Dissertation zur Erlangung des Doktorgrades

der Fakultät für Chemie und Pharmazie

der Ludwig-Maximilians-Universität München

Structural and functional analysis of MALT1 inhibition by phenothiazine derivatives

Florian Michael Schlauderer

aus

München, Deutschland

2015

This thesis has been prepared from October 2011 to October 2015 in the laboratory of Prof. Dr. Karl-Peter Hopfner at the Gene Center of the Ludwig-Maximilians-University of Munich (LMU).

Publications

During the work of this thesis, the following articles have been published:

Structural analysis of phenothiazine derivatives as allosteric inhibitors of the MALT1 paracaspase. Schlauderer F., Lammens K., Nagel D., Vincendeau M., Eitelhuber A.C., Verhelst S.H., Kling D., Chrusciel A., Ruland J., Krappmann D., Hopfner K.P.,
Angew Chem Int Ed Engl., 2013 Sep 23;**52**(39):10384-7.

Activity-based probes for detection of active MALT1 paracaspase in immune cells and lymphomas. Eitelhuber A.C., Vosyka O., Nagel D., Bognar M., Lenze D., Lammens K., Schlauderer F., Hlahla D., Hopfner K.P., Lenz G., Hummel M., Verhelst S.H., Krappmann D.,
Chem Biol., 2015 Jan 22;**22**(1):129-38.

Patents

During the work of this thesis, the following patents have been published:

WO 2014086478 A1: Inhibitors of malt1 protease.
Krappmann D., Nagel D., Schlauderer F., Lammens K., Hopfner K.P., Chrusciel R.A., Kling D.L., Bedore M.W.

WO 2014207067 A1: The (s)-enantiomer of mepazine.
Krappmann D., Nagel D., Schlauderer F., Lammens K., Hopfner K.P., Chrusciel R.A., Kling D.L.

Table of Contents

1 Zusammenfassung

Unser Immunsystem schützt uns vor Krankheitserregern wie Mikroorganismen und Fremdkörpern, aber auch defekten körpereigenen Zellen, durch ein stark reguliertes Netzwerk verschiedener Zelltypen. Funktionsstörungen des Immunsystems können zur Lymphom Entwicklung oder Autoimmunkrankheiten wie Multiple Sklerose führen. Das menschliche Immunsystem wird in die angeborene und adaptive Immunantwort unterteilt. In beiden Systemen besitzt der NF-κB Signalweg eine wichtige regulatorische Funktion und ist an der Kommunikation der Immunantworten untereinander beteiligt. Eine zentrale regulatorische Einheit in dem NF-κB Signalweg ist der CBM-Komplex, welcher aus den Proteinen CARMA1, BCL-10 und MALT1 besteht. Mutationen dieser Gene können zur Entwicklung von Lymphomen oder Autoimmunkrankheiten führen (Hailfinger, 2009; Mc Guire, 2013). MALT1 wurde durch die chromosomale Translokation t(11;18)(q21;21) entdeckt. Diese Translokation generiert das API2-MALT1 Fusionsprotein, welches die Entwicklung von Lymphomen durch konstitutive NF-κB Aktivierung fördert (Akagi, 1999; Morgan, 1999). Die proteolytische Aktivität der MALT1 Paracaspase ist an der NF-κB Signalübertragung beteiligt und steht im Zusammenhang mit der Lymphom Entwicklung (Ferch, 2009; Hailfinger, 2009). Die Inhibierung der proteolytischen Aktivität durch Phenothiazine ist selektiv toxisch für ABC-DLBCL Lymphome und besitzt ein immunsuppressives Potential (Nagel, 2012).

Die Hauptziele dieser Arbeit waren, mehr über die Aktivierung von MALT1 zu erfahren, die Bildung des CBM-Komplexes zu untersuchen und den Mechanismus der Inhibierung durch Phenothiazine zu erklären. Mit Hilfe von strukturbiologischen Methoden wie Elektron-Mikroskopie wurde die molekulare Anordnung des CBM-Komplexes visualisiert und durch Röntgenstrukturanalyse von Proteinkristallen konnte die Phenothiazine Bindungsstelle an MALT1 identifiziert werden. Die Bindungskonstanten für verschiedene Phenothiazin-Derivate wurden mit der biophysikalischen Methode des Fluoreszenzquenching bestimmt. Durch eine gezielte Mutation der allosterischen Bindungsstelle konnte der toxische Effekt von Phenothiazin-Derivaten für ABC-DLBCL auf die MALT1 Inhibierung zurückgeführt werden. Darüber hinaus stellt die Identifizierung des stereo-selektiven Inhibierungsmechanismus für (S)-Mepazine einen bedeutsamen Schritt zu einer effizienteren und MALT1 selektiveren Inhibierung dar.

1 Summary

Our immune system plays an important role in sensing of environmental conditions to protect us against pathogens including microorganisms, foreign substances or defect cells of our own body. It is a tightly regulated network of different cell types and disorders of the immune system can result in lymphoma development or serious autoimmune diseases like multiple sclerosis. The human immune system is divided into the innate and adaptive response. The NF-κB pathway has an important regulatory function in both systems and is involved in their communication. The CBM-complex is one central regulatory assembly in the NF-κB signaling cascade and consists of CARMA1, BCL-10 and MALT1. Mutations in one of these genes are connected with the development of lymphoma and autoimmune diseases (Hailfinger, 2009; Mc Guire, 2013). Especially, MALT1 was identified by the chromosomal translocation t(11;18)(q21;21). This translocation generates the API2-MALT1 fusion protein, which supports the development of B-cell lymphoma by constitutive NF-κB activation (Akagi, 1999; Morgan, 1999). MALT1 harbors a paracaspase domain, whose proteolytic activity is involved in NF-κB signal transduction. Several studies have shown that the proteolytic activity of MALT1 is closely connected to the undefined cell growth of lymphoma (Ferch, 2009; Hailfinger, 2009). Inhibition of the proteolytic activity by small molecules belonging to the class of phenothiazines is selectively toxic for ABC-DLBCL lymphoma and has an general immunosuppressive potential (Nagel, 2012).

The main goals of this thesis were to study MALT1 activation, CBM-complex formation and mechanism of MALT1 inhibition by phenothiazines. Therefore, structural approaches like electron-microscopy were used to determine the molecular assembly of the CBM-complex and x-ray crystallography to identify the binding site of phenothiazines on MALT1. Biochemical analysis by fluorescence quenching allowed the determination of association constants for different phenothiazines. In addition, mutation of the allosteric phenothiazine binding site verified the toxic effect of phenothiazines for ABC-DLBCL to origin from MALT1 inhibition. Moreover, the identified stereo-selective mechanism of inhibition by (S)-mepazine represents a significant step towards more efficient and MALT1 specific inhibition.

2 Introduction

The immune system is a concert of cells, sensing environmental conditions to protect us against a great variety of pathogens and defect cells of our own body. The human immune system consists of the innate and adaptive immune responses (Hoffmann, 1999). The innate response is in contrast to the adaptive response less specific, but usually the first reaction to pathogens like microorganism. The specificity of the adaptive immune response is based on the high receptor variability of antibodies (Agrawal, 1998) and the generation of an immunological memory to react against already known pathogens much more efficient. Both systems are closely connected and collaborate with each other, but use different types of cells and receptors to recognize pathogens (Medzhitov, 2007). Immune cells are derived from hematopoietic stem cells (HSCs) in the bone marrow and become multipotent progenitors (MPPs), before they differentiate into common myeloid progenitors (CMP) of the innate system or common lymphoid progenitors (CLP) of the adaptive immune system (Fig. 2-1) (Kondo, 1997; Akashi, 2000).
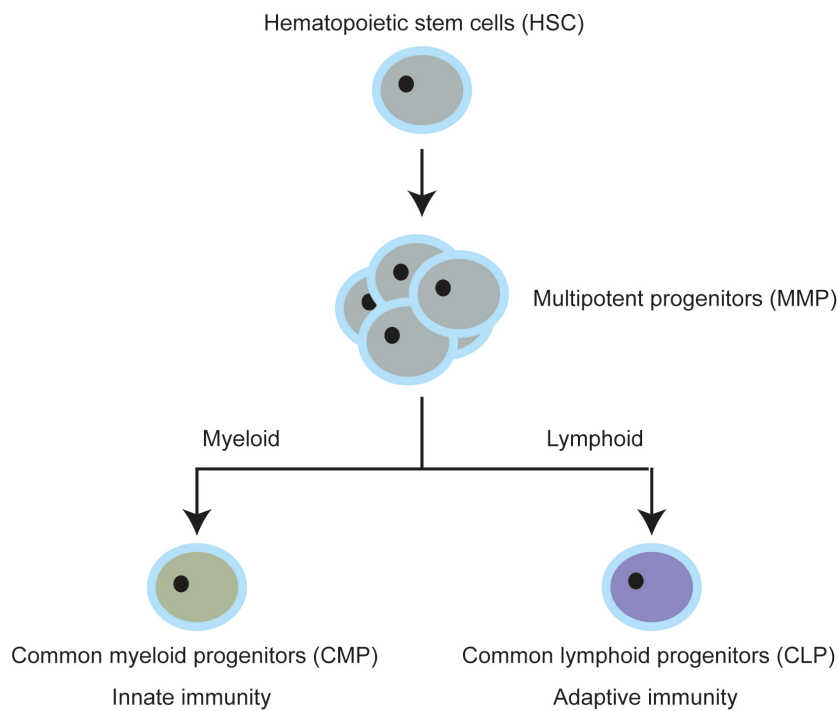
Figure 2-1: Overview of immune progenitor cells.

2.1 Innate immune system

Innate immune cells derived from CMPs differentiate in the bone marrow to granulocytes, mast cells or monocytes and subsequently enter the blood stream (Akashi, 2000) (Fig. 2-2). Granulocytes harbor big cytosolic granules with immune stimulatory or toxic molecules, which are released to the site of infection after activation. Granulocytes are further grouped into neutrophils, eosinophils and basophils (Arinobu, 2005) (Fig. 2-2). Neutrophils are mainly involved in phagocytosis, while eosinophils are antigen presenting cells with regulatory functions. Basophils and mast cells can release additional substances like histamine, resulting in increased permeability of surrounding capillaries to push the inflammatory response. Monocytes can further differentiate to macrophages and dentric cells (DCs) (Fogg, 2006) (Fig. 2-2). These are phagocytic leukocytes and recognize pathogen-associated molecular patterns (PAMP) by pattern-recognition receptors (PRR) to discriminate between host and pathogen derived molecules (Medzhitov, 2007). Extracellular PRRs like the family of Toll-like receptors (TLRs) recognize lipopolysaccharides (LPS) from bacteria or dsRNA from viruses, resulting in nuclear factor kappa-light-chain-enhancer of activated B-cells (NF-κB) activation and type-I interferon production (Alexopoulou, 2001), further stimulating immune cell differentiation and recruitment of additional immune cells. DCs are involved in antigen processing and presentation to T-cells of the adaptive system.

Figure 2-2: Overview of innate immune cells.

From CLPs derived innate immune cells are defined as innate lymphoid cells (ILCs) and include natural killer (NK) cells (Fig 2-2). ILCs have a classic lymphoid cell morphology, but unlike adaptive T-, and B-lymphocytes, ILCs lack B-cell receptor (BCR) or T-cell receptor (TCR) and do not show antigen specificity (Spits, 2011). ILCs have been further divided into three groups based on their cytokine production and transcription factor depending development (Spits, 2011).
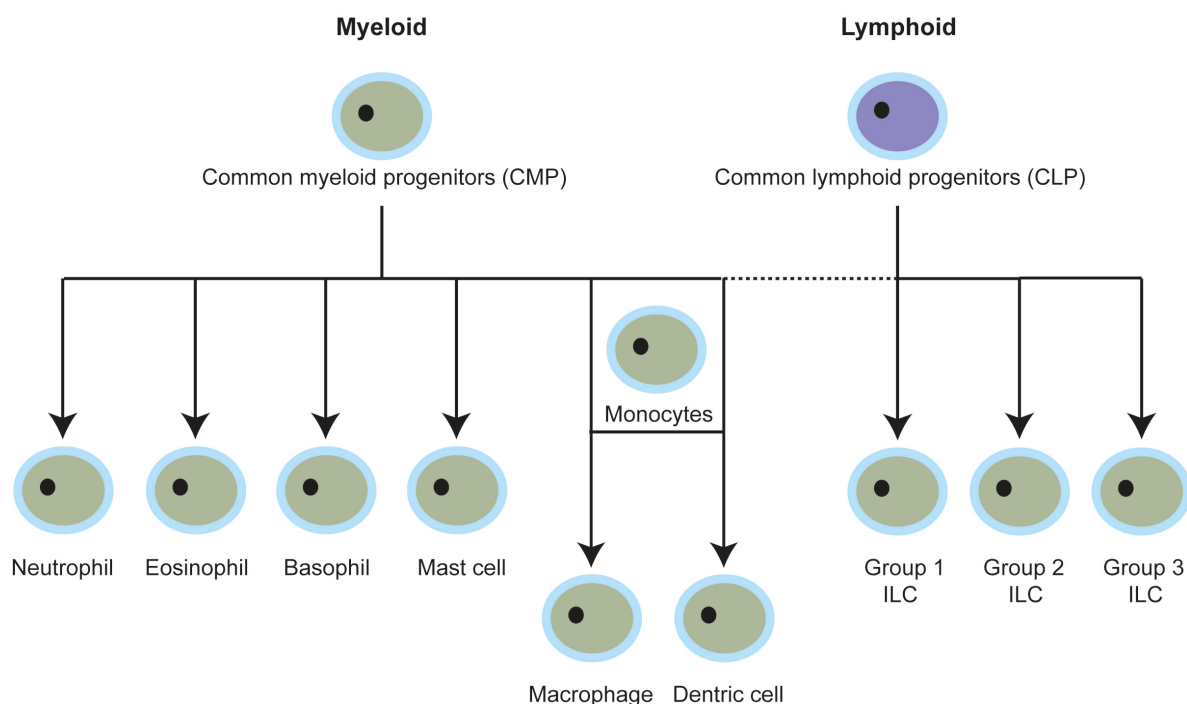
Group 1 includes NK cells and produces type-I cytokines like interferon gamma (IFN-γ) and tumor necrosis factor (TNF). These cytokines enhance the cellular immune response and inflammation. NK cells attack virus infected or tumor cells and have an essential role in amplifying inflammatory responses (Vivier, 2011). How NK cells discriminate between normal and infected or tumor cells, is generally described by the missing-self-signal hypothesis, meaning that sufficient levels of major histocompatibility complex (MHC) class-I molecules have to be recognized by inhibitory receptors on NK cells to prohibit attack (Karlhofer, 2006). More recently it was shown that several stimulatory receptors on NK cells recognize specific signals produced by infected cells or tumor cells (Brown, 2001) and the final decision for attack seems to depend on a balanced system between inhibitory and stimulatory signals. Signal transduction in NK cells depends among others on the NF-κB signaling cascade (Thome, 2004; Gross, 2008). Interestingly, dysregulation of NK cells is closely connected to autoimmune diseases (Baxter, 2002).

Group 2 ILCs are characterized by interleukin (IL) 25 and IL-33 stimulated expression of T-helper 2 (Th2) cell associated cytokines, like IL-5 and IL-13 (Klein Wolterink, 2012). Since ILC2 cells are able to express MHC class-II molecules, they might be involved in T-cell activation by antigen presentation (Wilhelm, 2011), connecting innate and adaptive immunity. Moreover, ILC2 cells have been shown to respond on signals produced by T-cells and B-cells, providing a feedback mechanism from adaptive to innate immunity (Neill, 2010).

Group 3 ILCs include lymphoid tissue-inducer (LTi) cells and are able to produce the cytokines IL-17 (Cupedo, 2009) and IL-22 (Cella, 2009) like Th17 cells of the adaptive immune system. LTi cells participate in lymphoid tissue formation and the maintenance of CD4^{+}-memory cells (Withers, 2012). Additionally, group 3 ILCs can produce granulocyte macrophage (GM) colony-stimulating factor (CSF) and generally promote immunity (Satoh-Takayama, 2008) and inflammation (Sonnenberg, 2011).

2.2 Adaptive immune system

Adaptive immune cells are derived from CLPs and separated into T-cells and B-cells, according to their defense mechanism. CLPs arriving in the thymus lose their ability to become B-cells (Pui, 1999) or NK cells (Michie, 2000) and will differentiate to the T-cell lineage, which depends among others on Notch signaling (Radtke, 1999).The interaction of the TCR with self-peptide-MHC complexes from antigen-presenting cells (APCs) plays an essential role in T-cell development. Initial thymocytes do not express the cluster of differentiation (CD) 4 or CD8 surface molecules, defining them as double negative (DN) (Fig. 2-3). These thymocytes are subdivided into four classes according to their expression of CD25 and CD44 surface molecules (Godfrey, 1993). The DN thymocytes begin to express either γδ or αβ chains of the TCR (Robey, 1994). Thymocytes expressing γδ-chain-TCRs develop to a small subset of less characterized T-cells. The majority of thymocytes express αβ-chain-TCRs and start after αβ-chain rearrangements (Shinkai, 1993) to expose CD4 and CD8 surface molecules, defining them as double positive (DP) thymocytes (Robey, 1994). These T-cell progenitors migrate through different thymic microenvironments, where they are selected according to their functionality and self-tolerance ability by positive and negative selection processes.

Positive selection appears in the cortex by the interaction with self-peptide bound MHC molecules of cortical thymic epithelial cells (cTECs). Thereby, the CD4 or CD8 lineage commitment depends on the TCR-CD4 interaction with MHC class-II presented molecules and on the TCR-CD8 interaction with MHC class-I presented molecules. The "strength of signal" model proposes a dependency of signal intensity and duration for correct lineage commitment (Matechak, 1996; Ohoka, 1997). Binding of MHC class-II presented molecules by the TCR and CD4 tends to produce more frequently a prolonged signal with moderate intensity compared to the TCR-CD8 interaction with MHC class-I presented molecules. (Veillette, 1989; Wiest, 1993). T-cell progenitors stop either expressing CD4 or CD8 molecules due to missing activation signals by MHC class-II or MHC class-I presented antigens in the different thymic niches. The positive selected T-cells migrate to the medulla, undergoing negative selection processing. In contrast to positive selection, high affinity to self-peptide bound MHC molecules of bone marrow derived APCs results in apoptosis. T-cell progenitors with improper commitment are eliminated during these selection processes. Especially, negative selection is essential to prohibit overreaction by self-peptide recognition and is connected to autoimmune diseases.

Finally selected <u>s</u>ingle <u>p</u>ositive (SP) CD8$^+$ T-cells leave the thymus as cytotoxic T-cells and screen for corresponding antigens on MHC class-I molecules, presented by virus infected cells or cancer cells. Activated cytotoxic T-cells produce IFN-ɣ, TNF-α and induce cell death by a cytolytic mechanism. In contrast, SP CD4$^+$ T-cells are responsible to activate or regulate the immune response and are defined as T-helper cells. Depending on the cytokine micro-environment, they develop into the specialized subgroups of Th1, Th2, Th17, <u>r</u>egulatory <u>T</u>-cells (T$_{reg}$) or <u>f</u>ollicular <u>h</u>elper <u>T</u>-cells (T$_{FH}$) (Table 2-1).

First were Th1 cells and Th2 cells identified (Mosmann, 1986). Th1 cell differentiation is mainly stimulated by IL-2 and IL-12, produced by activated APCs. Th1 cells express IFN-γ, GM-CSF and IL-2 to further stimulate the immune response. Th2 cell differentiation depends on IL-4 and activation results in IL-4, IL-5, IL-10 and IL-13 expression. In addition, Th2 cells are involved in B-cell activation. The development of Th17 cells depends on IL-6 and <u>t</u>ransforming <u>g</u>rowth <u>f</u>actor-β (TGF-β) (Mangan, 2006; Veldhoen, 2006). Th17 cells are IL-17, IL-23 or GM-CSF producing cells and are maintained long-term by IL-21 and IL-23 (Stritesky, 2008). IL-17 and IL-23 stimulate the immune response (Khader, 2007) and have been shown to be implicated in <u>m</u>ultiple <u>s</u>clerosis (MS) (Langrish, 2005; Veldhoen, 2006), inflammatory bowel disease (Duerr, 2006) and <u>r</u>heumatoid <u>a</u>rthritis (RA) (Stahl, 2010).

T$_{reg}$ cells are characterized by TGF-β and <u>f</u>orkhead-<u>b</u>ox-protein <u>P3</u> (FoxP3) (Chen, 2003; Hori, 2003) dependent CD25 expression (Sakaguchi, 2000). These cells express IL-4, IL-10 or TGF-β and are involved in maintenance of the immunological tolerance by controlling the T-cell response. Thus, dysfunction of T$_{reg}$ cells is likely to be implicated in autoimmune diseases (Sakaguchi, 1985; Chen, 1994). T$_{FH}$ cells develop after priming <u>i</u>nducible T-cell <u>co</u>-stimulator <u>l</u>igand (ICOSL) expressing DCs (Fazilleau, 2009b; Choi, 2011). These cells are located in T-cell zones, which are in proximity to follicular B-cells and are involved in the formation of germinal centers (Fazilleau, 2009a).

Table 2-1: T-helper cell differentiation and activation effects.

T-helper cell	Differentiation stimulation	Activation effects
Th1	IL-2, IL-12	IFN-γ, GM-CSF, IL-2 expression
Th2	IL-4	IL-4, IL-5, IL-10, IL-13 expression
Th17	IL-6, TGF-β / IL-21, IL-23	IL-17, IL-23, GM-CSF expression
T$_{reg}$	TGF-β, FoxP3	IL-4, IL-10, TGF-β expression
T$_{FH}$	ICOSL	GC formation

The T-cell immune response is divided into the expansion, contraction and memory phases. First, antigens presented by APCs in lymphoid tissues and costimulatory signals induce naive T-cells to clonally expand and differentiate into effector CD4$^+$ or CD8$^+$ T-cells (Swain, 1990). In the contraction phase, the majority of T-cells undergo apoptosis due to the decreasing abundance of specific antigens (Badovinac, 2002; Harbertson, 2002). Depending on the CD8$^+$ T-cell population size, some T-cells differentiate into a stabilized memory T-cell repertoire to provide an effective immune response upon pathogen re-exposure (Murali-Krishna, 1998). The differentiation and proliferation of CD4$^+$ memory T-cells differ from CD8$^+$ memory T-cells. According to their expression of C-C chemokine receptor type 7 (CCR7), which is responsible for locating T-cells to lymph nodes, CD4$^+$ and CD8$^+$ memory T-cells are divided into no CCR7 expressing effector memory (T_{EM}) T-cells and CCR7 expressing central memory (T_{CM}) T-cells (Sallusto, 1999). T_{EM} are located in non-lymphoid tissues and cannot undergo homeostatic turnover. T_{EM} convert to more proliferative T_{CM} and undergo efficient homeostatic turnover to store antigen information (Wherry, 2003).
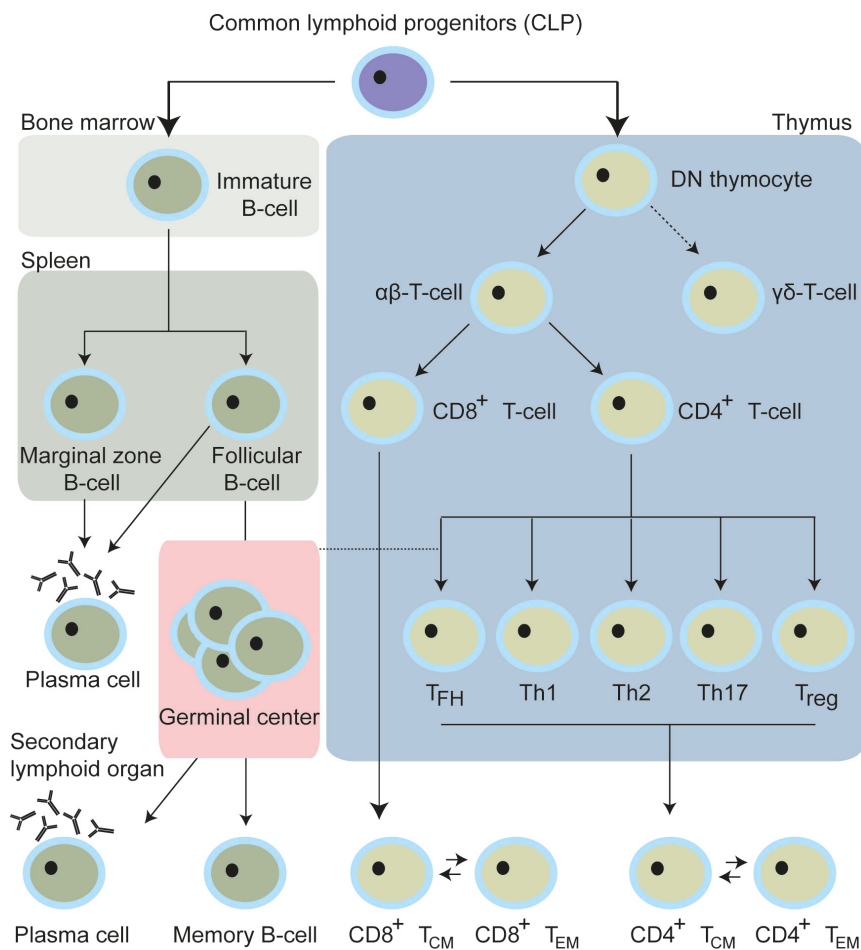

Figure 2-3: Overview of adaptive immune cells.

The second defense strategy of the adaptive immune system is represented by the B-cell lineage (Fig. 2-3). Initial differentiation from CLPs to pre-B-cells occurs in the bone marrow. Hereby, the BCR diversity is based on heavy-chain (HC) rearrangements of the variable (V), diversity (D) and joining (J) gene segments, forming the Ig HC (Hardy, 1991). Additional binding of surface molecules Igα, Igβ and surrogate immunoglobulin light chains (IgLC) λ5 and V_{preB} results in the pre-BCR formation. Pre-BCR signaling together with IL-7 stimulation is essential for the survival and proliferation of large pre-B-cells (Corfe, 2012). Highly auto-reactive pre-B-cells undergo receptor editing by additional immunoglobulin gene rearrangements or die by apoptosis (Nemazee, 2000). Subsequent signaling events lead to small resting pre-B-cells and rearrangement of LC genes. Immature B-cells express functional BCR in various HC and LC combinations and undergo negative selection in the bone marrow to prohibit expansion of auto-reactive clones (Ohashi, 2002). Immature B-cell development is continued through several transitional stages in the spleen (Loder, 1999) and further negative selection processes (Chung, 2003) prior differentiation to mature follicular or marginal zone B-cells (Fig. 2-3).

Lineage decision and survival of follicular and marginal zone B-cells depends among other factors on the BCR signal strength and NF-κB signal transduction by the CBM-complex (Ruefli-Brasse, 2003; Xue, 2003), consisting of the caspase-recruitment domain (CARD) containing membrane associated guanylate kinase (MAGUK) protein 1 (CARMA1), B-cell lymphoma 10 (BCL-10) and mucosa associated lymphoid tissue lymphoma translocation protein 1 (MALT1). Marginal B-cells are located in the marginal zone of the spleen and are responsible for immune response against bacterial infections (Oliver, 1997). They show generally a faster immune response than follicular B-cells and form antibody producing plasmablasts in a T-cell independent manner, although some marginal B-cells participate in a T-cell dependent manner by presenting antigens and costimulatory signals (Oliver, 1999). Follicular B-cells are primarily involved in the T-cell dependent immune response. They are circulating through the body and are preferentially located in follicles of secondary lymphoid organs close to T-cell zones (Hardy, 1983). Activation occurs by costimulatory signals and antigens, diffusing to follicles of secondary lymphoid organs (Pape, 2007) or presented by subcapsular sinus (SCS) macrophages (Junt, 2007) and DCs (Wykes, 1998). Initial plasma cells differentiated from either marginal or follicular B-cells have a rather short life-time and do not produce highly specific antibodies (Smith, 1996). Additional interactions of follicular B-cells with T_{FH}-cells and follicular dendritic cells (FDCs) result in formation of germinal centers (McHeyzer-Williams, 2001). The architecture of germinal centers is divided into a

dark zone and a light zone. The dark zone harbours highly proliferating B-cells, defined as centroblasts. In the dark zone occurs the affinity maturation of antibodies by somatic hypermutation (SHM) and class-switch recombination (CSR) (Shan, 1990; Jacob, 1991). The light zone consists of not proliferating centrocytes. High affinity antibody producing cells are selected in the light zone according to their BCR signal strength and differentiate to plasma cells or memory B-cells. These cells exit the germinal centers and migrate to the mucosal tissues, bone marrow or site of infection (Blink, 2005; Phan, 2006). The interaction between CD40 of centrocytes with CD154 of T_{FH} cells is essential for germinal center exit and underlies NF-κB mediated transcriptional repression of BCL-6 (Saito, 2007). Binding of antibodies to correlating antigens on pathogens initiates macrophage mediated phagocytosis, antibody-dependent cell-mediated cytotoxicity (ADCC) by NK cells and neutrophil activation (Chan, 1971; Titus, 1987; Anderson, 1990).

2.3 NF-κB pathway in immune cells

The NF-κB pathway was discovered by the observation of a protein, selectively binding to the κ-light-chain enhancer of B-cell tumors extracts (Sen, 1986) and has evolved to one of the central signaling pathways, controlling immune cell development, survival, proliferation and differentiation by the regulation of cytokine, chemokine, apoptosis regulator and growth factor expression (Pahl, 1999). Notable is, the dysregulation of NF-κB signaling is implicated in chronic inflammation, lymphoma or autoimmune diseases (Toubi, 2004; Bassères, 2006). Transcription factors of the NF-κB family are p50, p52, RelA (p65), c-Rel and RelB. These proteins bind as homo-, or hetero-dimers to κB-elements in promoter or enhancer regions to activate or repress transcription (Ruben, 1992; Ryseck, 1992).

Generally, NF-κB signaling has been divided into the canonical and alternative pathway according to the activation mechanism (Bonizzi, 2004; Gilmore, 2006). Canonical NF-κB signaling is initiated by tumor necrosis factor receptor (TNFR), TLR, BCR or TCR stimulation, resulting in formation of the CBM-complex and TNF receptor associated factor (TRAF6) assisted recruitment of the inhibitor of NF-kB (IκB) kinase (IKK) complex to the membrane (Fig. 2-4) (Hayden, 2004; Landström, 2010). The canonical IKK complex consists of the active kinases IKKα, IKKβ and the regulatory IKKγ (NEMO) subunit. Activation requires TGF-β activated kinase 1 (TAK1) dependent phosphorylation of the IKKβ kinase. Subsequent phosphorylation of NF-κB inhibitor α (IκBα) by IKKβ (Perkins, 2006) leads to

K48-ubiquitination of IκBα and following proteasomal degradation of IκBα to release the nuclear localization signal (NLS) of RelA, c-Rel, RelB and p50 dimers (Fig. 2-4).
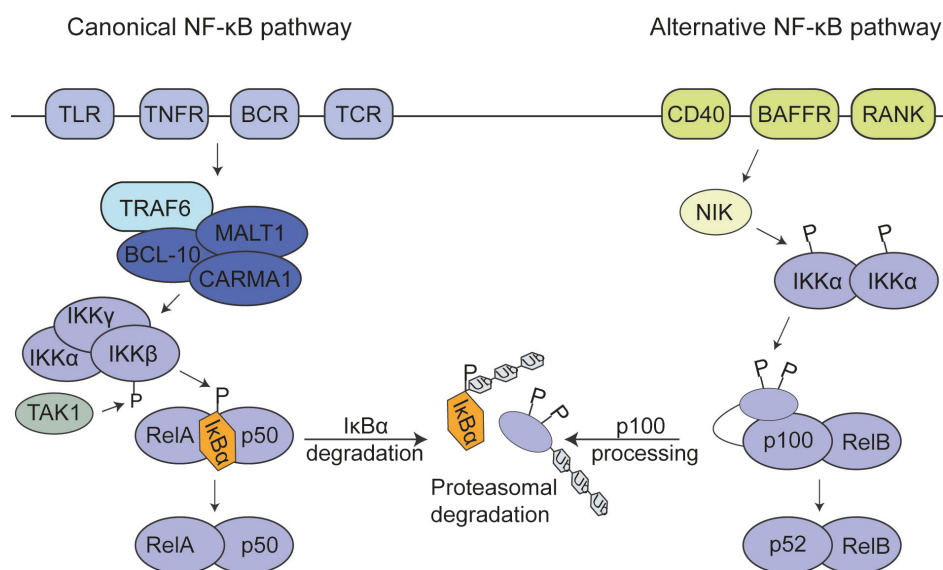

Figure 2-4: Overview of canonical and alternative NF-κB pathway.

Alternative NF-κB signaling is initiated by B-cell activating factor receptor (BAFFR), TNF receptor CD40 or RANK stimulation and results in activation of NF-κB inducing kinase (NIK) (Fig. 2-4) (Claudio, 2002; Coope, 2002; Dejardin, 2002). In contrast to the canonical pathway, the alternative IKK complex consists of two IKKα subunits and activation depends on phosphorylation by NIK (Senftleben, 2001; Xiao, 2004). The processing of p100 to p52 is mediated by the active IKK complex and results in nuclear translocation of the p52-RelB dimers (Fig. 2-4) (Xiao, 2004) .

2.4 MALT1 paracaspase

The MALT1 paracaspase was discovered by identification of the chromosomal translocation t(11;18)(q21;21) in MALT lymphoma and has been described as binding partner of BCL-10 (Akagi, 1999; Morgan, 1999). MALT1 consists of a central proteolytic active domain, which is homolog to caspases or metacaspases. In contrast to caspases, the paracaspase MALT1 cleaves substrates after an arginine in P1 position (Uren, 2000; Vercammen, 2007). The active site of MALT1 prefers an uncharged residue in P2 position and a hydrophobic residue in P4 position (Table 2-2) (Hachmann, 2012). The active site of human MALT1 isoform 1 harbors the in caspases highly conserved, catalytic active residues, histidine (H415) and cysteine (C464) (Uren, 2000). The homolog residues of mouse MALT1 are H423 and C472 (Fig. 2-5).

The first identified substrate of MALT1 was BCL-10 (Rebeaud, 2008), but processing of BCL-10 is rather involved in T-cell adhesion than NF-κB signaling (Rueda, 2007). First evidence for proteolytic dependent NF-κB regulation was shown by MALT1 processing of tumor necrosis factor, alpha-induced protein 3 (TNFAIP3 or A20) (Coornaert, 2008). A20 inhibits NF-κB signaling by removing K63-polyubiquitin chains from TRAF6, IKKɣ and MALT1 (Mauro, 2006). MALT1 dependent cleavage of A20 after R439 diminishes the deubiquitinase activity of A20 (Düwel, 2009). Afterwards, the substrates cylindromatosis (CYLD) (Staal, 2011), RelB (Hailfinger, 2011), Roquin-1 and Regnase-1 have been identified (Uehata, 2013; Jeltsch, 2014). Similar to A20, MALT1 dependent processing of CYLD inhibits deubiquitination of TRAF2, TRAF6, IKKɣ and TAK1. In contrast to A20, MALT1 dependent CYLD processing promotes JNK signaling and does not influence NF-κB signaling (Staal, 2011). The transcription factor RelB negatively regulates NF-κB signaling by inhibiting RelA and c-Rel dependent gene transcription, which is abrogated by MALT1 processing (Hailfinger, 2011). The ribonucleases Roquin-1 and Regnase-1 are involved in mRNA stability and decay. MALT1 dependent cleavage of Roquin-1 results in inactivation of ribonuclease activity and achieves efficient translation of NF-κB transcription factor mRNAs, essential for Th17 differentiation and IL-17 expression (Jeltsch, 2014).

Table 2-2: Substrates of MALT1.

Protein	Cleavage site	Effects of processing
A20	$GASR_{439}$	promotes NF-κB signaling
BCL-10	$LRSR_{228}$	involved in T-cell adhesion
RelB	$LVSR_{85}$	promotes NF-κB signaling
CYLD	$FMSR_{324}$	promotes JNK signaling
Regnase-1	$LVPR_{111}$	promotes NF-κB signaling
Roquin-1	$LIPR_{510}$, $MVPR_{579}$	promotes NF-κB signaling

The proteolytic activity of MALT1 depends on substrate mediated dimerization of the paracaspase domain, which is supported by close proximity within the CBM-complex (Wiesmann, 2012; Qiao, 2013). C-terminal mono-ubiquitination on K644 stabilizes MALT1 dimers and enhances the proteolytic activity (Pelzer, 2013). MALT1 plays a key role in T-cell development and activation, but the proteolytic activity is not essential for NF-κB activation and rather promotes signal transduction. In contrast, the scaffolding function of MALT1 within the CBM-complex is absolutely necessary for NF-κB mediated gene transcription

(Lucas, 2001; Rebeaud, 2008). The scaffolding function of MALT1 relies mostly on the additional N-terminal and C-terminal domains. The C-terminal part of MALT1 consists of an Ig-like domain (Ig3) and comprises binding sites for TRAF2, TRAF6 and Ubc13 (Sun, 2004; Zhou, 2005). TRAF6 binding to MALT1 initiates auto-ubiquitination of TRAF6 and subsequent ubiquitination of C-terminal lysine residues of MALT1. This ubiquitination is responsible for ubiquitin binding domain (UBDN) mediated recruitment of IKKγ to MALT1 (Wagner, 2008; Düwel, 2009). The C-terminal region of MALT1 is additionally involved in further CBM-complex stabilization by interacting with the *coiled-coiled* region of CARMA1 (Che, 2004). The N-terminal part of MALT1 consists of a death domain (DD) followed by two immunoglobulin like domains and is mainly involved in BCL-10 binding (Langel, 2008). The region between the second Ig-like domain and the paracaspase domain distinguishes the two isoforms of MALT1. In contrast to isoform-1, isoform-2 lacks 10 amino acids (309-319), which include an additional TRAF6 binding site, represented by the glutamate residues E313 and E316 (Fig. 2-5) (Noels, 2007).
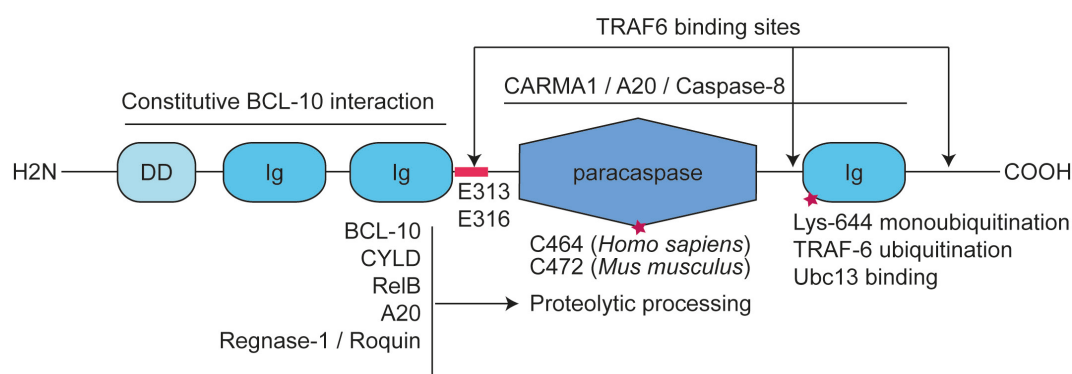
Figure 2-5: MALT1 domain architecture.

Moreover, a proteolytic independent role of MALT1 has been proposed for the regulation of caspase-8 activity in NF-κB dependent lymphocyte proliferation and activation (Salmena, 2003; Su, 2005; Kawadler, 2008). The proteolytic inactive caspase homolog cellular FLICE-like inhibitory protein (cFLIP) participates in regulation of caspase-8 and CD95 stimulated apoptosis (Chang, 2002). Caspase-8 mediated processing of cFLIP is involved in TCR mediated NF-κB signaling, IL-2 production and reduces the ability to induce apoptosis (Micheau, 2002; Misra, 2007). Caspase-8 interacts with the MALT1-BCL-10 complex and is recruited with TRAF6 and the IKK complex to lipid-rafts (Su, 2005; Misra, 2007). Hetero-dimerization of caspase-8 with MALT1 has been proposed to mediate auto-proteolytic activation of caspase-8, leading to a specific conformation, which favors cFLIP cleavage, but does not allow cleavage of substrates like caspase-3 (Kawadler, 2008).

2.5 API2-MALT1 fusion protein

The chromosomal translocation t(11;18)(q21;21) is frequently observed in MALT lymphoma and generates a fusion protein of the C-terminal part from MALT1 and the N-terminal region of the inhibitor of apoptosis 2 (API2) (Akagi, 1999; Lucas, 2001). API2 belongs to the family of inhibitors of apoptosis (IAP) and consists of three N-terminal baculoviral IAP repeat (BIR) domains, central ubiquitin associated (UBA) domain, followed by a CARD domain and C-terminal really interesting new gene (Ring) domain. In most lymphoma cases is the BIRC3 gene, which encodes API2, translocated after N442 to several loci in the MALT1 gene before the paracaspase encoding region (Fig. 2-6) (Motegi, 2000; Ye, 2003; Isaacson, 2004).
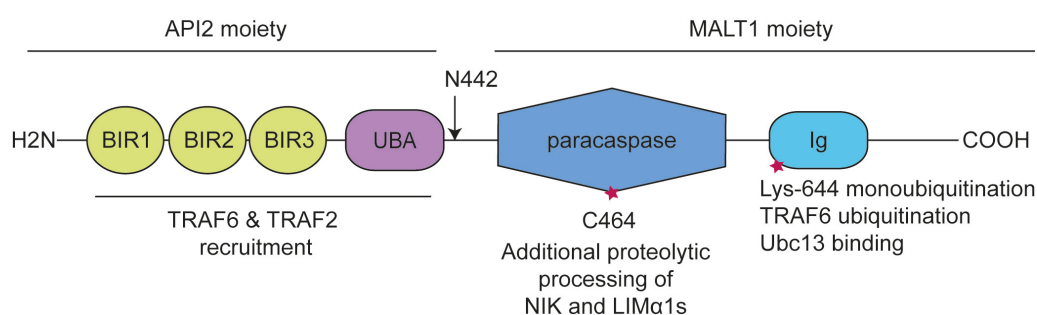

Figure 2-6: API2-MALT1 domain architecture.

The BIR and UBA domains of API2 are mostly involved in TRAF2 or TRAF6 recruitment (Shu, 1996; Lucas, 2007). In addition, the BIR domains of API2 are able to inhibit the activity of caspase-3 and caspase-7 (Roy, 1997; Takahashi, 1998). Of particular importance is that API2-MALT1 fusion leads to an enhanced proteolytic activity and shows constitutive expression of canonical and alternative NF-κB genes, independent of antigen stimulation (Lucas, 2001; Zhou, 2005). Mutational studies proposed that constitutive canonical NF-κB signaling is due to additional interactions with TRAF2 and TRAF6 by the API2 part (Garrison, 2009). Another study proposed BIR1 domain supported oligomerization of API2-MALT1 to be responsible for the constitutive NF-κB activation (Zhou, 2005). The identification of NF-κB-inducing kinase (NIK) as unique substrate of API2-MALT1 explains constitutive activation of alternative NF-κB genes by proteolytic activity dependent formation of a less proteasomal degradation prone, but still active kinase fragment (Rosebeck, 2011). Most recently, LIM domain and actin binding 1 (LIMα1) has been identified as unique substrate of API2-MALT1. LIMα1 is generally known to act as tumor suppressor and cleavage by API2-MALT1 results in formation an oncogenic LIM domain only (LMO)-like protein fragment (Nie, 2015).

2.6 CBM-complex architecture

The CBM-complex was initially described as Polkadots, which represent big spotted cytosolic structures (Rossman, 2006), regulating NF-κB signaling in immune and non-immune cells. CBM-complex formation is mediated by protein kinase C (PKC) dependent phosphorylation of CARMA proteins (Table 2-3), downstream of immunoreceptor tyrosine-based activation motif (ITAM) containing receptors or G-protein coupled receptors (GPCR) (Hara, 2003; Matsumoto, 2005; Gross, 2008; Blonska, 2011). CARMA1, also termed CARD11, is specific for the spleen, thymus, peripheral blood lymphocytes and functions downstream of antigen receptors in T-cells and B-cells or natural-killer group 2, member D (NKG2D) receptor in NK-cells (Bertin, 2001; Gaide, 2001; Hara, 2003; Gross, 2008). CARMA3, also known as CARD10, functions in immune and non-immune cells downstream of GPCRs and is highly expressed in the liver, kidney, heart and brain (McAllister-Lucas, 2001; Wang, 2007). CARD9 shows high expression levels in the bone marrow, thymus, spleen (Hsu, 2007) and functions downstream of monocyte-activating receptor dectin-1 in macrophages and DNAX-activation protein 12 (DAP12) associated triggering receptor expressed on myeloid cells 1 (TREM1) in myeloid and NK-cells (Taylor, 2002; Gross, 2006; Hara, 2007).

Table 2-3: Overview of CARMA family proteins.

Protein	Alternative name	Tissue specificity	Cell types
CARMA1	CARD11	Spleen, thymus	Immune cells
CARMA3	CARD10	Liver, kidney, heart, brain	Immune-, non-immune cells
CARD9	-	Bone marrow, thymus, spleen	Myeloid and NK-cells

These CARMA family members share a similar domain architecture that comprises an N-terminal CARD domain followed by a *coiled-coil* containing linker region. CARMA1 and CARMA3 contain an additionally PDZ domain, Src homology (SH) 3 domain and C-terminal MAGUK domain (Fig. 2-7) (Bertin, 2001). Upon receptor stimulation, PKC dependent phosphorylation of the CARMA1 linker region results in conformational changes from an inhibitory to an active state (Matsumoto, 2005; Sommer, 2005). During this thesis a study was published that revealed CARMA1 in its active state to function as a nucleator for directional BCL-10 polymerization (Qiao, 2013). BCL-10 consists of an N-terminal CARD domain followed by an unstructured, serine and threonine rich region (Fig. 2-7). The CARD domain of BCL-10 is prone for cooperative polymerization to filaments with a left-handed, single-

stranded helical symmetry. These filaments are built of intrastrand and interstrand interfaces similar to the type II and type I interactions of DD family complexes like in the myddosome (Ferrao, 2012; Qiao, 2013). The intrastrand and interstrand interfaces within BCL-10 filaments are mostly electrostatic, similar to the BCL-10 and CARMA1 interface at the filament end (Qiao, 2013). BCL-10 filament growth mediates signal amplification upon a certain threshold, sensed by CARMA1 nuclei formation. BCL-10 filament structures enhance the proteolytic activity of MALT1 by inducing for activation required proximity of MALT1 paracaspase domains (Wiesmann, 2012; Qiao, 2013).
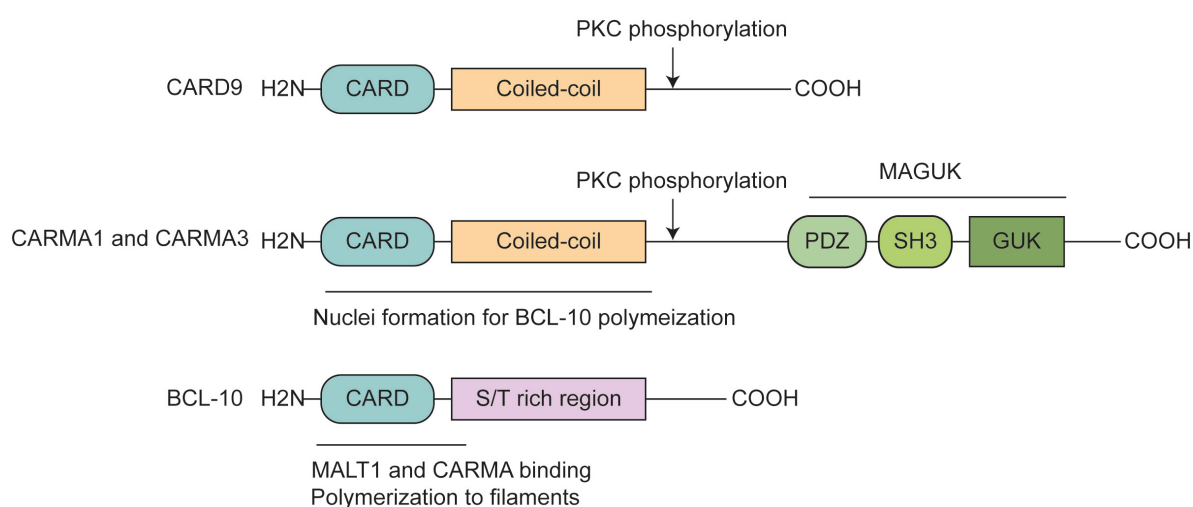

Figure 2-7: Overview CBM-complex members.

2.7 CBM-complex dependent NF-κB signaling in T-cells and B-cells

Canonical NF-κB signaling in adaptive immune cells depends on BCR or TCR signal intensity and contact duration with APCs (Gett, 2003; Ruefli-Brasse, 2003). In CD4^{+} T-cells, α-β-chain dimers of the TCR form complexes with CD3 surface molecules (Fig. 2-8). Upon TCR stimulation the protein tyrosine kinase (PTK) p56Lck phosphorylates the ITAM of CD3 molecules (Raab, 1995). Subsequently, the PTK zeta-associated protein-70 (ZAP70) is activated by p56Lck dependent phosphorylation and mediates several phosphorylation events to recruit phosphatidyl-inositol-3-kinase (PI-3-K) and phospholipase-C-gamma-1 (PLCγ1) (Weiss, 1994; Raab, 1995; Yablonski, 1998). PLCγ1 stimulates the hydrolysis of phosphatidyl-inositol-2-phosphat (PIP2) to diacylglycerol (DAG) and inositol triphosphate (IP$_3$) (Homma, 1992). The generation of IP$_3$ is involved in calcium ion release from intracellular storages (Streb, 1983; Berridge, 1993), which participates in signal amplification by stimulating the dissociation of the cytoplasmic CD3 domain from the membrane to ensure

solvent exposure of tyrosine residues for phosphorylation (Shi, 2012). Additional interactions of CD80 and CD86 on APCs with the CD28 receptor on T-cells stimulate PI-3-K mediated phosphorylation of the membrane lipid PIP2, resulting in phosphatidyl-inositol-3-phosphat (PIP3) formation (Linsley, 1991; Pentcheva-Hoang, 2004; Park, 2009). Auto-phosphorylation dependent activation of phosphoinositide-dependent kinase 1 (PDK1) occurs due to PIP3 assisted membrane recruitment and results in phosphorylation induced activation of PKCθ. The activity of PKCθ is additionally enhanced by DAG or calcium ions and initiates CBM-complex formation by CARMA1 phosphorylation (Fig.2-8) (Lee, 2005; Sommer, 2005).
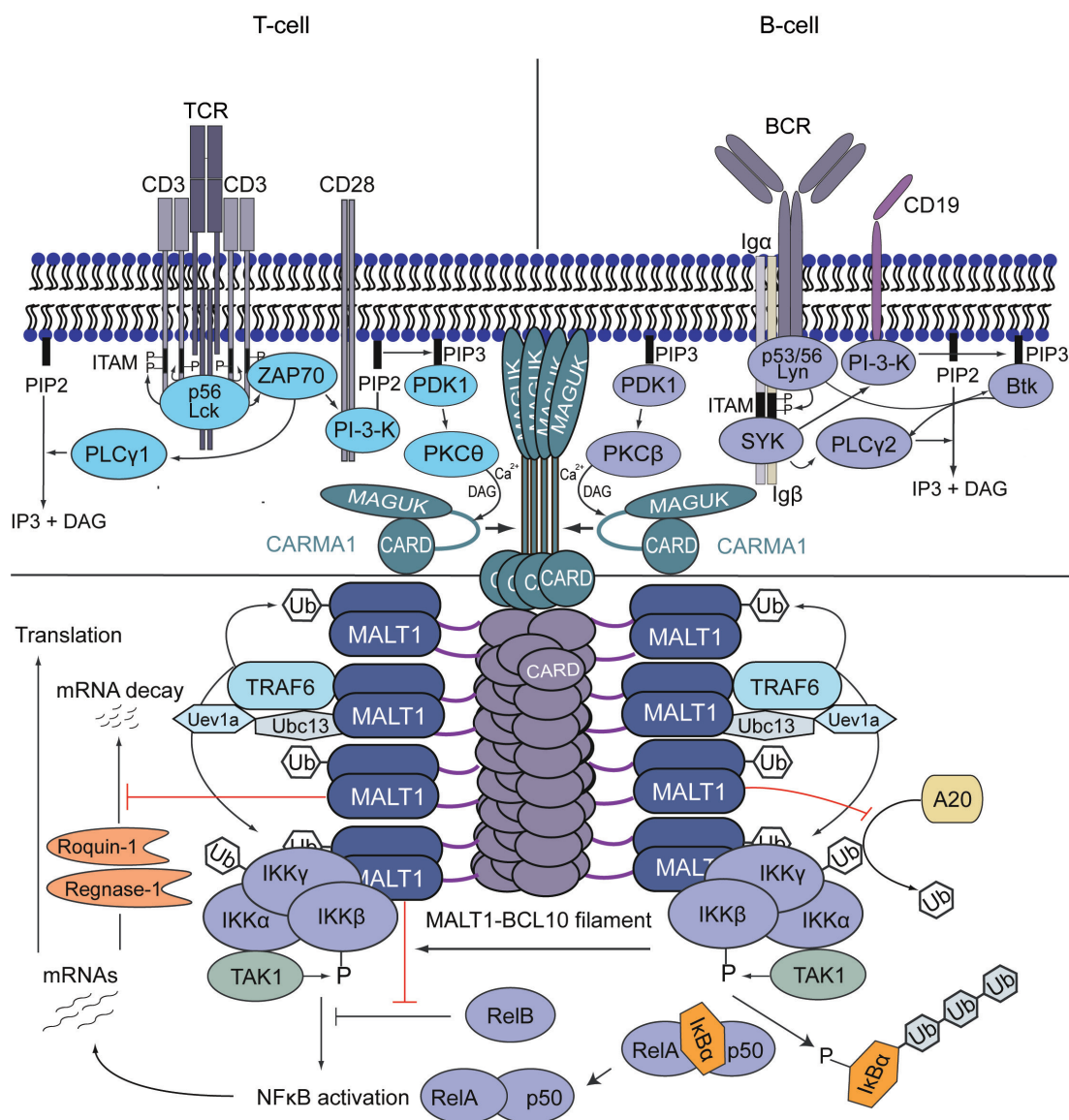

Figure 2-8: Model of CBM-complex in NF-κB signaling.

A similar mechanism is employed by B-cells, where antigen stimulation induces PTK p53/56Lyn to phosphorylate ITAMs in α-β chain dimers of the BCR (Pleiman, 1994). This leads to recruitment and activation of SYK, subsequent CD19 assisted PI-3-K activation and phospholipase-C-gamma-2 (PLCγ2) phosphorylation (Fig. 2-8). Activation of PLCγ2 is promoted by PIP3 mediated Bruton's tyrosine kinase (Btk) activation and results in the generation of IP3 and DAG (Saouaf, 1994; Salim, 1996; Suzuki, 2003). Formation of PIP3 is essential for phosphoinositide-dependent kinase-1 (PDK1) recruitment and initiates PKCβ dependent phosphorylation of CARMA1 (Lee, 2005; Sommer, 2005).

Phosphorylation of CARMA1 induces a conformational change that favors the CARD-CARD domain interaction with BCL-10 to mediate directional BCL-10 polymerization (Qiao, 2013). Finally, constitutive association between MALT1 and BCL-10 results in CBM-complex formation (Matsumoto, 2005; Su, 2005; Shinohara, 2007) and interactions of CARMA1 with MALT1 further stabilize the CBM-complex (Che, 2004). The following IKK complex recruitment to the CBM-complex depends on K63-ubiquitination by TRAF6, ubiquitin conjugating enzyme (Ubc13) and Uev1a. The regulatory IKKɣ subunit binds via the UBDN domain to the CBM-complex (Sun, 2004; Zhou, 2004; Wagner, 2008). Additional K63-ubiquitination of IKKɣ by TRAF6 stimulates recruitment to the plasma membrane, where the IKK complex activation is mediated by TAK1 dependent phosphorylation of IKKβ (Sun, 2004). The inhibitory IκBα protein is marked for proteasomal degradation by IKKβ dependent phosphorylation and subsequent K48-polyubiquitination by the E3 ubiquitin ligase SCFIκB. The NLS of NF-κB transcription factors is now accessible for import factor facilitated nuclear translocation.

2.8 Role of MALT1 in B-cell lymphoma

Lymphoma derived from marginal zone B-cells are MALT lymphoma among others. MALT lymphoma are non-Hodgkin lymphoma occurring in the stomach, lung, bowel and salivary gland. MALT lymphoma can arise from gastric inflammation caused by chronic *Helicobacter pylori* infection or autoimmune diseases related effects, frequently observed in patients with Sjogren's syndrome (Isaacson, 2004; Streubel, 2004). Chromosomal translocations of the MALT1, BCL-10 and BIRC3 genes have been identified in patients with MALT lymphoma. In 15-40% of those patients, API2-MALT1 fusion is caused by the chromosomal translocation t(11;18)(q21;q21) (Akagi, 1999). In about 20% of the patients, the chromosomal translocation t(1;14)(q32;q21) translocates the MALT1 gene under control of the Ig-heavy-chain enhancer and results in MALT1 overexpression (Zhang, 1999; Streubel, 2003). Similarly enhanced overexpression of BCL-10 was identified in 5% of the patients, caused by the chromosomal translocation t(1;14)(p22;q32).

Moreover, MALT1 dependent lymphoma can derive from highly proliferative germinal center compartments, where B-cells mature to high affinity antibody producing plasma cells. Normal germinal center B-cells can develop germinal center B-cell like (GCB) diffuse large B-cell lymphoma (DLBCL) and post-germinal center B-cells can give rise to activated B-cell like (ABC)-DLBCL (Lenz, 2008b). Several mutations of CARMA1 have been identified in ABC-DLBCL. These mutations favor the active like conformation and result in antigen independent CBM-complex formation, enhanced MALT1 proteolytic activity and constitutive NF-κB signaling (Lenz, 2008a; Ferch, 2009; Hailfinger, 2009). Mutations of tyrosine residues located in ITAMs of CD79A (Igα) and CD79B (Igβ) have been identified in ABC-DLBCL patients. These mutations result in increased BCR expression and inhibit the Lyn kinase activity (Davis, 2010). Generally, the Lyn kinase has been shown to play an important role in balancing signal transduction and prohibits hyperresponsiveness (Xu, 2005). Depending on the stimulus and the B-cell activation state, Lyn kinase either inhibits or promotes NF-κB signaling. Signal transduction is achieved by ITAM phosphorylation of Igα and Igβ, mediating SYK binding and CD19 phosphorylation supported PI-3-K binding (Xu, 2005). The negative regulatory role of Lyn results from ITAM phosphorylation of FcγRIIB or CD22. It is worth noting, that mutations in CD79B are responsible for chronic BCR-signaling, promoting CBM-complex formation and proteolytic activity of MALT1 (Davis, 2010).

2.9 Role of MALT1 in autoimmunity

Autoimmune diseases are characterized by a defect self-tolerance balance, responsible for the development of chronic inflammation and tissue damage. NF-κB signaling regulates immune cell development, proliferation, survival and lymphocyte activation. Dysregulation of NF-κB signaling is likely to be implicated in various autoimmune diseases. In particular, MALT1 has been shown to be involved in rheumatoid arthritis (RA) (Wang, 2014) and multiple sclerosis (MS) (Brüstle, 2012).

Rheumatoid arthritis causes chronic inflammation in joint tissues of feet, knees and hands, primarily driven by pro-inflammatory cytokines like IL-1, TNF-α and IL-6. The expression of these cytokines depend on NF-κB signaling in activated T-cells and macrophages to stimulate the immune response (Campbell, 2000). The function of MALT1 in RA was proposed by identification of A20 as negative regulator for pro-inflammatory cytokine expression and T-cell activation (Elsby, 2010). A further study identified lower expression levels of A20 and MALT1 in RA patients and proposed MALT1 to cause dysregulation of T-cell differentiation in RA, similar to multiple sclerosis (MS) (Wang, 2014).

Multiple sclerosis is caused by an aberrant immune response, leading to tissue damage and demyelination of the central nervous system (CNS). The experimental autoimmune encephalomyelitis (EAE) is a murine MS model, usually induced by myelin oligodendrocyte glycoprotein (MOG) peptide and pertussis toxin (PT), resulting in auto-reactive T-cells, infiltrating the CNS similar to MS. Especially, Th1 cells and Th17 cells are proposed to play a major role in EAE induction (Jager, 2009). In inflammatory CNS lesions stimulates IL-12 Th1 cells to activate macrophages by IFN-γ secretion (Merrill, 1992). Th1 differentiation and IFN-ɣ expression depends on the NF-κB transcription factors c-Rel and RelB (Kontgen, 1995; Corn, 2005). Conversely, further studies revealed that IFN-γ deficient mice are more susceptible to EAE and not resistant as expected (Ferber, 1996). Another study identified Th17 cells expanded with IL-23 to be responsible for EAE induction (Langrish, 2005). Th17 differentiation depends on TGF-β, IL-6, IL-21 and IL-23 secretion by APCs (Langrish, 2005; Park, 2005; Mangan, 2006; Veldhoen, 2006). Of particular importance is that only IL-23 driven GM-CSF secretion is indispensable for EAE pathogenesis (El-Behi, 2011). GM-CSF expression is either directly mediated by c-Rel activated transcription or indirectly by c-Rel dependent Rorɣt expression (Himes, 1996; Codarri, 2011). In addition, c-Rel mediated Foxp3 expression is involved in T_{reg} differentiation (Zhang, 1999). Interestingly, RelA and RelB are essential for ɣδ-T-cells development to restrain T_{reg} responses during EAE by an IL-23 dependent mechanism (Petermann, 2010; Powolny-Budnicka, 2011).

The role of MALT1 in EAE was initially analyzed by MALT1 deficient mice (Brüstle, 2012; Mc Guire, 2013). These mice were resistance against EAE induction, similar to previously described NF-κB1 (p50), c-Rel and IKKβ deficient mice (Hilliard, 1999; Hilliard, 2002; Greve, 2007). The resistance of MALT1 deficient mice is proposed to origin from an impaired auto-reactive T-cell immune response. MALT1 deficiency abolishes lymphocyte and macrophage infiltration into the spinal cord and results in no detectable pro-inflammatory cytokine expression, thus preventing demyelination and axonal damage (Mc Guire, 2013). MALT1 deficient mice harbor a reduced amount of Th17 cells with normal expression levels of c-Rel and Rorγt, but show significantly high levels of RelB, primarily located in the nucleus. In addition, decreased expression levels of the Th17 effector cytokines IL-17 and GM-CSF were identified (Brüstle, 2012). In contrast to the effects on Th17 cells, Th1 differentiation and their ability for IFN-γ and GM-CSF expression is not impaired in MALT1 deficient mice. Furthermore, MALT1 deficiency has no effect on IL-4 secretion of Th2 cells or FoxP3 expression in T_{reg} cells (Brüstle, 2012). Of importance is that Th17 cells show generally higher MALT1 expression levels compared to Th1 or T_{reg} cells. In addition, Th cells isolated from spinal cord or brain express IFN-γ and IL-17A in contrast to Th cells of MALT1 deficient mice, expressing either IFN-γ or IL-17A (Brüstle, 2012).

Further analysis towards the role of MALT1 proteolytic activity was performed by using the inhibitor carbobenzoxycarbonyl-val-arg-pro-arg-fluoromethylketone (Z-VRPR-FMK). This peptide inhibitor binds covalently to the active site cysteine of MALT1. These experiments show a dependency of the proteolytic activity for IL-17A expression by Th17 cells, but no effect on Th1 differentiation (Brüstle, 2012). Addressing the proteolytic activity of MALT1, the NF-κB and JNK signaling inhibitory proteins A20 and CYLD are completely processed in splenic CD4$^+$ T-cells of EAE induced mice, which is mostly abolished in MALT1 deficient mice (Mc Guire, 2013). In addition, MALT1 dependent cleavage of Regnase-1 and Roquin-1 promotes Th17 differentiation (Jeltsch, 2014).

Most recently, C472A mutant knock-in mice have been characterized in context of EAE (Gewies, 2014; Jaworski, 2014). Similar to MALT1 deficient mice, MALT1-C472A mutant mice are resistant to EAE induction, represented by reduction of CD4$^+$ T-cells infiltrating the CNS and no detectable expression of IFN-γ, IL-17A and GM-CSF by CD4$^+$ T-cells (Fig. 2-9). In contrast to MALT1 deficient T-cells, increased expression of IFN-γ by Th1 cells and IL-4 by Th2 cells have been observed in MALT1 knock-in mice, resulting in lymphocyte expansion and accumulation of T-cells in lymph nodes (Jaworski, 2014). Interestingly, no effect on IL-17 expression could be identified in MALT1 C472A mice (Jaworski, 2014).

Moreover, JNK signaling is not affected in MALT1 C472A mice. In contrast, MALT1 deficient mice show partial reduced JNK activation. This indicates that the scaffolding function of MALT1 is rather responsible for JNK signaling than the proteolytic activity (Ruland, 2003; Jaworski, 2014).
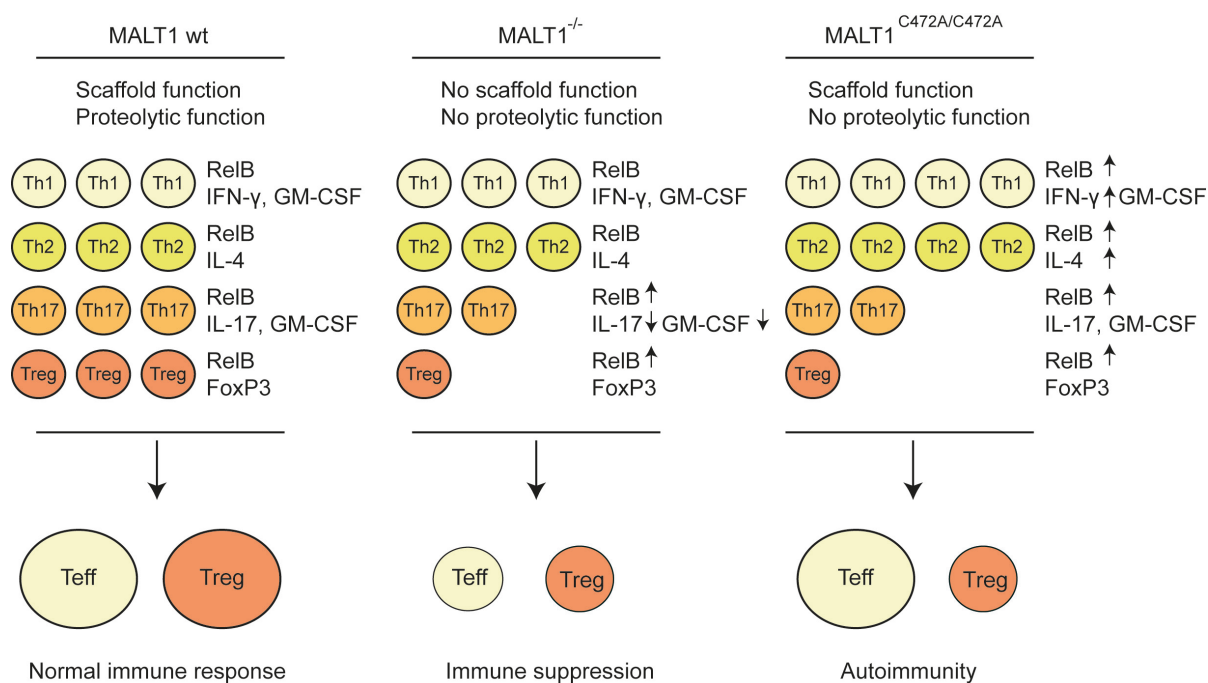

Figure: 2-9: Influence of MALT1 on the immune response (adapted from Bertossi, 2014).

MALT1 deficient and MALT1 C472A mutant mice show increased RelB levels, proposed to be responsible for inhibition of FoxP3 dependent T_{reg} cell differentiation, since significantly reduced T_{reg} cell population were identified in the thymus, spleen and lymph nodes (Fig. 2-9) (Mc Guire, 2013; Jaworski, 2014). However, no altered FoxP3 mRNA levels could be detected and impaired T_{reg} cell differentiation is proposed to depend on MALT1 protease activity in a cell-intrinsic manner. MALT1 C472A mutant mice show increased serum levels of IgE and IgG1 and are prone to develop spontaneous autoimmune gastritis due to the reduced T_{reg} cell population. This is suggested to shift the balance towards autoimmunity (Jaworski, 2014). Besides effects in T-cells, MALT1 C472A mutant mice support an essential role of MALT1 proteolytic activity for DC and NK cell activation and development of B1 B-cells or MZ B-cells (Ruefli-Brasse, 2003; Ruland, 2003; Jaworski, 2014).

2.10 Inhibitors for MALT1

The proteolytic activity of MALT1 is inhibited by the inhibitor Z-VRPR-FMK. This peptide inhibitor binds covalently to the active site cysteine (C464). Initially, this inhibitor was used for the inhibition of metacaspases in plants and could be used for MALT1 inhibition due to high homology of the MALT1 active site (Vercammen, 2006). MALT1 inhibition results in reduced NF-κB activation, IL-2 expression in T-cells (Rebeaud, 2008; Düwel, 2009) and is selectively toxic for ABC-DLBCL (Ferch, 2009). Similar to caspases, tetra-peptide binding to the active site of MALT1 induces dimerization of the paracaspase domain (Wiesmann, 2012).

Afterwards, small molecules belonging to the class of phenothiazines were identified by establishment of a MALT1 specific cleavage assay, used for high throughput screening (HTS) of 18,000 compounds from the ChemBioNet collection (Lisurek, 2010; Nagel, 2012). The proteolytic activity of MALT1 was displayed by cleavage induced release of the 7-amido-4-methylcoumarin (AMC) fluorophore from the substrate Ac-LRSR-AMC, which origins from the cleavage site in BCL-10 (Rebeaud, 2008). The identified phenothiazine derivatives thioridazine, mepazine and promethazine have a historical clinical use as antipsychotic or sedative drugs, suggested to function as dopamine D2 receptor antagonists (Seeman, 1976). In particular, MALT1 inhibition by thioridazine or mepazine prevents RelB cleavage, IL-2 expression in activated T-cells and downregulates NF-κB gene transcription in ABC-DLBCL (Nagel, 2012). Moreover, MALT1 inhibition by thioridazine and mepazine reduces the growth of ABC-DLBCL due to induction of apoptosis. The toxic effect is specific for ABC-DLBCL and does not affect GCB-DLBCL, HBL1 or TM8 cells (Nagel, 2012). Impaired T-cell activation by MALT1 inhibition, already suggested an immunosuppressive potential for phenothiazines. Recently, mepazine has been shown to attenuate EAE progression without affecting T_{reg} development, previously observed in MALT1 deficient mice (Mc Guire, 2014).

In parallel, MI-2 was identified as a small molecule inhibitor for MALT1 by HTS, using the Ac-LRSR-AMC based protease cleavage assay (Fontan, 2012). Similar to phenothiazines results MALT1 inhibition by MI-2 in downregulation of NF-κB target genes, prevents nuclear localization of RelB and is selective toxic for ABC-DLBCL. In contrast to phenothiazines, MI-2 contains a reactive chloromethyl amide group and is proposed to bind covalently to the active site of MALT1 (Fontan, 2012).

2.11 Objectives

The CBM-complex is one central regulatory assembly in the NF-κB signaling cascade and defects in CARMA1, BCL-10 or MALT1 have been shown to be connected with lymphoma development and various autoimmune diseases (Akagi, 1999; Mc Guire, 2013). Especially, the proteolytic activity of MALT is involved in NF-κB signal transduction and connected to the undefined cell growth of lymphoma (Ferch, 2009; Hailfinger, 2009) or development of autoimmune diseases (Mc Guire, 2013). Inhibition of the proteolytic activity by small molecules belonging to the class of phenothiazines is selectively toxic for ABC-DLBCL lymphoma and proposed to have immunosuppressive effects (Nagel, 2012).

The focus of this thesis was to study the mechanism of MALT1 inhibition by phenothiazines. Since no crystal structure of MALT1 was known at the beginning of this thesis, x-ray crystallography was the method of choice to identify the binding site of these small molecules on MALT1. The crystal structure of MALT1 in complex with a phenothiazine will be of significant importance to understand the mechanism of MALT1 inhibition. The molecular assembly of the CBM-complex was also not known at the beginning of this thesis. Electron microscope approaches could give insights into the scaffolding within the CBM-complex and further explain effects of CBM-complex formation on the proteolytic activity of MALT1.

3 Materials and methods

3.1 Materials

Chemicals used in this work were ordered from Sigma-Aldrich (Deisenhofen, DE), Carl Roth (Karlsruhe, DE), Merck (Darmstadt, DE) and Enzo Life Sciences (Lausen, DE) or synthesized by the chemical institute of the Technische Universität München (TUM) (Munich, DE) and Kalexsyn, Inc. (Kalamazoo, US).

3.1.1 Bacterial strains

The *E.coli* XL1 blue strain was used for cloning and the *E. coli* Rosetta (DE3) strain was used for recombinant expression. In particular, the methionine auxotroph B834 (DE3) strain was used for expression of seleno-methionine (SeMet) containing protein.

Table 3-1: Bacterial strains.

E.coli strain	Genotype	Source
XL1- Blue	*recA1 endA1 gyrA96 thi-1 hsdR17 supE44 relA1* lac [F' proAB lacI^{q}ZΔM15 Tn10 (Tet^R)]	Stratagene (Heidelberg)
Rosetta (DE3)	F$^-$ *ompT hsdS$_B$* (r$_B^-$ m$_B^-$) *gal dcm* (DE3) pRARE (Cam^R)	Novagen (USA)
B834 (DE3)	F$^-$ *ompT hsdS$_B$* (r$_B^-$ m$_B^-$) *gal dcm met* (DE3) pRARE (Cam^R)	Novagen (USA)

3.1.2 cDNA

Cloning procedures were performed with the synthetic synthesized complementary deoxyribonucleic acid (cDNA) ordered from GeneArt (Thermo Fisher Scientific, DE). The DNA sequences were not modified or codon-optimized and used as template DNA.

Table 3-2: cDNA used for cloning.

Gene	Species	Plasmid	Source
BCL-10	*Homo sapiens*	pCMV6-XL	Thermo Fisher Scientific
BIRC3	*Homo sapiens*	pCMV6-XL	Thermo Fisher Scientific
MALT1 isoform 1a	*Homo sapiens*	pCMV6-XL	Thermo Fisher Scientific

3.1.3   Oligonucleotides

Oligonucleotides were ordered HPLC purified from Eurofins MWG Operon (Ebersberg, DE) or Thermo Fisher Scientific (Ulm, DE).

Table 3-3: Oligonucleotides used for cloning.

Name	Gene	Sequence	Restriction site
B3_D25f	BIRC3	TACATCATATGGACTTGTCATGTGAACTGTACC	Nde- I
B3_N119r& M1_D320f	BIRC3 MALT1	CCAAGATTATTTAATTCATCATTTGTTACTGAAGA AGGAAAAGTAGG	No
M1_D320f& B3_N119r	MALT1 BIRC3	CCTACTTTTCCTTCTTCAGTAACAAATGATGAATTA AATAATCTTGG	No
M1_T29f	MALT1	CCCTTATCAGCCATATGACCCTCAACCGCCTG	Nde- I
M1_L339f	MALT1	AAGGAGATATACATATGTTGGCGAAGGACAAG	Nde- I
M1_K128f	MALT1	AAGGAGATATACATATGAAGATTACTGTAAACCCA	Nde- I
M1_T29f_sd	MALT1	GTTTAACTTTAAGAAGGAGATATACCATGACCCTC AACCGCCTG	No
sd_M1_T29	MALT1	CCCTGGCAAGCCATGTCGACTGATAATTTTGTTTA ACTTTAAGAAGGAGA	Sal-1
M1_R719r	MALT1	GGTGGTGGTGCTCGAGTCGATGCATGTCTAA	Xho-I
M1_G722r	MALT1	GGTGCTCGAGTCCCAAACCTCGATGCATGTC	Xho-I
M1_G722r_s	MALT1	GGTGGTGGTGCTCGAGTCATCCCAAACCTCGATGC ATGTC	Stop + Xho-I
M1_E397Af	MALT1	CGTAATGCTGTGGATGCGTTTTTACTCCTTTTAG	No
M1_E397Ar	MALT1	CTAAAAGGAGTAAAAACGCATCCACAGCATTACG	No
M1_K524Ef	MALT1	TAGAAGATAAGGAAATCACTGTGTTACTGG	No
M1_K524Er	MALT1	CCAGTAACACAGTGATTTCCTTATCTTCTA	No
B10_M1f	BCL-10	CCCTGTTCAGCCATATGGAGCCCACCGCA	Nde-1
B10_E220r	BCL-10	AGTCACGATGCGGCCGCTCACTCACTAGAGTTTGC	Stop + Not

3.1.4   Plasmids

Table 3-4: Plasmids used for cloning.

Plasmid	Description	Resistance	Source
pet21a	C-terminal 6xHis Tag	Amp	Novagen
pet28a	Cleavable N-terminal 8xHis Tag	Kan	Novagen
pGEX6PII	Cleavable N-terminal GST Tag	Amp	GE Healthcare
pCMV6-XL	Cloning vector	Amp	Thermo Fisher Scientific

3.1.5   Media and antibiotics

Liquid Lysogeny Broth (LB) media and LB agar plates (1 % NaCl, 1 % bacto-tryptone, 0.5 % yeast extract and 1.5 % agar) were prepared according to standard protocols (Sambrook, 2001). For expression of SeMet protein, synthetic M9 minimal medium supplemented with glucose, vitamins and amino acids with the exception of L-methionine (Molecular Dimensions, US) was prepared. Antibiotic stock solutions of ampicillin (amp), kanamycin (kan) and chloramphenicol (cam) were prepared with a final concentration of 250 mM. These stock solutions were sterile filtered prior to use or storage at -20 °C. Antibiotic stock solutions were diluted in LB media to a final concentration of 30-50 μg/ml.

3.1.6   Inhibitors for MALT1

Table 3-5: Inhibitors for MALT1 paracaspase.

Small molecule	Stock concentration	Source
Z-VRPR-FMK	10 mM	Enzo Life Sciences
Hex-LRSR-AOMK	10 mM	TU Munich
Promethazine	50 mM	Kalexsyn, Inc
Mepazine	25 mM	Kalexsyn, Inc
(S)-mepazine	25 mM	Kalexsyn, Inc
(R)-mepazine	25 mM	Kalexsyn, Inc
Thioridazine	50 mM	Kalexsyn, Inc
(S)-thioridazine	50 mM	Kalexsyn, Inc
(R)-thioridazine	50 mM	Kalexsyn, Inc

3.1.7   Crystallization screens

Table 3-6: Commercial crystallization screens.

Name	Company
Index HTS	Hampton Research
Magic 2	MPI Martinsried
Procomplex	Qiagen
ClassicI	Jena Bioscience

3.2 Molecular biology methods

Molecular biology methods were performed according to published standard protocols (Sambrook, 2001) or indicated separately. Commercial kits and enzymes were used according to the manufacturer recommendations. Enzymes used for cloning were purchased from Fermentas (St. Leon-Rot, DE) or New England Biolabs (Frankfurt, DE).

3.2.1   Cloning

The construct design is based on homology of domain architecture and secondary structure prediction by the PSIPRED webserver (Bryson, 2005). Oligonucleotide design and analysis was performed by the GeneRunner software. Oligonucleotides contain the desired restriction site or hybridizing regions for fusion protein construct generation. DNA fragments were amplified by polymerase chain reaction (PCR) using the Phusion® Flash High-Fidelity PCR Master Mix (Finnzymes, Espoo, FI). Usually, PCR reactions were performed by a variable program (Table 3-7) in a total volume of 20 µl containing 50 ng of template DNA and 50 pmol of each DNA oligonucleotide. In particular, API2-MALT1 fusion construct generation was performed by overlap-PCR (Table 3-7). Amplified DNA fragments were purified by mi-PCR Purification Kit (Metabion, DE) and subsequently digested with restriction enzymes. DNA fragments were further analyzed by agarose gel electrophoresis and purified by mi-Gel Extraction Kit (Metabion, DE). In parallel, plasmids were digested with the corresponding restriction enzymes, dephosphorylated by FastAP (Fermentas, DE), analyzed by agarose gel-electrophoresis and finally purified by mi-Gel Extraction Kit (Metabion, DE). DNA fragments were ligated into the corresponding vector by T4 DNA Ligase (Fermentas, DE). Specific clones were selected after transformation in *E.coli* and sequenced by MWG Biotech (Ebersberg, DE).

Table 3-7: Program for PCR and overlap PCR.

Step	Temperature [°C]	Time [s]	Cycles	Cycles overlap PCR
Initial denaturation	98	120	1 x	
Denaturation	98	15		4x without oligonucleotides
Annealing	52-57	15	30 x	28x with oligonucleotides
Elongation	72	(bp/2500)x60		
Final elongation	72	180	1 x	
Stop	4	120	1 x	
Pause	12	oo	1 x	

3.2.2 Transformation in *E.coli*

Transformations for cloning procedures were performed with *E.coli* XL-1 Blue and for recombinant expression with Rosetta (DE3) (Table 3-1). Cells were made competent chemically according to the published protocol (Hanahan, 1983) and frozen in liquid nitrogen. Transformations were performed with 150 ng of plasmid from ligation reactions or 10 ng of plasmid from a sequenced clone. For transformation, cells were incubated with the plasmid for 10 min on ice and subsequently a heat-shock was performed at 42 °C followed by 2 min incubation on ice. Afterwards 800 μl of LB were added and cells grew for 1 h at 37 °C before plated on LB-agar plates containing the respective antibiotics. Finally, cells were incubated at 37 °C overnight and selected clones were used for further experiments.

3.2.3 Plasmid expression

Plasmids were expressed in *E.coli* Rosetta (DE3) cells (Table 3-1). Therefore, selected clones from LB-agar plates were grown overnight at 37 °C in 50-100 ml LB media supplemented with the respective antibiotics to a final concentration of 50 μg/ml. Afterwards, 10 ml of these pre-cultures were diluted in 3 l LB supplemented with respective antibiotics at similar concentrations. Cells were grown at 37 °C until they reached an OD_{600} of 0.4 and were subsequently cooled to 18 °C. The expression was induced at an OD_{600} of 0.8 by addition of 0.5 mM isopropyl β-D-1-thiogalactopyranoside (IPTG) and performed overnight. Cells were harvested by centrifugation, frozen in liquid nitrogen and stored at -80 °C. Expression of SeMet labeled protein was performed in the *E.coli* B834 (DE3) strain. Therefore, synthetic M9 minimal medium (Molecular Dimensions, DE) was used. Finally, 1 ml of 50 mg/ml seleno-L-methionine was added to 1 l of media.

3.3 Biochemistry methods

3.3.1   Recombinant protein purification

The purification strategy depended on the affinity-tag of the construct. Cells containing recombinant proteins with C-terminal 6xHis-tag or N-terminal 8xHis-tag were resuspended in Lysis Buffer A (Table 3-8), disrupted by sonication at 40 % duty cycle for 15 min and centrifuged at 17,000 rpm for 40 min (SLC-6000 Rotor, Sorvall, DE). The supernatant was incubated for 20 min with in Buffer A (Table 3-8) equilibrated nickel-nitrilotriacetic acid (Ni-NTA) beads (Qiagen, DE) and loaded on 15 ml columns for further washing steps with Buffer B (Table 3-8). Afterwards, the proteins were eluted with Buffer C (Table 3-8). Proteins containing a C-terminal His-tag were concentrated to 5 ml and centrifuged at 16,000 rpm for 10 min prior to size-exclusion chromatography or ion-exchange chromatography. Proteins containing a cleavable N-terminal 8xHis-tag were dialyzed against 5 l Buffer D (Table 3-8). In parallel, cleavage of the His-tag was performed overnight at 12 °C by addition of 1 unit PreScission protease per 50 μg of protein (GE Healthcare). Afterwards, the glutathione S-transferase (GST) tagged PreScission protease (GE Healthcare, DE) was removed by glutathione sepharose affinity chromatography and the flow-through was incubated with pre-equilibrated Ni-NTA beads (Qiagen, DE) for 20 min at 4 °C. Ni-NTA beads were loaded on 15 ml column and the flow-through was collected and prepared similarly for size-exclusion chromatography or ion-exchange chromatography.

For purification of proteins containing a GST-tag, cells from 3 l culture were resuspended in 50 ml Buffer A1 (Table 3-8), disrupted by sonication at a duty cycle of 40 % for 15 min and centrifuged at 17,000 rpm for 1 h (SLC-6000 Rotor, Sorvall, DE). The supernatant was sterile filtered prior loading on a 5 ml glutathione sepharose column (GE Healthcare) with a flow-rate of 0.3 ml/min. Several washing steps were performed with a flow rate of 2 ml/min using Buffer B1 (Table 3-8). The protein elution was initiated by addition of Buffer C1 (Table 3-8). Afterwards, the protein solution was dialyzed against Buffer D1 (Table 3-8). In parallel, cleavage of the GST-tag was performed overnight at 12 °C by addition of 1 unit PreScission protease per 50 μg of protein (GE Healthcare, DE). The protein solution was loaded with a flow rate of 0.3 ml/min on a 5 ml glutathione sepharose column (GE Healthcare, DE). Since uncleaved protein and PreScission (GE Healthcare, DE) protease bind to the sepharose column, only the flow-through was collected and prepared for size-exclusion chromatography by centrifugation at 16,000 rpm for 10 min.

Table 3-8: Buffers for cell lysis and affinity chromatography.

Name	Composition
Buffer A	50 mM Hepes pH 7.5, 300 mM NaCl, 7 mM imidazole, 4 mM ß-mercaptoethanol
Buffer B	25 mM Hepes pH 7.5, 300 mM NaCl, 21 mM imidazole, 4 mM ß-mercaptoethanol
Buffer C	25 mM Hepes pH 7.5, 300 mM NaCl, 250 mM imidazole, 4 mM ß-mercaptoethanol
Buffer D	20 mM Tris pH 7.2, 150 mM NaCl, 2 mM ß-mercaptoethanol
Buffer A1	50 mM Hepes pH 7.5, 300 mM NaCl, 4 mM ß-mercaptoethanol
Buffer B1	25 mM Hepes pH 7.5, 300 mM NaCl, 4 mM ß-mercaptoethanol
Buffer C1	25 mM Hepes pH 7.5, 300 mM NaCl, 20 mM glutathione, 4 mM ß-mercaptoethanol
Buffer D1	20 mM Tris pH 7.2, 150 mM NaCl, 2 mM ß-mercaptoethanol

Ion-exchange chromatography was performed on an ÄKTA (BASIC) system equipped with a 5 ml HiTrap Q HP anion exchange column (GE Healthcare, DE) using Buffer E and Buffer F (Table 3-9). Peak fractions were analyzed by sodium dodecyl sulfate polyacrylamide gel electrophoresis (SDS-PAGE) and prepared for size-exclusion chromatography.

Size-exclusion chromatography was performed on an ÄKTA Purifier10 or Purifier100 system equipped with a HiLoad 26/60 Superdex 200 pg column or Superose 6 26/60 column (GE Healthcare, DE) using Buffer G (Table 3-9). The peak fractions were analyzed by SDS-PAGE and selected fractions were pooled, concentrated and frozen in liquid nitrogen.

Analytical size-exclusion chromatography was performed to determine homogeneity and oligomeric state of protein samples. Therefore, an ÄKTA micro or ÄKTA Ettan system equipped with a Superdex 200 5/150 GL or Superose 6 PC 3.2/30 (GE Healthcare, DE) and Buffer G (Table 3-9) were used. The prepared samples were centrifuged at 16,000 rpm for 10 min prior to injection and peak fractions were analyzed by SDS-PAGE.

Table 3-9: Buffers for ion-exchange chromatography and size-exclusion chromatography.

Name	Composition
Buffer E	25 mM Hepes pH 7.5, 100 mM NaCl, 4 mM ß-mercaptoethanol
Buffer F	25 mM Hepes pH 7.5, 1 M NaCl, 4 mM ß-mercaptoethanol
Buffer G	25 mM Hepes pH 7.5, 300 mM NaCl, 5 mM DTT

3.3.2   Denaturing polyacrylamide gel-electrophoresis (SDS-PAGE)

Polyacrylamide gel electrophoresis was performed according to the published protocol (Laemmli, 1970) using a vertical Mini-PROTEAN 3 system (BioRad). Mostly SDS-gels with 12 % acrylamide were used. In particular for proteins with a molecular weight below 30 kDa, SDS-gels containing 15 % acrylamide were used. Protein samples were prepared with 4x loading dye (110 mM Tris pH 6.8, 16 % glycerol, 4 % SDS, 5 % ß-mercaptoethanol, 0.6 % bromphenol blue) diluted to 1-fold final concentration. Electrophoresis was performed at 180 V in running buffer (25 mM Tris, 192 mM glycine, 0.1 % SDS). Afterwards, SDS-gels were stained in coomassie staining solution (7 % acetic acid, 50 % ethanol, 0.2 % Coomassie Brilliant Blue R-250) and destained with deionised water. The relative molecular weight of protein bands was determined by comparison with the PAGE RULER^{TM} protein ladder (Fermentas, DE).

3.3.3   Dimerization of MALT1

Dimerization of MALT1 was induced by addition of the covalent binding, substrate like peptide inhibitors carbobenzoxycarbonyl-valin-arginine-prolin-arginine-fluoromethyl ketone (Z-VRPR-FMK) (Enzo Life Sciences, US) or hexyl-leucine-arginine-serine-arginine-acyloxy-methyl ketone (hex-LRSR-AOMK) (TUM, DE). The dimerization reaction was performed by incubation with 2x excess of inhibitor at 12 °C overnight. The samples were centrifuged at 16,000 rpm for 10 min prior to size-exclusion chromatography with Buffer G (Table 3-9). The peak fractions of monomeric and dimeric MALT1 were collected, analyzed by SDS-PAGE, concentrated and used for crystallization.

3.3.4   MALT1 activity assay

The MALT1 cleavage assay was performed with 20 ng of the MALT1 construct and variable concentrations of inhibitor, compound or DMSO. Protein samples were incubated in 384-well non-binding microplates and 50 μM of the MALT1 substrate Ac-LRSR-AMC was added. After 30 min incubation at 30 °C, the fluorescence of cleaved AMC was measured over 1 h by a Synergy 2 Microplate Reader (Biotek, US). The MALT1 protease activity is represented in relative fluorescence units. Determination of inhibitory concentration (IC)$_{50}$ values includes data from at least three independent experiments and was performed in PRISM 5 (GraphPad) by Nagel D. (AG Krappmann). The Z-VRPR-FMK inhibitor was dissolved in water and the compounds were dissolved in DMSO.

3.3.5   Fluorescence quenching assay

The fluorescence spectrometer FluoroMax-P (HORIBA Jobin Yvon, DE) was used to determine fluorescence quenching of tryptophan W580 residue in the respective MALT1 construct. The measurement was performed at an extinction wavelength of 285 nm and emission wavelength of 329 nm by 2 μl titration steps of 400 μM, 800 μM, 4 mM, 8 mM thioridazine, mepazine or promethazine stock solutions in water against 0.5 μM wt or E397A mutant MALT1(L339-R719) in 1.6 ml assay buffer (5 mM Hepes pH=7.0, 300 mM NaCl) For promethazine measurements, additional stock solutions (25 mM, 50 mM) were used. The tryptophan fluorescence of monomeric and ligand free dimeric MALT1 were recorded with increasing amounts of compound. The titration was continued until saturation of quenching was observed. The collected data were processed in OriginLab and association constant (K_D) determination is based on a one binding site curve fitting method.

3.4   Structural biology methods

3.4.1   Crystallization

Initial crystallization setups were either performed manually with the Phoenix Crystallization Robot (Art Robbins, US) or by the crystallization facility of the MPI Martinsried. Typically, 350 nl of reservoir and protein solution were used for crystal setups. Crystal plates were sealed immediately and stored at 10 °C or 20 °C. The Protein solutions were centrifuged at 16,000 rpm for 20 min and the reservoir solutions were centrifuged at 3000 rpm for 2 min prior to crystallization setups. Generally, a protein concentration of 7 mg/ml was optimal for crystallization of API2-MALT1 constructs (Table 3-10).

The API2(D25-N119)-MALT1(D320-G722) construct with C-terminal His-Tag crystallized only in the substrate bound dimeric state. This construct was dimerized with the inhibitor Z-VRPR-FMK and crystals could be observed by screening all available crystal screens (Table 3-6). Initial crystals were observed in the conditions Hampton Index E11 (0.1 M Hepes pH 7.5, 0.2 M magnesium chloride hexahydrate, 22 % poly(acrylic acid sodium salt) 5,100) and Magic2 G4 (50 mM Tris pH=7.8, 0.2 NaCl, 22 % PEG 8000). These crystals were further refined by hanging-drop vapor diffusion and sitting drop vapor diffusion methods.

In addition to native protein setups, seleno-methionine containing protein of the His-Tag containing construct was used to refine the Magic2 G4 condition (50 mM Tris pH=7.2, 0.2 NaCl, 18 % PEG 8000).

Moreover, in-drop proteolysis was used to obtain high-resolution diffracting crystals. Therefore, the protease subtilisin (Sigma-Aldrich, DE) was added to the concentrated protein solution with a final concentration of 2 μg/ml and incubated at 20 °C for 30 min prior to crystallization setups. In particular, crystals obtained in the Jena Bioscience ClassicI G2 condition (0.1 M Hepes pH 7.5, 10 % PEG 8000) were used for data collection. These crystals were cryo-protected with 25 % glycerol in reservoir solution and frozen in liquid nitrogen.

Furthermore, crystals of the similar construct with cleaved N-terminal His-Tag were observed in the Hampton Index G11 condition (0.1 M Bis-Tris pH 6.5, 0.2 M magnesium chloride hexahydrate, 25 % PEG 3350) and were further refined by the hanging drop vapor diffusion method. Best crystals were yielded with a protein concentration of 7 mg/ml and the reservoir solution (0.1 M Bis-Tris pH 5.5, 50 mM magnesium chloride hexahydrate, 18 % PEG 3350). In order to improve diffraction, the decoupling of nucleation and crystal growth method was used (Saridakis, 2000). The initial step in crystallization is nuclei formation and occurs if protein solution is supersaturated. In contrast, crystal growth is an ordered process and is maintained in the metastable zone. In order to separate nucleation and crystal growth, the cover-slides of hanging-drop plates were transferred after 14 h from a 18 % PEG 3350 containing condition to a less precipitant containing condition (14 % PEG 3350). These crystals were cryo-protected with 25 % ethylenglycol or 15 % 2,3-butandiol in reservoir solution and frozen in liquid nitrogen.

Table 3-10: Crystallization conditions of API2-MALT1 constructs.

Protein	Condition	Method
Native protein (7 mg/ml), C-terminal 6xHis-tag, Z-VRPR-FMK dimerized	Index E11: 0.1 M Hepes pH 7.5, 0.2 M magnesium chloride hexahydrate, 22 % Poly(acrylic acid sodium salt) 5,100	Hanging drop vapor diffusion
Native protein (7 mg/ml), C-terminal 6xHis-tag Z-VRPR-FMK dimerized	Magic2 G4: 50 mM Tris pH=7.8, 0.2 NaCl, 22 % PEG 8000	Hanging drop vapor diffusion
SeMet protein (5 mg/ml), C-terminal 6xHis-tag, Z-VRPR-FMK dimerized	Magic2 G4: 50 mM Tris pH=7.2, 0.2 NaCl, 18 % PEG 8000	Hanging drop vapor diffusion
Native protein (7 mg/ml), C-terminal 6xHis-tag, Z-VRPR-FMK dimerized	ClassicI G2: 0.1 M Hepes pH 7.5, 10 % PEG 8000	In drop proteolysis
Native protein (7 mg/ml), No tag Z-VRPR-FMK dimerized	Index G11: 0.1 M Bis-Tris pH 5.5, 50 mM magnesium chloride hexahydrate, , 18 % PEG 3350	Decoupling of nucleation and growth

The MALT1(L339-R719) construct crystallized in the ligand-free dimeric and substrate bound dimeric state. Initial crystals were observed by using the Hampton Index crystallization screen (Table 3-6) with a protein concentration of 8 mg/ml and were further refined to optimize crystal growth (Table 3-11).

For crystallization of Z-VRPR-FMK bound to MALT1(L339-R719), the published condition (0.1 M MES pH 6.0, 0.2 M calcium acetate and 2 % benzamidine hypochlorite) (Yu, 2011) was used. These crystals were refined by the hanging drop vapor diffusion method. Best crystals were yielded by using 1 µl of protein solution at 5 mg/ml and 1 µl of reservoir (0.1 M MES pH 5.5, 0.2 M calcium acetate, 10 % benzamidine hypochlorite) at 20 °C. These crystals were cryo-protected with 20 % glycerol in reservoir solution and flash frozen in liquid nitrogen.

Crystals of hex-LRSR-AOMK in complex with MALT1(L339-R719) were produced by micro-seeding with Z-VRPR-FMK bound crystals. Micro-seeding was performed with the Seed Bead kit (Hampton Research, US) by mixing 1 µl of protein solution at 5 mg/ml with 1 µl of reservoir solution (25 mM MES pH=5.5, 75 mM calcium acetate, 10 % benzamidine hypochlorite) and addition of seed-dilutions by using the streak seeding tool (Hampton Reasearch, US). The crystal plates were stored at 20 °C. These crystals were cryo-protected with 20 % glycerol in reservoir solution and frozen in liquid nitrogen.

Crystals of ligand-free dimeric MALT1(L339-R719) were observed in the Hampton Index-H8 condition (0.1 M magnesium formate dihydrate, 15 % PEG 3350), in parallel to publication of the crystal structure (Wiesmann, 2012) and were further refined by the hanging drop vapor diffusion method. Best crystals were produced by mixing 1 µl of protein solution at 8 mg/ml with 1 µl reservoir solution (0.2 M magnesium formate, 13 % PEG 3350) at 20 °C. These crystals were cryo-protected with 15 % 2,3-butandiol in reservoir solution and frozen in liquid nitrogen.

The ligand free dimeric MALT1 crystals were soaked with 1.5 mM thioridazine in reservoir solution (0.2 M magnesium formate, 13 % PEG 3350) for 14 h to yield crystals of MALT1 in complex with thioridazine. Stock solutions of 25 mM thioridazine were freshly prepared with deionized water and further diluted in reservoir solution. These crystals were cryo-protected with 15 % 2,3-butandiol in reservoir solution and flash frozen in liquid nitrogen.

The MALT1(K128-G722) construct crystallized only in the substrate bound state. Initial crystals were observed in the A12 condition (100 mM Tris pH=8.0, 1 M NaCl) of the Hampton Index crystallization screen. These crystals were further refined by the hanging drop vapor diffusion method. Best crystals were yielded by using a protein concentration of 1 mg/ml. To improve diffraction, methods like seeding and dehydration have been tried.

Table 3-11: Crystallization conditions of MALT1 constructs.

Protein	Condition	Method
MALT1(L339-R719) Concentration:5 mg/ml Z-VRPR-FMK dimerized	0.1 M MES pH 5.5, 0.2 M calcium acetate, 10 % benzamidine hypochlorite	Hanging drop vapor diffusion
MALT1(L339-R719) Concentration:5 mg/ml Hex-LRSR-AOMK dimerized	25 mM MES pH=5.5, 75 mM calcium acetate, 10 % benzamidine hypochlorite	Hanging drop vapor diffusion
MALT1(L339-R719) Concentration:8 mg/ml Ligand free, dimeric	Index H8: 0.2 M magnesium formate, 13 % PEG 3350	Hanging drop vapor diffusion
MALT1(L339-R719) Thioridazine bound, dimeric	Index H8: 0.2 M magnesium formate, 13 % PEG 3350	Soaking of ligand free crystals
MALT1(K128-G722) Concentration:1 mg/ml Z-VRPR-FMK dimerized	Index A12: 100 mM Tris pH=8.0, 1 M NaCl	Seeding and dehydration

3.4.2   Data collection, processing and structure solution

Data collection of seleno-methionine containing API2(D25-N119)-MALT1(D320-G722) crystals was performed at the ID29 beamline (European Synchrotron Radiation Facility, Grenoble, FR) at a wavelength of 0.939270 Å, equipped with a PILATUS 6M pixel detector (DECTRIS, CH). Data were processed by XDS (Kabsch, 2010). The final structure was solved at 3.9 Å by molecular replacement (MR) using PHASER (McCoy, 2007) with the published MALT1 structure (pdb entry: 3UOA) as search model (Yu, 2011) and AutoBuster (Bricogne, 2011) for refinement.

Data of the construct with cleaved N-terminal His-Tag were collected at the X06SA beamline (Swiss Light Source (SLS), Villigen, CH) at a wavelength of 1.000010 Å, equipped with a PILATUS 6M pixel detector (DECTRIS, CH). Data were processed by XDS (Kabsch, 2010) and the final structure was solved at 3.6 Å similar to the above described structure solution.

Data collection of crystals from subtilisin digested API2(D25-N119)-MALT1(D320-G722) was performed at the X06SA beamline (SLS, Villigen, CH) at a wavelength of 1.000000 Å, equipped with a PILATUS 6M pixel detector (DECTRIS, CH). Data were processed by XDS (Kabsch, 2010) and the structure solved by MR using PHASER (McCoy, 2007) and the MALT1 structure (pdb entry: 3V4O) as search model (Wiesmann, 2012). The final structure was solved at 3.0 Å by using Phenix (Adams, 2010) for refinement.

Data collection of crystals containing MALT1(L339-R719) bound to hex-LRSR-AOMK was performed at the X06SA beamline (SLS, Villigen, CH) at a wavelength of 1.000010 Å, equipped with a PILATUS 6M pixel detector (DECTRIS, CH). Data were processed by XDS (Kabsch, 2010) and the structure solved by MR using PHASER (McCoy, 2007) and the published MALT1 structure (pdb entry: 3UOA) as search model (Yu, 2011). The final structure of MALT1(L339-R719) in complex with hex-LRSR-AOMK was solved at 2.4 Å using Phenix (Adams, 2010) for refinement and Coot (Emsley, 2004) for model building.

Table 3-12: Data collection and structure solution.

Crystal	Synchrotron	Wavelength	Diffraction	MR model
API2(D25-N119)-MALT1(D320-G722) SeMet protein (Magic2 G4)	ESRF ID29	0.939270 Å	Anisotropic,3.9 Å	3UOA
API2(D25-N119)-MALT1(D320-G722) No tag (Index G11)	SLS X06SA	1.000010 Å	Anisotropic,3.6 Å	3UOA
API2(D25-N119)-MALT1(D320-G722) In drop proteolysis (ClassicI G2)	SLS X06SA	1.000000 Å	3.0 Å	3V4O
MALT1(L339-R719) Hex-LRSR-AOMK bound	SLS X06SA	1.000010 Å	2.4 Å	3UOA
MALT1(L339-R719) Thioridazine bound	ESRF ID29	0.972390 Å	2.7 Å	3V55
MALT1(L339-R719) Thioridazine bound	ESRF ID29	1.900000 Å	2.9 Å	-

Data collection of thioridazine bound MALT1(L339-R719) crystals was performed at the ID29 beamline (European Synchrotron Radiation Facility, Grenoble, FR) at a wavelength of 0.972390 Å, equipped with a PILATUS 6M pixel detector (DECTRIS, CH). Additionally, a second data set collected of the same crystal was collected at a wavelength of 1.90 Å. Data were processed by XDS (Kabsch, 2010). The structure was solved by MR with PHASER (McCoy, 2007), using the paracaspase domain and Ig3 domain of the published ligand free MALT1 structure (pdb entry: 3V55) as separate search models (Wiesmann, 2012). The final structure of MALT1(L339-R719) bound to thioridazine was solved at 2.7 Å by iterative AutoBuster (Bricogne, 2011) refinement and model building steps in Coot (Emsley, 2004).

All figures used for this thesis were generated in PyMol (Schrödinger, 2015).

3.4.3   Negative staining and electron-microscopy

All samples were centrifuged 15 min at 16,000 rpm prior to staining with uranyl-acetate. The grids were glow-discharged by high voltage supplied for 30 s at 0.3 mbar to render the carbon support film hydrophilic. Typically, 3.5 µl of sample were added to the grid, following 45 s of incubation and washing with 5 drops of Buffer G (Table 3-9). Subsequently, samples were stained with 3.5 µl of uranyl acetate, which was removed immediately by blotting paper. Afterwards, samples were stained again with 3.5 µl uranyl acetate and incubated for 15 s. Remaining uranyl acetate was removed by blotting paper. Stained particles were visualized by the 100 kV "Morgagni" electron microscope.

4 Results

4.1 API2-MALT1 fusion protein

The chromosomal translocation t(11;18)(q21;q21) generates a fusion protein of the C-terminal region from MALT1 and the N-terminal region of API2, frequently observed in MALT lymphoma (Akagi, 1999; Lucas, 2001). Generally, expression of API2-MALT1 results in constitutive NF-κB activation and supports lymphoma development. In particular, the BIR1 domain is proposed to participate in the constitutive activation mechanism. Mutational studies showed that only the first of the three BIR domains in the API2-MALT1 fusion protein is responsible for the constitutive activation mode (Zhou, 2005). Additional TRAF2 interaction motifs within the BIR1 domain suggested a crucial role of TRAF2, but mutational studies did not approve a TRAF2 dependent mechanism (Varfolomeev, 2007). Another study reproved TRAF2 binding to be essential for the constitutive NF-κB activation (Garrison, 2009). In concert with the importance of MALT1 oligomerization mediated by BCL-10 (Zhou, 2004) and the fact that BIR domains generally tend to oligomerize (Hozak, 2000), BIR1 domain induced oligomerization is likely to support MALT1 activation (Zhou, 2005). Moreover, the C-terminal Ig3 domain is required for NF-κB activation (Zhou, 2005). Since the mechanism of API2-MALT1 activation by the BIR1 domain and function of the Ig3-domain was not known, structural studies with recombinant API2-MALT1 fusion protein were performed in this thesis. The most promising construct contains the BIR1 domain (D25-N119) from API2 fused to paracaspase-Ig3 domain part (D320-G722) of MALT1. Both regions were amplified separately by PCR using the respective cDNA as template and fused together by overlap-PCR. Subsequently, DNA fragments were digested by respective restriction enzymes and purified prior to ligation into the pet28a vector, containing a cleavable N-terminal 8xHis-Tag or into the pet21a vector, containing a C-terminal 6xHis-Tag (Fig. 4-1).
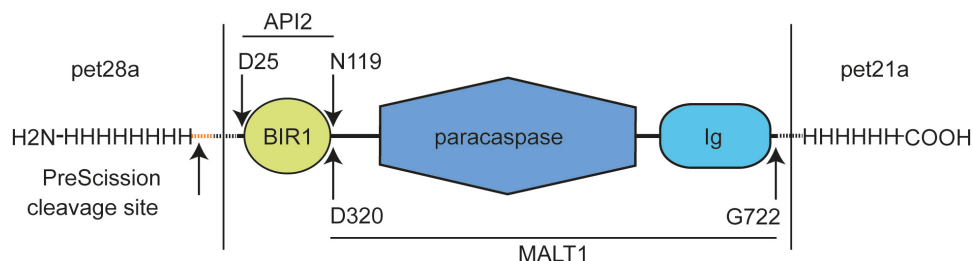
Figure: 4-1: Construct architecture of API2-MALT1.

4.1.1 Expression and purification of API2(D25-N119)-MALT1(D320-G722)

The API2-MALT1-6xHis construct has a calculated molecular weight of 57 kDa. Expression was analyzed by the SDS-samples before induction (bI) and before harvesting cells (bH), which did not show an upcoming band. Soluble API2-MALT1 protein was bound to the Ni-NTA beads and impurities (IP) were partially removed by washing steps prior to protein elution (Fig. 4-2 A). Further purification and separation of oligomeric species was performed by size-exclusion chromatography. Monomeric API2-MALT1 was eluted at 216 ml and less dimeric protein was eluted at 195 ml (Fig. 4-2 B). The Protein fractions were analyzed by SDS-PAGE (Fig. 4-2 C) and pooled according to the oligomeric state. Monomeric protein was concentrated to 12 mg/ml and dimeric protein to 7 mg/ml. The concentrated samples were analyzed by SDS-PAGE and the purity was determined to be suitable for crystallization (Fig. 4-2 C). Dimerization of monomeric protein was achieved by incubation with the peptide inhibitor Z-VRPR-FMK. Dimeric API2-MALT1 bound to Z-VRPR-FMK was separated from the monomeric species by size-exclusion chromatography (Fig. 4-2 D).
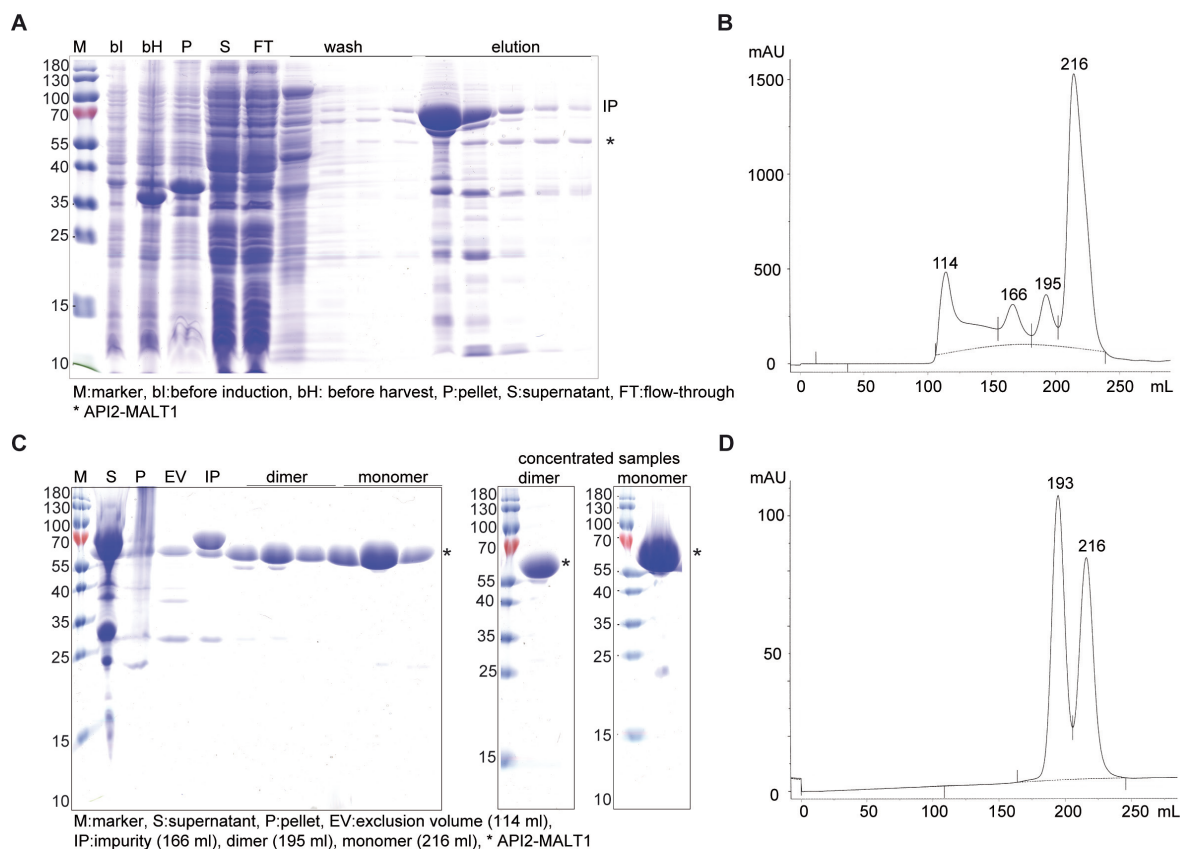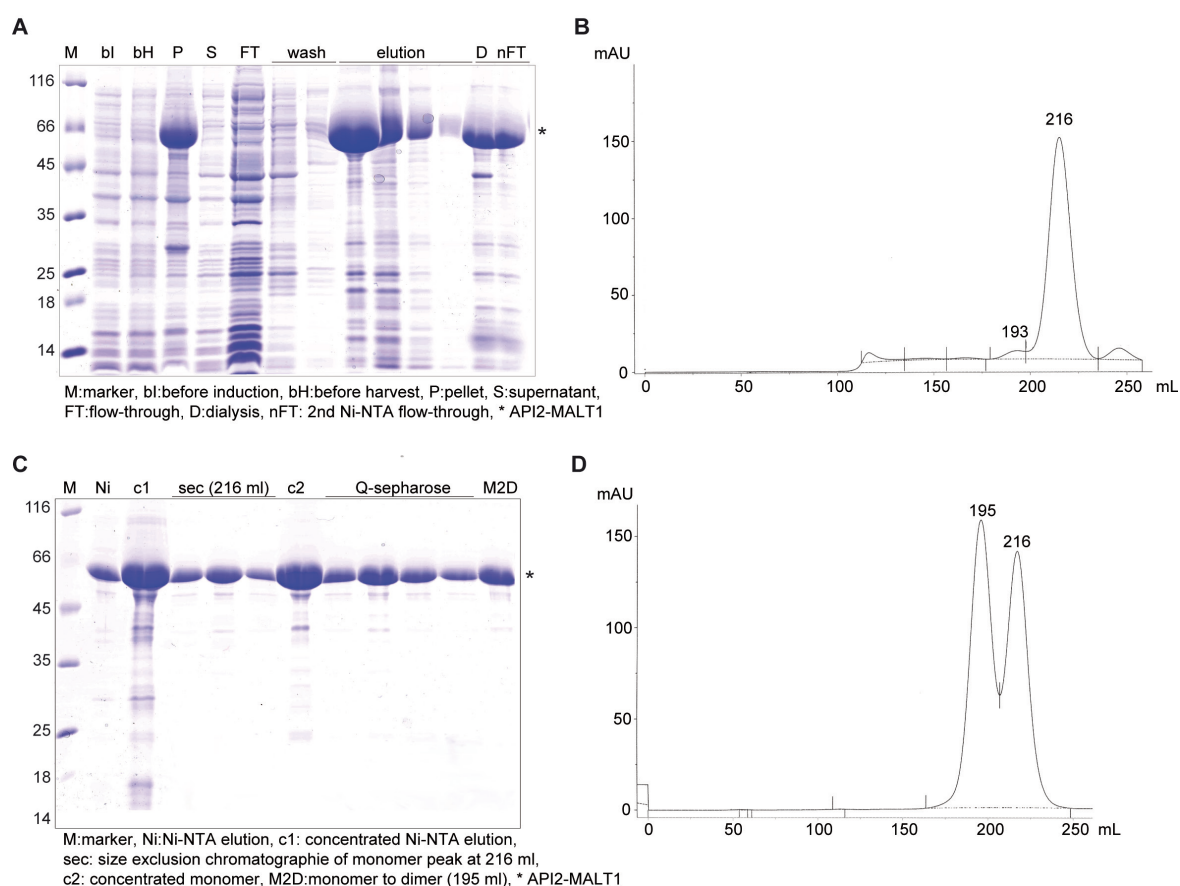

Figure: 4-2: Purification of API2-MALT1 (pet21a construct).
A) SDS-PAGE of Ni-NTA purification.
B) Size-exclusion chromatogram of purification (S200 26/60).
C) SDS-PAGE of size-exclusion chromatography fractions and of concentrated samples.
D) Size-exclusion chromatogram of Z-VRPR-FMK dimerized API2-MALT1 (S200 26/60).

Similarly, expression of the 8xHis-API2-MALT1 construct was analyzed by the SDS-samples before induction (bI) and before harvesting cells (bH), which did not indicate successful expression. The pellet (P) indicated that some protein was insoluble, but enough soluble API2-MALT1 protein was bound to Ni-NTA beads and impurities were partially removed by washing steps prior to protein elution. The N-terminal His-Tag was cleaved during dialysis (D) by PreScission protease, which was afterwards removed by glutathione-sepharose affinity chromatography. The uncleaved protein was removed by a second Ni-NTA step and the flow-through (nFT) (Fig. 4-3 A) was used for size-exclusion chromatography. Monomeric API2-MALT1 protein was eluted at 216 ml (Fig. 4-3 B) and additionally purified by ion-exchange chromatography using a Q-sepharose column. The samples were analyzed by SDS-PAGE to determine the purity (Fig. 4-3 C) and pooled accordingly. Monomeric protein was concentrated to 12 mg/ml and dimerization of API2-MALT1 was performed by incubation with the peptide inhibitor Z-VRPR-FMK. The dimeric species was separated again from the monomeric species by size-exclusion chromatography (Fig. 4-3 D).

Figure: 4-3: Purification of API2-MALT1 (pet28a construct).
  A) SDS-PAGE of Ni-NTA purification.
  B) Size-exclusion chromatogram of purification (S200 26/60).
  C) SDS-PAGE of size-exclusion chromatography fractions.
  D) Size-exclusion chromatogram of Z-VRPR-FMK dimerized API2-MALT1 (S200 26/60).

4.1.2   Crystallization of API2(D25-N119)-MALT1(D320-G722)

In order to gain knowledge about API2-MALT1 interfaces and in particular about the role of the BIR1 domain, the API2(D25-N119)-MALT1(D320-G722) construct was crystallized. Crystals of C-terminal His-Tag containing protein were obtained in the Hampton Index E11 and Magic2 G4 conditions (see 3.4.1 Crystallization). Best crystals of the refined Hampton Index E11 condition (Fig. 4-4 A) diffracted to about 8 Å, but indexing of these images failed. Native protein crystals of the Magic2 G4 condition built intergrown crystals, not suitable for data collection (Fig. 4-4 B). SeMet protein crystals produced single plate shaped crystals (Fig. 4-4 C), but diffracted highly anisotropic to about 3.9 Å. These crystals belong to the space group $I2_12_12_1$ (Table 4-1).
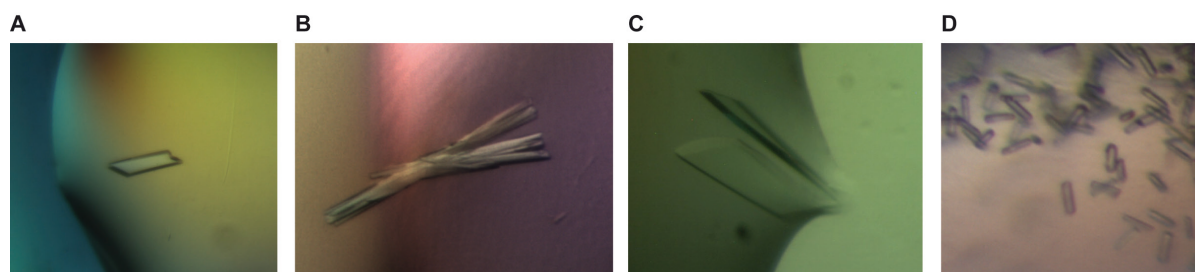
Figure: 4-4: Crystals of API2-MALT1-6xHis.
A) Crystals of native API2-MALT1 (Hampton Index E11).
B) Crystals of native API2-MALT1 (Magic2 G4).
C) Crystals of SeMet containing API2-MALT1 (Magic2 G4).
D) Crystals of subtilisin digested API2-MALT1 (Jena Biosience ClassicI G2).

Table 4-1: Data processing, Magic2 G4 condition (SeMet protein).

Data processing	
Space group	$I2_12_12_1$
Cell dimensions	
a,b,c (Å)	167.9 255.5 251.6
α, β, γ (°)	90.0 90.0 90.0
Wavelength (Å)	0.939270
Resolution (Å)	3.9
Rsym (%)	19.0 (112.7)
I / σI	4.19 (1.10)
Completeness (%)	90.5 (87.6)
Redundancy	2.2 (2.1)

* Values in parentheses are for highest-resolution shell.

Best crystals of cleaved His-Tag protein were yielded by refining the Hampton Index G11 condition and using the decoupling of nucleation and growth method (Fig. 4-5 A). Similarly, these crystals showed anisotropic diffraction to about 3.5 Å (Fig. 4-5 B) and analysis by SDS-PAGE indicated no degradation (Fig. 4-5 C).
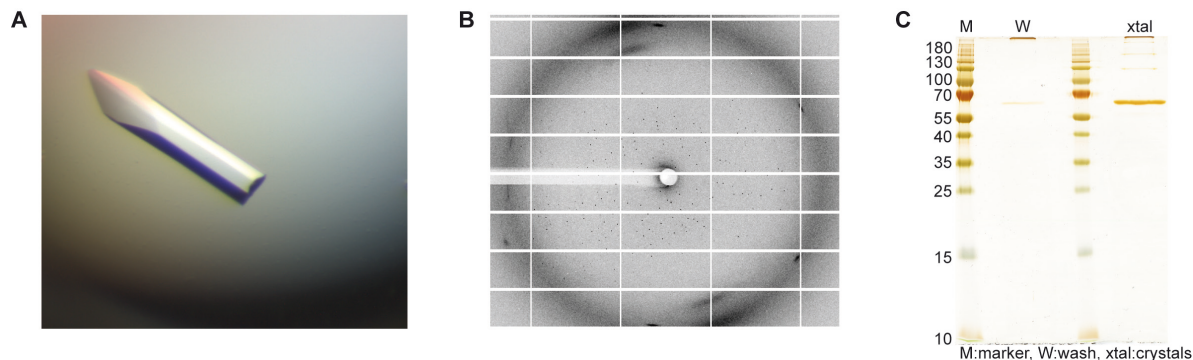
Figure: 4-5: Crystals and diffraction pattern of API2-MALT1 (pet28a construct).
   A) Crystal of native API2-MALT1 (Hampton Index G11).
   B) Diffraction image shows anisotropic pattern.
   C) SDS-PAGE of washed API2-MALT1 crystals shows no degradation.

4.1.3   Crystal structure of MALT1(L339-I564)

First high-resolution diffracting crystals were produced by the in-drop proteolysis method, using API2-MALT1-6xHis and subtilisin. Initial crystals (Fig. 4-4 D) diffracted to 3.0 Å and belong to the space group $P6_1$. Since the crystals lost diffraction power during data collection, two data sets were merged, resulting in a completeness of 81.6 % (Table 4-2).

Table 4-2: Data processing and refinement statistics for MALT1 paracaspase domain.

Data processing				Refinement	
Space group	$P6_1$			Resolution (Å)	35.92 -3.00
Cell dimensions				No. reflections	23154
a,b,c (Å)	79.1	79.1	181.2	R_{work} / R_{free}	0. 185/ 0. 246
α, β, γ (°)	90.0	90.0	120.0	**No. atoms**	
Wavelength (Å)	1.000000			Protein	3684
Resolution (Å)	3.0			**B-factor (Å²)**	
Rsym (%)	9.0 (59.8)			Protein	84.52
I / σI	5.70 (1.01)			**R.m.s deviations**	
Completeness (%)	81.6 (82.2)			Bond lengths (Å)	0. 009
Redundancy	1.1 (1.1)			Bond angles (°)	1.248

* Values in parentheses are for highest-resolution shell. $R=\dfrac{\sum||F_{obs}|-|F_{calc}||}{\sum|F_{obs}|}$ (Brünger, 1992)

This structure contains only the paracaspase domain and was solved by MR with the in parallel published paracaspase domain (pdb: 3V4O) (Wiesmann, 2012). The asymmetric unit contains two molecules of the fragment L339 to I564 (Fig. 4-6).
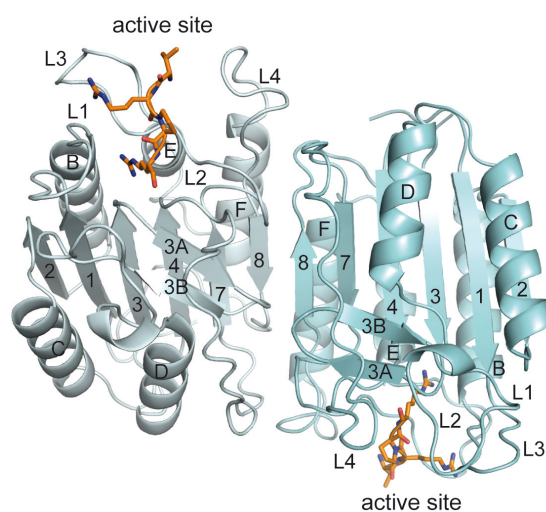
Figure: 4-6: Structure of MALT1 paracaspase domain.
One monomer is colored light cyan and the other monomer cyan. In both monomers is the substrate like inhibitor Z-VRPR-FMK covalently bound to the active site cysteine C464.

4.1.4 Crystal structure of API2(D25-N119)-MALT1(D320-G722)

Crystals of the cleaved His-Tag API2(D25-N119)-MALT1(D320-G722) protein belong to the space group $I2_12_12_1$ and diffracted anisotropic to 3.6 Å (Table 4.3). The structure was solved by MR using the published MALT1 structure (pdb: 3UOA) as search model (Yu, 2011).

Table 4-3: Data processing of crystals from Hampton Index G11 condition.

Data processing		Refinement	
Space group	$I2_12_12_1$	Resolution (Å)	49.86-3.49
Cell dimensions		No. reflections	66588
a,b,c (Å)	166.0 249.8 255.2	R_{work} / R_{free}	0.260/ 0.332
α, β, ɣ (°)	90.0 90.0 90.0	**No. atoms**	
Wavelength (Å)	1.000010	Protein	24119
Resolution (Å)	3.6	**B-factor (Å²)**	
Rsym (%)	15.8 (176.5)	Protein	136.52
I / σI	8.42 (1.19)	**R.m.s deviations**	
Completeness (%)	99.5 (97.1)	Bond lengths (Å)	0. 020
Redundancy	6.9 (6.3)	Bond angles (°)	1.703

* Values in parentheses are for highest-resolution shell. $R = \frac{\sum ||F_{obs}| - |F_{calc}||}{\sum |F_{obs}|}$ (Brünger, 1992)

Unfortunately, the BIR1 domain is not visible in the electron density, although by SDS-PAGE analyzed crystals show one band, indicating no degradation (Fig. 4-5 C). The asymmetric unit contains 8 molecules of the fragment from L339 to R719. Therefore, building of the final structure (Fig. 4-7) was not finished completely. Partially, crystal packing leads to clashes between the loops connecting β-sheet GIg3 and FIg3, resulting in minor reorganizations of the Ig3 domains.
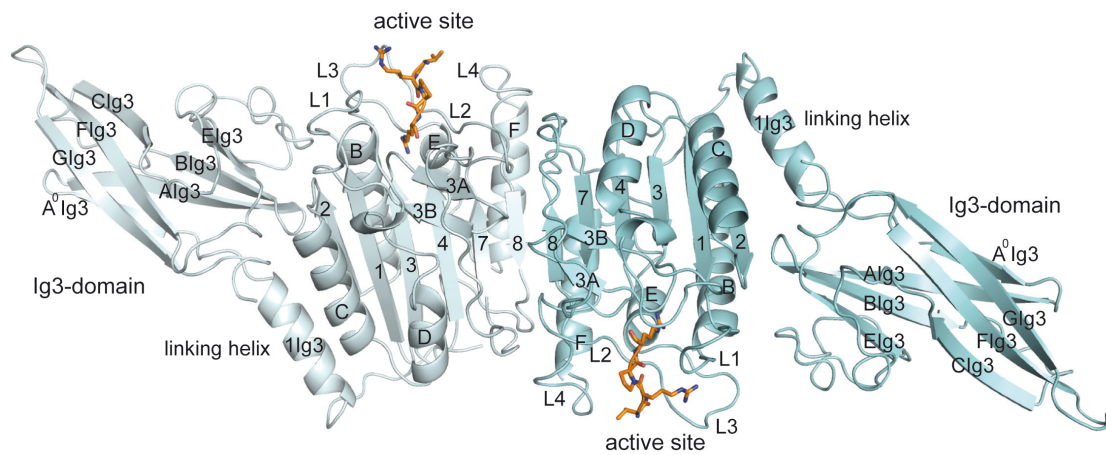
Figure: 4-7: Crystal structure of API2-MALT1.

API2-MALT1 crystal structure shows the paracaspase-Ig3 domain of MALT1 with Z-VRPR-FMK (orange) bound to the active sites. One monomer of the MALT1 dimer is colored light cyan and the other monomer cyan. Indexes for α-helices and β-sheets are according to standard caspase nomenclature.

4.2 MALT1 activation and allosteric inhibition by phenothiazines

Crystal structures for the MALT1 paracaspase domain and paracaspase-Ig3 domain were published during the thesis (Yu, 2011; Wiesmann, 2012). In parallel, our collaborators identified promising small-molecule inhibitors, belonging to the class of phenothiazines (Fig. 4-8 A) (Nagel, 2012). Since the mechanism of inhibition was not known, the focus of this thesis was to identify the binding-site of these molecules on MALT1. Moreover, binding constants for different phenothiazine derivatives could be determined by a fluorescence quenching assay. Additionally, our collaborators developed activity based probes for MALT1, based on the BCL-10 derived cleavage sequence (LRSR) (Eitelhuber, 2015). In particular, additional interactions of the P2 serine residue were of interest. Since all substrate bound crystal structures were published with the peptide inhibitor Z-VRPR-FMK, crystallographic approaches with the synthesized inhibitor hex-LRSR-AOMK and the published construct MALT1(L399-R719) (Yu, 2011; Wiesmann, 2012) (Fig. 4-8 B) were performed.
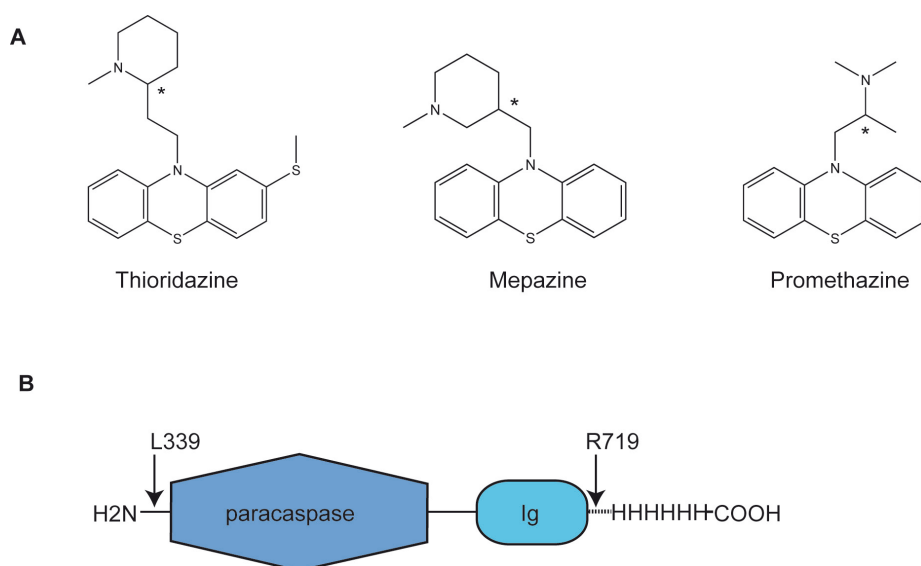
Figure: 4-8: Phenothiazine derivatives and construct architecture of MALT1(L339-R719).
  A) Chemical structures of phenothiazine derivatives.
  B) Construct design of MALT1(L339-R719).

4.2.1   Expression and purification of MALT1(L339-R719)

Expression of MALT1(L339-R719) was performed in *E.coli* Rosetta (DE3) cells. Following cell lysis, the supernatant was incubated with Ni-NTA beads. Impurities could be partially removed during washing steps prior to protein elution (Fig. 4-9 A). Separation of monomeric and dimeric species was performed by size-exclusion chromatography. Monomeric MALT1 was eluted at 232 ml and dimeric MALT1 was eluted at 208 ml (Fig. 4-9 B). The protein fractions were analyzed by SDS-PAGE (Fig. 4-9 A) and pooled accordingly. Monomeric MALT1 fractions were concentrated to 12 mg/ml and dimeric MALT1 fractions to 7 mg/ml. Dimerization of monomeric MALT1 was performed by incubation with the covalent binding peptide inhibitors Z-VRPR-FMK or hex-LRSR-AOMK. Inhibitor bound dimeric MALT1 was separated from the monomeric species by size-exclusion chromatography (Fig. 4-9 C and D).
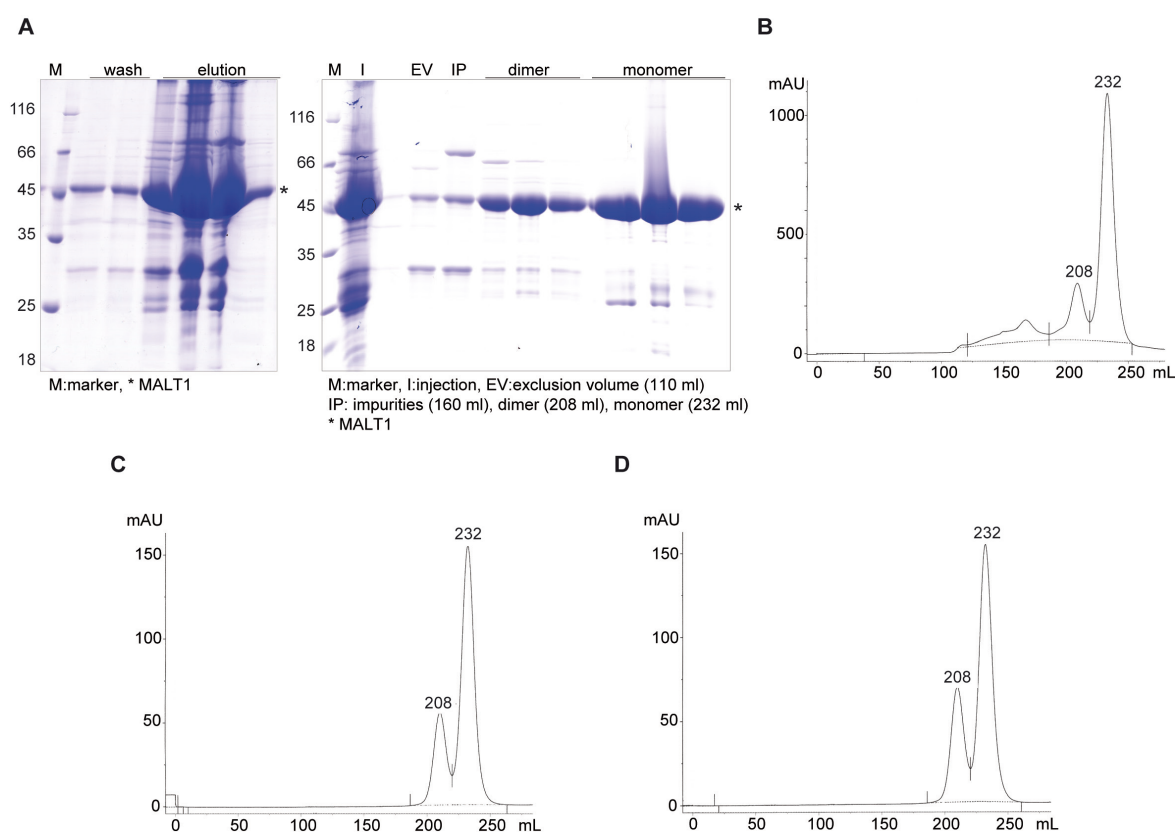
Figure: 4-9: Purification of MALT1(L339-R719).
  A) SDS-PAGE of purification and size-exclusion fractions.
  B) Size-exclusion chromatogram of purification (S200 26/60).
  C) Size-exclusion chromatogram of Z-VRPR-FMK dimerized MALT1 (S200 26/60).
  D) Size-exclusion chromatogram of hex-LRSR-AOMK dimerized MALT1 (S200 26/60).

4.2.2   Crystallization of MALT1(L339-R719)

Initially, crystallization of MALT1(L339-R719) was performed with the Z-VRPR-FMK dimerized protein, generating single crystals (Fig. 4-10 A). These crystals were further used for seeding to produce crystals of MALT1 bound to hex-LRSR-AOMK (Fig. 4-10 B). Crystals of ligand free dimeric MALT1 (Fig. 4-10 C) were soaked with thioridazine.
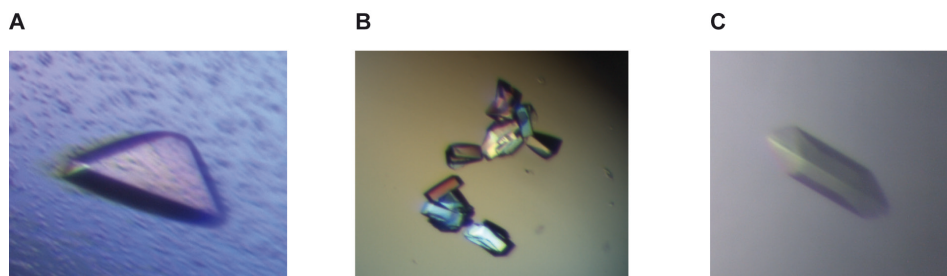
Figure: 4-10: Crystals of MALT1(L339-R719).
  A) Crystal of MALT1 bound to Z-VRPR-FMK.
  B) Crystals of MALT1 bound to hex-LRSR-AOMK.
  C) Crystal of ligand free MALT1 used for thioridazine soaks.

4.2.3   Crystal structure of MALT1(L339-R719) bound to hex-LRSR-AOMK

Crystals of MALT1 bound to hex-LRSR-AOMK (Fig. 4-10 B) diffracted to 2.4 Å and belong to the space group C_2 (Table 4-4). These crystals harbor 2 molecules per asymmetric unit. The final structure has 734 (96.45 %) residues in the preferred region of the Ramachandran Plot, 26 (3.42 %) residues are in the allowed region and 1 (0.13 %) residue is defined as outlier.

Table 4-4: Data processing of MALT1(L339-R719) bound to hex-LRSR-AOMK.

Data processing		Refinement	
Space group	C_2	Resolution (Å)	43.94-2.40
Cell dimensions		No. reflections	27345
a,b,c (Å)	178.24, 53.48, 78.74	R_{work} / R_{free}	0.198 / 0.245
α, β, ɣ (°)	90.00, 103.80, 90.00	**No. atoms**	
Wavelength (Å)	1.000010	Protein	6100
Resolution (Å)	43.94 - 2.40	**B-factors (Å²)**	
Rsym (%)	2.8 (38.1)	Protein	73.06
I / σI	15.06 (1.82)	**R.m.s deviations**	
Completeness (%)	91.1 (69.2)	Bond lengths (Å)	0.010
Redundancy	1.72 (1.37)	Bond angles (°)	1.307

* Values in parentheses are for highest-resolution shell. $R=\frac{\Sigma||F_{obs}|-|F_{calc}||}{\Sigma|F_{obs}|}$ (Brünger, 1992)

The biological relevant dimeric species was generated by symmetry operations. In both monomers is the substrate like inhibitor hex-LRSR-AOMK covalently bound to the active site cysteine C464 (Fig. 4-11 A). Electrostatic surface representation shows the positively charged S1 and S3 pocket, coordinating the P1 and P3 arginine. In contrast, the S4 pocket is mostly hydrophobic (Fig. 4-11 B). Substrate binding induced reorganization of the active site Loops (L1-L4), in particular of the L4 loop, is connected to the dimerization interface of β-sheet 8 (Fig. 4-11 C). Moreover, the L4-loop and β-sheet 8 represent a direct connection to the linking helix and Ig3 domain.
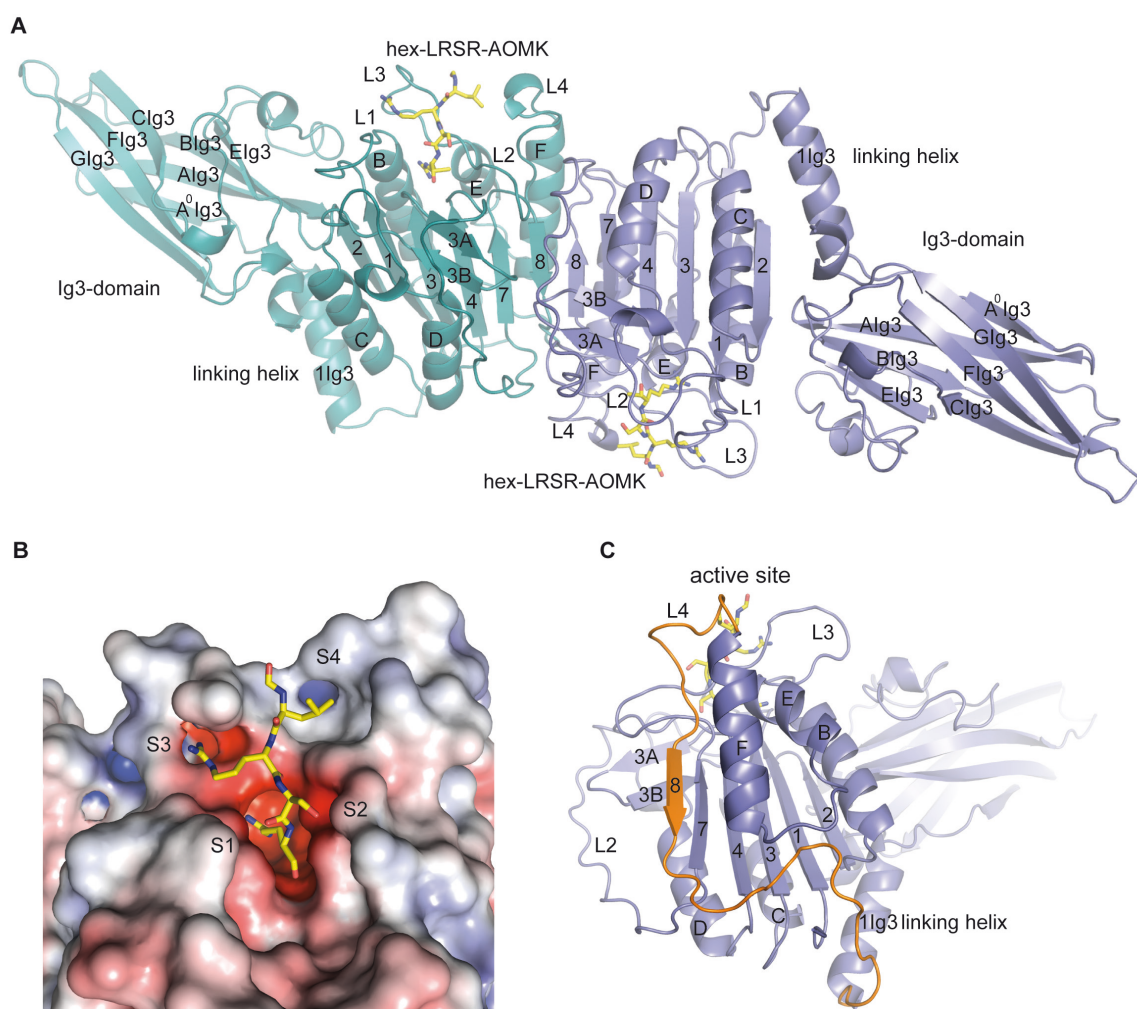
Figure: 4-11: Crystal structure of MALT1(L339-R719) bound to hex-LRSR-AOMK.

A) Overview of MALT bound to hex-LRSR-AOMK crystal structure. One monomer is colored blue and the other monomer in cyan. In both monomers is the inhibitor hex-LRSR-AOMK illustrated in yellow and covalently bound to the active site cysteine C464. Indexes for α-helices and β-sheets are according to standard caspase nomenclature.

B) Electrostatics surface representation of active site pocket (red -6 kT to blue +6 kT).

C) Connection from active site to Ig3 domain is highlighted in orange.

Besides the already published dimerization mutant R551E, which is located in β-sheet 8 and abolishes MALT1 protease activity (Wiesmann, 2012), lysine 524 (K524) is located next to α-helix F and expected to play an important role in dimerization. The crystal structure of MALT1 in complex with hex-LRSR-AOMK shows K524 to interact with aspartate (D330') and glutamate (E534') of α-helix F' from the opposing monomer (Fig. 4-12 A). Furthermore, E534 is stabilized in this position by electrostatic interactions with K557, which is located in the loop emerging from β-sheet 8 and connects the paracaspase domain with the Ig3 domain (Fig. 4-12 A). Mutation of K524 to glutamate was expected to disrupt the interaction with D530 and E534, permitting structural reorganization and dimerization. To further verify the effect of K524E mutation in solution, dimerization by incubation with the substrate like peptide inhibitor Z-VRPR-FMK was analyzed by analytical size-exclusion chromatography, showing no formation of dimeric species for K524E mutant MALT1 (Fig. 4-12 B). Thus, the stabilizing interaction of K524 is required for dimerization of MALT1.
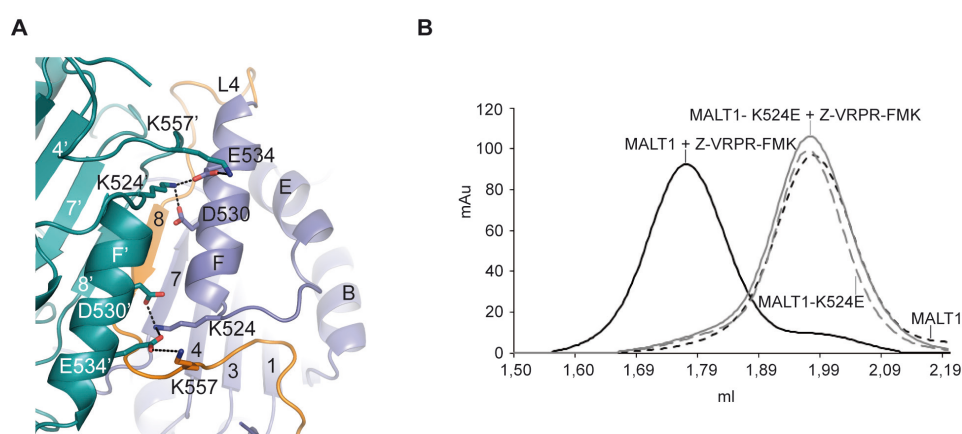
Figure: 4-12: Dimerization interface and K524E mutation of MALT1.
A) Detailed view of MALT1 dimerization interface with interacting residues as stick model. One monomer is colored blue and the other monomer cyan. The connection between the active site and Ig3 domain is highlighted in orange.
B) Overlay of analytical size-exclusion chromatograms shows no dimeric species for K524E mutant MALT1 after incubation with the covalent binding peptide inhibitor Z-VRPR-FMK.

Biochemical studies revealed by using a positional-scanning substrate combinatorial library that residues P2 and P3 are less selective with the greatest tolerance in P3, while in position P4 leucine or phenylalanine are clearly preferred residues (Hachmann, 2012). These data fit well with the observation that the LRSR bound crystal structure possess a well ordered L4 substrate binding loop and the non-polar P4 leucine fits perfectly in the hydrophobic S4 pocket composed of the residues F499, I501, I510 and L541 (Fig. 4-13 A). In contrast, the P3 arginine is mainly coordinated by electrostatic interactions with Q502 and E500. The

backbone of the peptide inhibitor shows additional interactions to E500 and A498. The P2 serine of the inhibitor does not show any additional interactions. The P1 arginine is highly coordinated by electrostatic interactions with D365 and D462. The L2 loop contains the active site cysteine C464, which forms a covalent bond to the inhibitor peptide upon reacting with the AOMK molecule. Thereby, the caspase typical active site histidine (H415) stabilizes the negatively charged tetrahedral intermediate with the δN atom. Additionally, the backbone oxygen of proline (P357) is responsible to keep H415 in place (Fig.4-13 B).
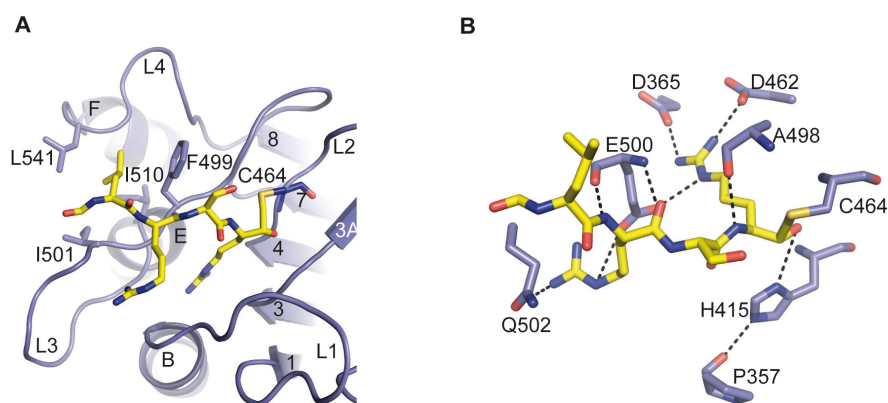
Figure: 4-13: Detailed view of active site containing hex-LRSR-AOMK.

A) Top view of the MALT1 active site with hex-LRSR-AOMK represented in standard orientation, hydrophobic S4 pocket building residues are represented as stick model.

B) Illustration of electrostatic inhibitor coordination. Interacting residues are represented as stick model and the peptide inhibitor hex-LRSR-AOMK is presented in standard orientation.

4.2.4   Crystal structure of MALT1(L339-R719) in complex with thioridazine

Diffraction of thioridazine soaked crystals (Fig. 4-10 C) depended extremely on thioridazine concentration and incubation time. Either crystals lost diffraction power or did not contain the inhibitor. In contrast to native crystals, which diffracted to about 1.9 Å, only one thioridazine containing crystal diffracted to 2.7 Å and belongs to the space group C_2 (Table 4-5). This crystal harbors one molecule per asymmetric unit. In addition to the native dataset at $\lambda = 0.972390$ Å, a second dataset at $\lambda = 1.900000$ Å was collected to visualize the anomalous sulfur signal of thioridazine (Table 4-5). The final structure has 328 (95.35 %) residues in the preferred region of the Ramachandran Plot, 15 (4.36 %) residues fall in the allowed region and 1 (0.29 %) residue is defined as outlier. The biological relevant dimeric species was generated by crystallographic operations (Fig. 4-14). Most important, the structure reveals that compounds of this tri-cyclic inhibitor class bind in a pocket located on the opposite site relative to the caspase active site, in the interface between the caspase domain and the Ig3 domain connecting α-helix Ig3 of MALT1. The active site and in particular the L2 loop are mostly unstructured, similar to the ligand free structure (Fig. 4-14) (Wiesmann, 2012)

Table 4-5: Data processing of MALT1(L339-R719) in complex with thioridazine.

Data collection			Refinement	
	native data	anomalous data		
Space group	C_2	C_2	Resolution (Å)	41.09 - 2.70
Cell dimensions			No. reflections	10386
a,b,c (Å)	94.8, 70.6, 57.5	94.9, 70.7, 57.5	R_{work} / R_{free}	0.200/ 0.249
α, β, γ (°)	90.0, 93.6, 90.0	90.0, 93.6, 90.0	**No. atoms**	
Wavelength (Å)	0.972390	1.900000	Protein	2803
Resolution (Å)	47.32 - 2.70	47.34 - 2.84	**B-factor (Å²)**	
Rsym (%)	3.8 (61.2)	5.4 (51.5)	Protein	86.51
I / σI	17.69 (1.75)	11.79 (1.80)	**R.m.s deviations**	
Completeness (%)	98.6 (97.8)	97.4 (94.7)	Bond lengths (Å)	0.013
Redundancy	3.08 (3.11)	2.83(2.74)	Bond angles (°)	1.26

* Values in parentheses are for highest-resolution shell. $R=\frac{\sum||F_{obs}|-|F_{calc}||}{\sum|F_{obs}|}$ (Brünger, 1992)
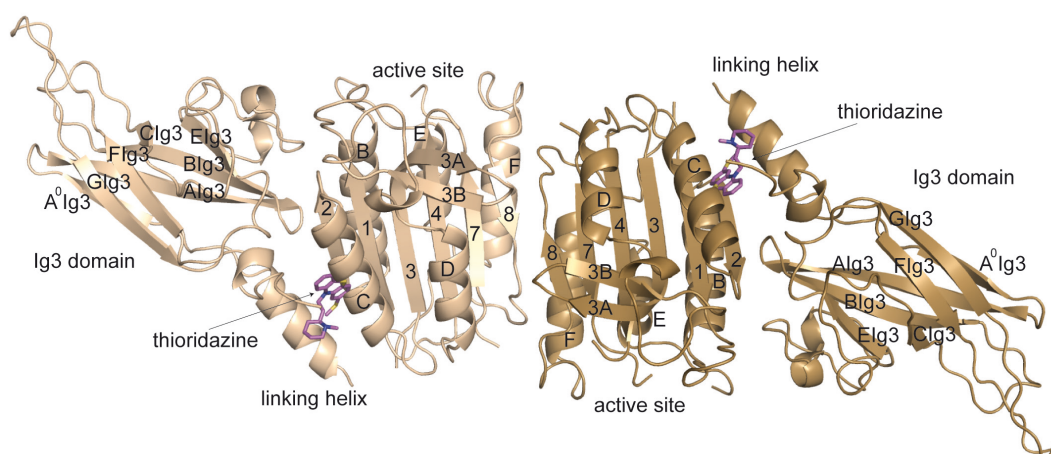
Figure: 4-14: Crystal structure of MALT1 in complex with thioridazine.
Crystal structure shows the MALT1 dimer with one monomer colored gold and the other monomer colored sand. The small molecule inhibitor thioridazine binds in the interface between the paracaspase and Ig3 domain and is represented as magenta stick model. Indexes for α-helices and β-sheets are according to standard caspase nomenclature.

The anomalous difference density map of sulfur atoms was used to determine the orientation of the 2-methylsulfanylphenothiazine ring. In detail, the tri-cyclic ring system of thioridazine is bound in a hydrophobic pocket composed of residues A394, F398, L401 in α-helix C and L346, V344 and V381 in β-sheets 1 and 2, respectively (Fig. 4-15 A). Additional to this hydrophobic pocket, residue E397 forms a prominent hydrogen bond to the nitrogen of the N-methylpiperidine group of thioridazine (Fig. 4-15 A). Moreover, a detailed inspection of the refined $2F_o$ - F_c electron density map suggests only the S-enantiomer of thioridazine to be bound in the crystal structure. Electrostatic surface representation of the binding site illustrates perfect fitting of thioridazine into the allosteric binding pocket (Fig. 4-15 B).
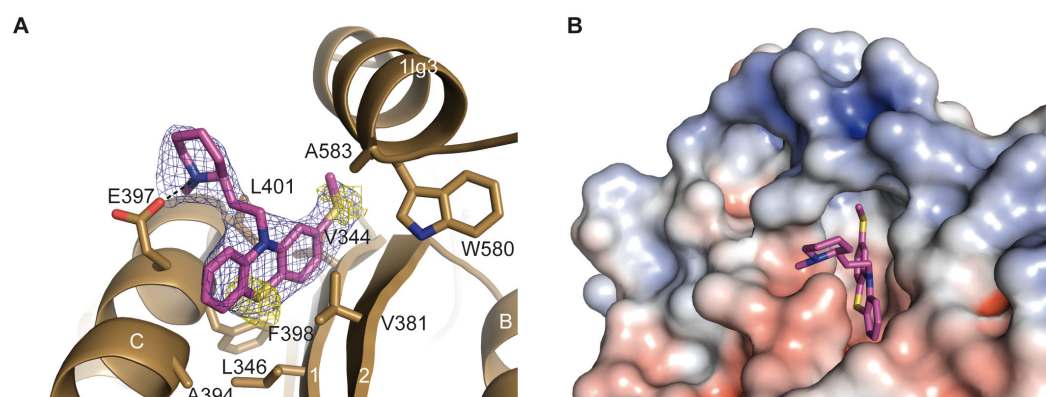
Figure: 4-15: Detailed view of thioridazine binding site.
A) A detailed view of the thioridazine binding site shows the compound as magenta stick model surrounded by the in blue illustrated refined $2F_o - F_c$ electron density map (contoured at 1 σ). The anomalous difference density map (contoured at 2,2 σ) is highlighted in yellow.
B) Surface representation of thioridazine binding pocket (red -6 kT to blue +6 kT).

4.2.5 MALT1 fluorescence quenching assay

In order to verify the mechanism of inhibition in solution and the binding site to be universal for phenothiazines, a tryptophan fluorescence quenching assay was developed. Upon binding, the side chain of residue tryptophan 580 (W580) on α-helix 1Ig3 is flipped out of the hydrophobic groove into a solvent exposed environment (Fig. 4-16 A). For this assay, advantage was taken from the fact, that W580 is the only tryptophan residue in the MALT1(L339-R719) construct and in close proximity to the tri-cyclic compound. As expected by the binding mode of thioridazine observed in the crystal structure, the intrinsic fluorescence of W580 is quenched by the presence of the compound. The high magnitude of quenching suggests that in addition to the solvent quenching effect, a process of energy transfer might occur by the close proximity of the drug to the tryptophan residue. Mutation of E397 to alanine prevents the main interaction between MALT1 and thioridazine and verifies the proposed binding mechanism.
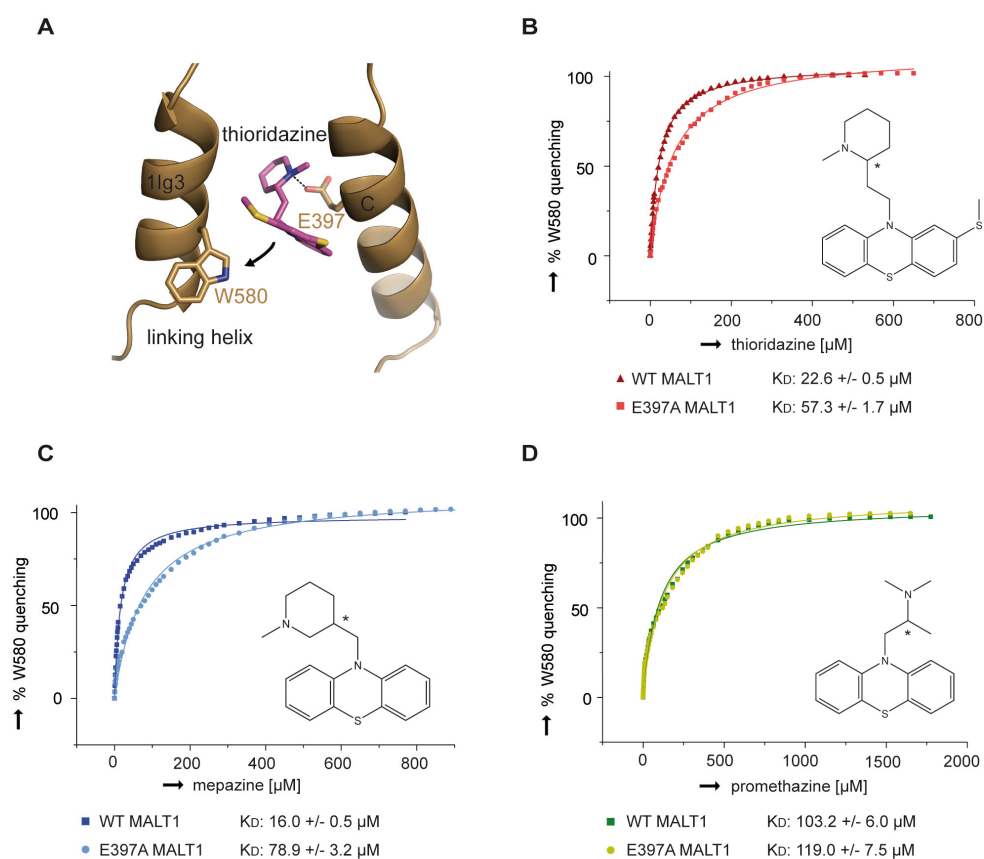
Figure: 4-16: Fluorescence quenching assay of monomeric MALT1.
  A) Tryptophan flipping mediated by thioridazine binding.
  B) Fluorescence quenching assay of monomeric MALT1 with thioridazine.
  C) Fluorescence quenching assay of monomeric MALT1 with mepazine.
  D) Fluorescence quenching assay of monomeric MALT1 with promethazine.

Indeed, the E397A mutation has significant effects on association constants of all analyzed compounds (Table 4-6). The determined association constants for thioridazine are 22.6 µM using wt MALT1 and 57.3 µM using E397A mutant MALT1 (Fig. 4-16 B). The association constants for mepazine are 16.0 µM for wt MALT1 and 78.9 µM for E397A mutant MALT1 (Fig. 4-16 C). Importantly, the fluorescence quenching assay verifies the binding site to be universal for several phenothiazine derivatives and shows mepazine to have the greatest inhibitory potential of all analyzed compounds. Mepazine has similar to thioridazine a strong dependency on the interaction between E397 and the N-methylpiperidine group. In contrast, promethazine is lacking the N-methylpiperidine group and has less inhibitory potential, represented by association constants of 103.2 µM for wt MALT1 and 119.0 µM for E397A mutant MALT1 (Fig. 4-16 D). The oligomeric state of MALT1 has no influence on the inhibitory potential, since association constants for monomeric and dimeric MALT1 are in comparable range, represented by association constants for thioridazine of 22.4 µM for monomeric MALT1 and 20.9 µM for dimeric MALT1 (Fig. 4-17 A). Similarly, comparable association constants for mepazine of 16.1 µM using monomeric MALT1 and 19.8 µM using dimeric MALT1 were determined (Fig. 4-17 C).
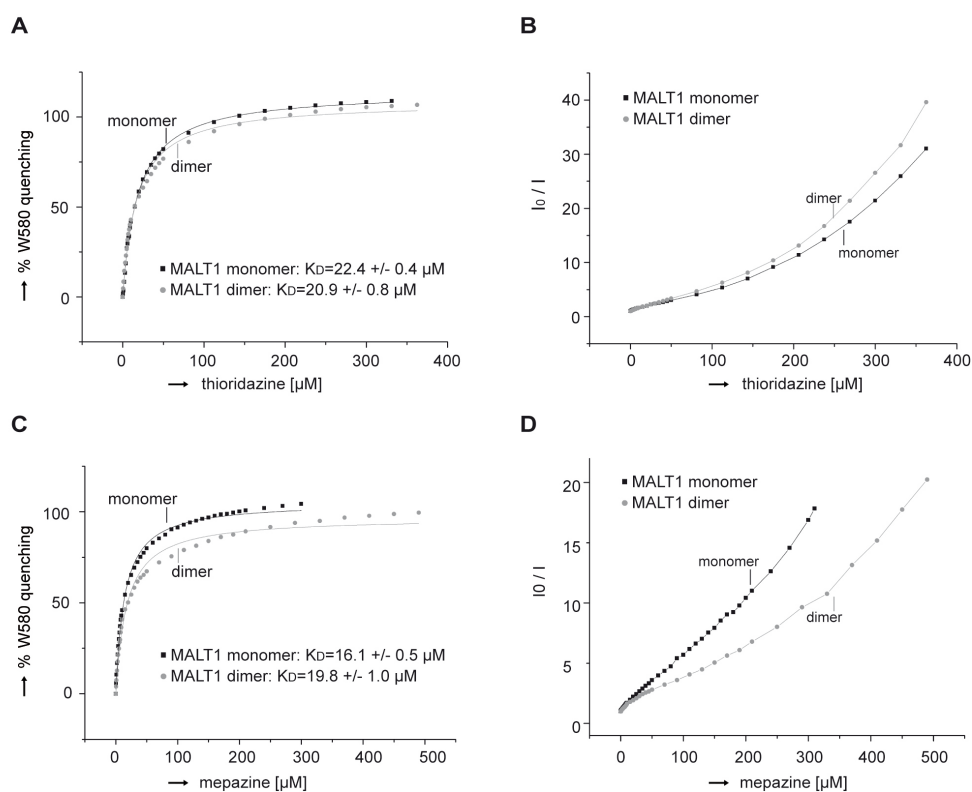
Figure: 4-17: Fluorescence quenching assay.
A) Fluorescence quenching assay of monomeric and dimeric MALT1 with thioridazine.
B) Stern-Volmer plot of monomeric and dimeric MALT1 with thioridazine.
C) Fluorescence quenching assay of monomeric and dimeric MALT1 with mepazine.
D) Stern-Volmer plot of monomeric and dimeric MALT1 with mepazine.

Table 4-6: Association constants for phenothiazine derivatives.

Small molecule	wt MALT1, K_D [µM]	E397A MALT1, K_D [µM]
Promethazine	103.2	119.0
Mepazine	16.0	78.9
(S)-mepazine	8.5	-
(R)-mepazine	29.9	-
Thioridazine	22.6	57.3
(S)-thioridazine	21.3	-
(R)-thioridazine	23.0	-

The fluorescence data were analyzed according to the Stern-Volmer law (Eftink, 1981) (Fig. 4-17 B and D), pointing to a combination of dynamic and static fluorescence quenching effects. Most importantly, the refined $2F_o - F_c$ electron density map around thioridazine suggests preferentially binding of (S)-thioridazine (Fig. 4-15 A). Regarding the inhibitory potential of thioridazine enantiomers, no significant effect could be observed by fluorescence quenching, represented by comparable association constants of 23.0 µM for (R)-thioridazine and 21.3 µM for (S)-thioridazine (Fig. 4-18 A). Surprisingly, the fluorescence quenching assay shows significant different association constants for the mepazine enantiomers. In particular, preferential binding of (S)-mepazine was observed, represented by associations constant of 8.5 µM for (S)-mepazine and 29.9 µM for (R)-mepazine (Fig. 4-18 B).
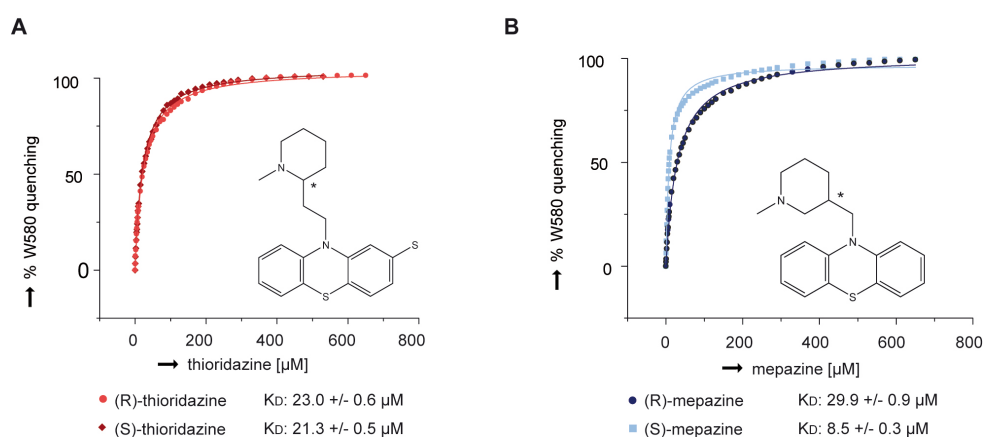
Figure: 4-18: Fluorescence quenching assay of thioridazine and mepazine enantiomers.
  A) Fluorescence quenching assay of monomeric MALT1 with thioridazine enantiomers.
  B) Fluorescence quenching assay of monomeric MALT1 with mepazine enantiomers.

4.3 Molecular assembly of MALT1 and BCL-10

In order to gain insights in the interplay between the different domains of MALT1, death domain truncated MALT1(K128-G722) (Fig. 4-19 A) was recombinant expressed and used for crystallization setups. In addition, MALT1(T29-G722) (Fig. 4-19 B) in complex with BCL-10(M1-E220) (Fig. 4-19 C) was either co-expressed or expressed by a polycistronic expression system and analyzed by EM to visualize the molecular assembly.
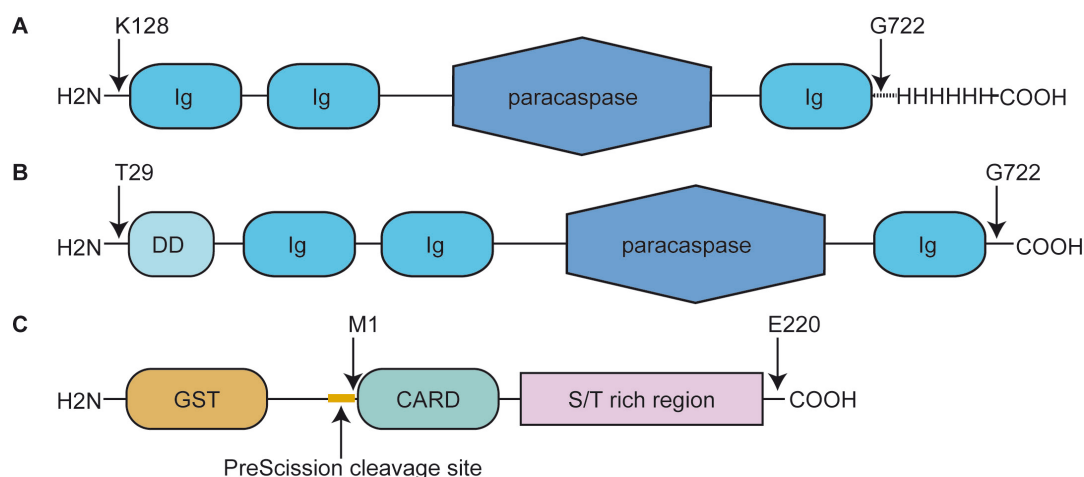
Figure: 4-19: MALT1 and BCL-10 construct architecture.
  A) Construct design of MALT1(K128-G722).
  B) Construct design of MALT1(T29-G722).
  C) Construct design of BCL-10(M1-E220).

4.3.1 Expression, purification and crystallization of MALT1(K128-G722)

The MALT1(K128-G722) construct was cloned into the pet28a vector and expression was performed in *E.coli* Rosetta (DE3) cells. Soluble recombinant protein was bound to Ni-NTA beads by its N-terminal His-Tag. Some impurities were removed during the washing step (W). The proteins were eluted and cleavage of the N-terminal His-Tag was performed during dialysis. The cleavage efficiency was visualized by the SDS-samples before dialysis (bD) and after dialysis (aD). The PreScission protease was removed by an additional affinity chromatography step using a glutathione-sepharose column (-PP). Afterwards, cleaved protein could be separated from uncleaved protein by a second Ni-NTA affinity chromatography (Fig. 4-20 A). The flow-through (nFT) was used for further purification by size-exclusion chromatography. MALT1 was eluted at 214 ml (Fig. 4-20 B), the respective protein fractions were analyzed by SDS-PAGE, showing the final purity (Fig. 4-20 C). Dimerization of MALT1 was performed by incubation with the substrate like peptide inhibitor Z-VRPR-FMK and subsequent size-exclusion chromatography. Substrate bound dimeric MALT1 was eluted

at 175 ml (Fig. 4-20 D), the respective fractions were pooled, concentrated to 4 mg/ml and used for crystallization (Fig. 4-20 E). These crystals diffracted to 20 Å, but could not be improved by refinement or different crystallization methods like seeding and dehydration.
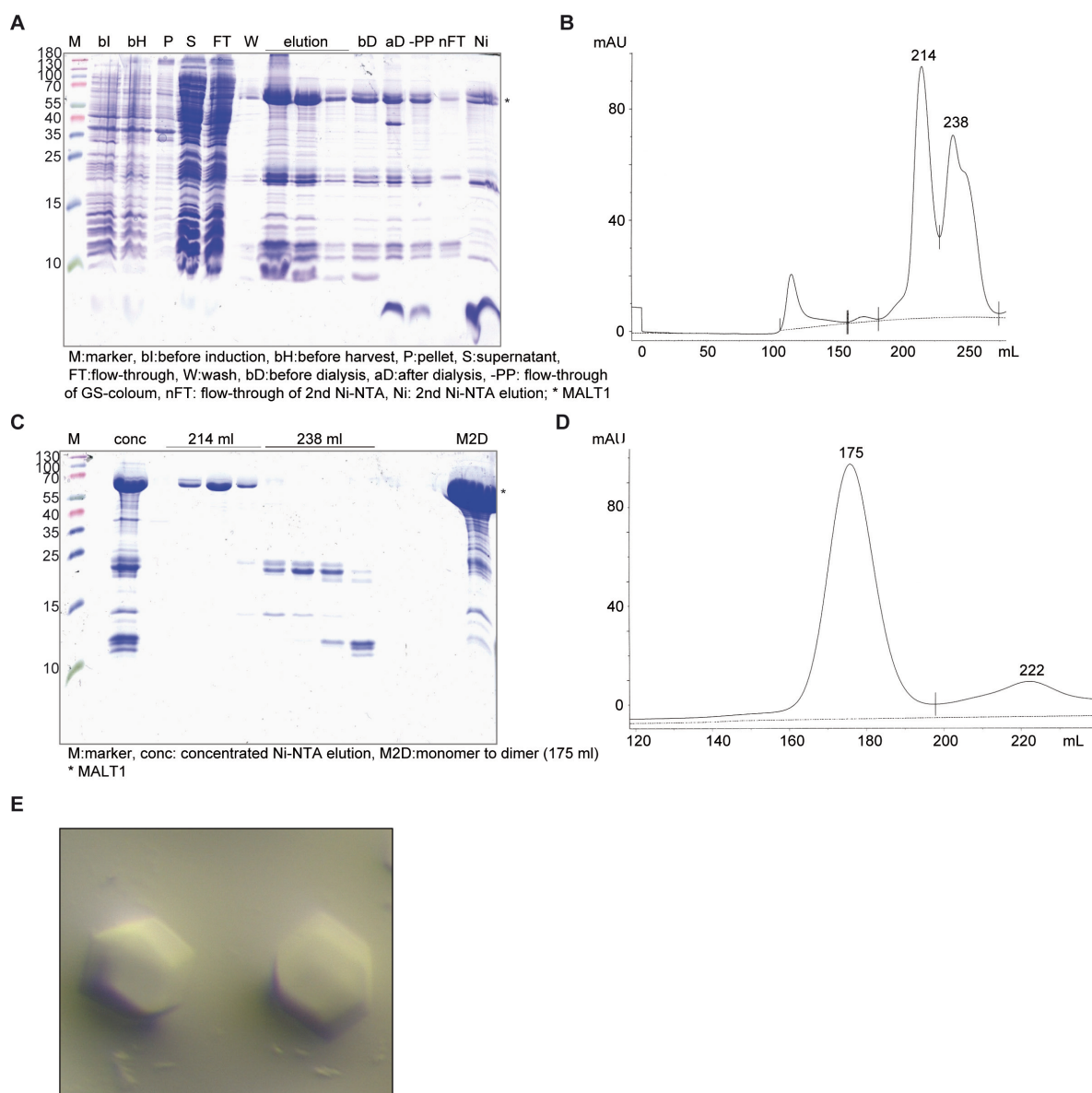

Figure: 4-20: Purification and crystallization of MALT1(K128-G722).
  A) SDS-PAGE of purification.
  B) Size-exclusion chromatogram (S200 26/60).
  C) SDS-PAGE of size-exclusion fractions.
  D) Size-exclusion chromatogram of Z-VRPR-FMK dimerized MALT1 (Superose-6 26/60).
  E) Crystals of MALT1(K128-G722).

4.3.2   Expression, purification and structural analysis of BCL-10 and MALT1

Initially, MALT1(T29-G722) was cloned into the pet28a vector and BCL-10(M1-E220) was cloned into the pGEX6PII vector. Co-expression was performed in *E.coli* Rosetta (DE3) cells. After cell lysis, the SDS-sample of the pellet (P) indicated that proteins were partially insoluble. However, soluble recombinant BCL-10 was bound to the glutathione-sepharose column and was eluted together with MALT1. Cleavage of the N-terminal GST-Tag of BCL-10 and N-terminal His-Tag of MALT1 was performed by addition of PreScission protease prior to dialysis. The cleavage efficiency was visualized by SDS-PAGE of the samples before dialysis (bD) and after dialysis (aD), showing complete cleavage of both tags (Fig. 4-21 A). The PreScission protease and cleaved GST were removed by an additional glutathione-sepharose affinity chromatography step. During concentration of the flow-through (FT2), aggregation was observed. The aggregates were separated from the supernatant by centrifugation and the supernatant was used for initial negative staining with uranyl-acetate.
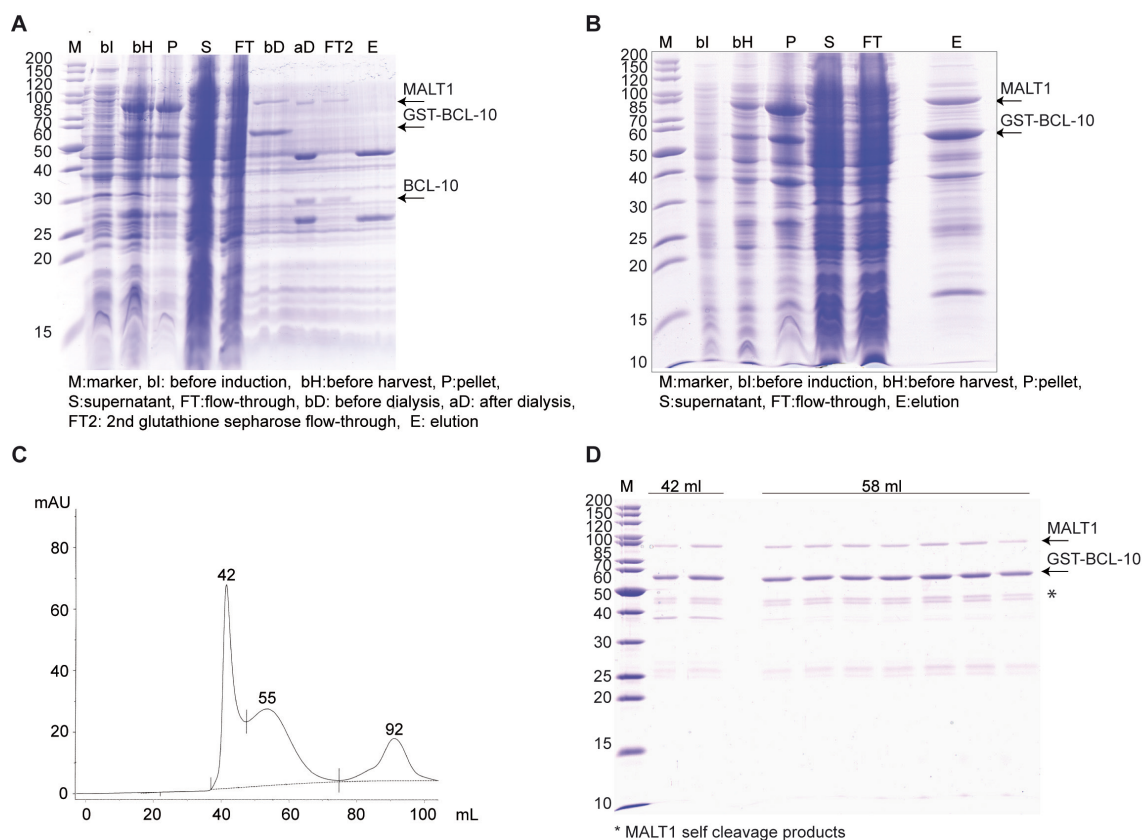
Figure: 4-21: Purification of BCL-10 and MALT1.
  A) SDS-PAGE of first GST purification.
  B) SDS-PAGE of second GST purification.
  C) Size-exclusion chromatogram of GST containing complex (Sepharose-6 26/60).
  D) SDS-PAGE of size-exclusion fractions from GST containing complex.

Surprisingly, filamentous structures with cross interactions could be observed (Fig. 4-22 A). Afterwards, similar expression and initial glutathione-sepharose affinity chromatography were performed and visualized by SDS-PAGE (Fig. 4-21 B). Since the complex of GST-BCL10 and MALT1 was partially stable, the eluted complex was further purified by size-exclusion chromatography. Aggregates of GST-BCL-10 and MALT1 were eluted at the exclusion volume of 42 ml and some soluble complex was eluted at 55 ml (Fig. 4-21 C). Size-exclusion fractions indicated auto-proteolytic processing of MALT1 (Fig. 4-21 D). The soluble complex was used for negative staining and EM analysis showed sphere shaped particles with an approximate diameter of 0.05 μm (Fig. 4-22 B).
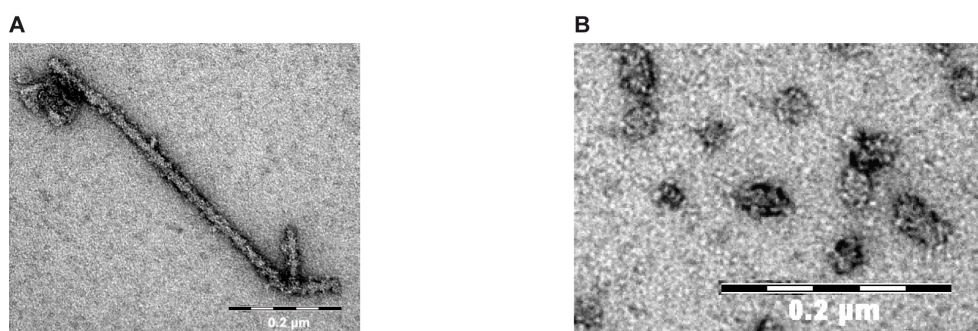
Figure: 4-22: EM analysis of BCL-10-MALT1 complex.
 A) Negative stained BCL-10-MALT1 complex shows filamentous structures (110kx).
 B) Negative stained GST-BCL-10-MALT1 complex shows sphere shaped particles (110kx).

Due to relatively low expression, MALT1(T29-G722) was cloned into the BCL-10 containing pGEX6PII vector. Polycistronic expression was achieved by addition of an N-terminal Shine-Dalgarno (SD) sequence to the MALT1 construct. The expression was analyzed by the SDS-samples before induction (bI) and before harvesting cells (bH), indicating successful expression by an upcoming band. Following cell lysis, purification was performed by glutathione-sepharose affinity chromatography. One half of the protein solution was used for GST-tag cleavage by PreScission protease. The cleavage efficiency was visualized by the SDS-samples before dialysis (bD) and after dialysis (aD). The PreScission protease and GST were completely removed by an additional glutathione-sepharose affinity step (Fig. 4-23 A). The collected flow-through (FT2) was used for size-exclusion chromatography (Fig. 4-23 B) and subsequent negative staining. The EM analysis revealed again filamentous structures with cross interactions (Fig. 4-23 C). The other half of protein solution was not cleaved by PreScission protease and directly analyzed by size-exclusion chromatography. Similar to previous results, aggregates were eluted at 42 ml and the soluble complex was eluted at 58 ml (Fig. 4-23 D). The corresponding fractions were visualized by SDS-PAGE, indicating

MALT1 self-cleavage products (Fig. 4-23 E). The soluble complex was used for negative staining and further analysis by EM showed sphere shaped particles with an approximate diameter of 0.05 µm (Fig. 4-23 F).
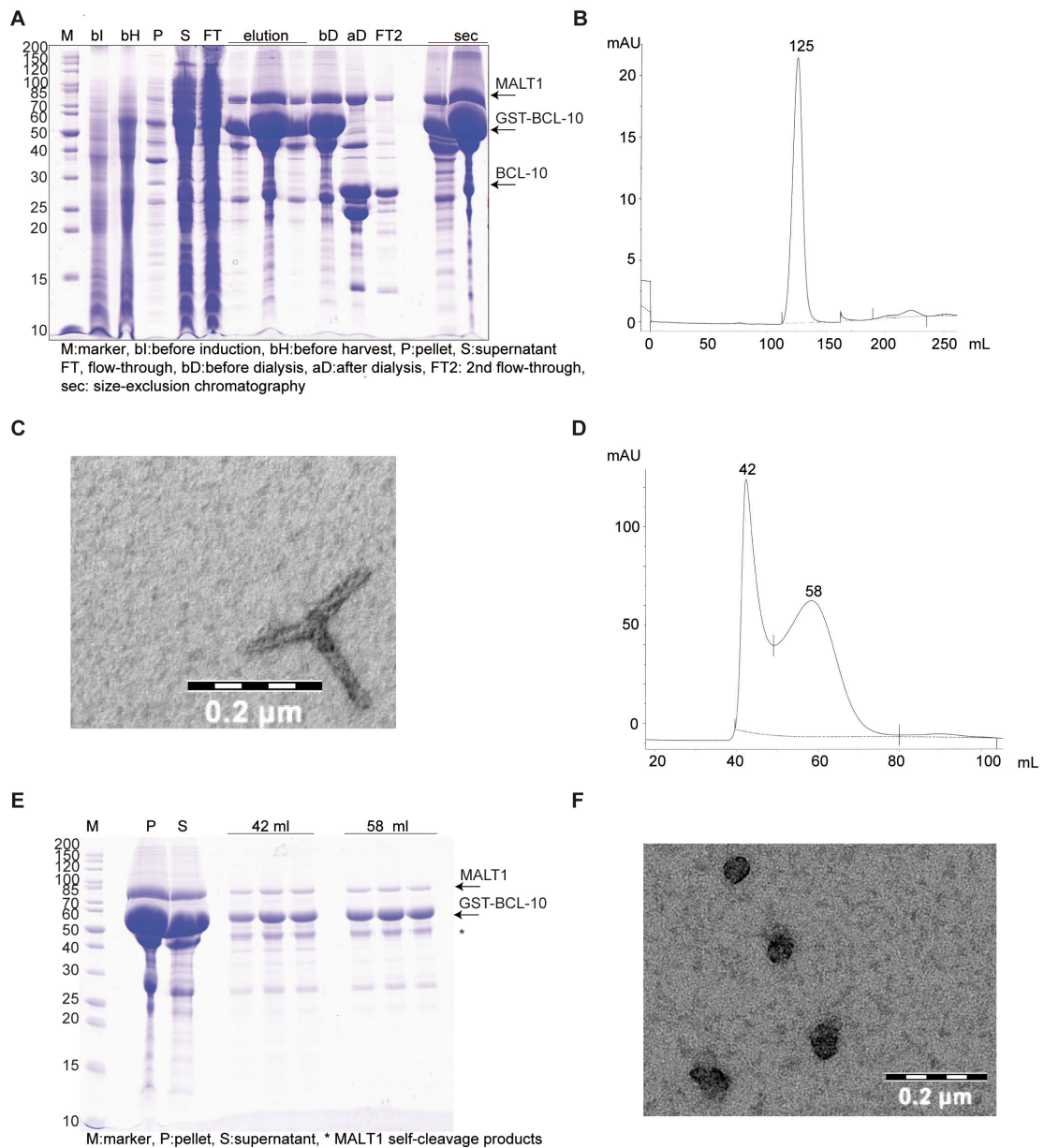

M:marker, bI:before induction, bH:before harvest, P:pellet, S:supernatant
FT, flow-through, bD:before dialysis, aD:after dialysis, FT2: 2nd flow-through,
sec: size-exclusion chromatography

M:marker, P:pellet, S:supernatant, * MALT1 self-cleavage products

Figure: 4-23: Purification and EM analysis of polycistronic expressed BCL-10-MALT1.
A) SDS-PAGE of Ni-NTA purification.
B) Size-exclusion chromatogram of GST cleaved BCL-10-MALT1 complex (S200 26/60).
C) Negative stained BCL-10-MALT1 complex shows filamentous structures (56kx).
D) Size-exclusion chromatogram of GST-BCL-10-MALT1 complex (Sepharose-6 26/60).
E) SDS-PAGE of size-exclusion fractions from GST-BCL-10-MALT1 complex.
F) Negative stained GST-BCL-10-MALT1 complex shows sphere shaped particles (110kx).

5 Discussion

The API2-MALT1 fusion protein is frequently observed in MALT lymphoma and supports lymphoma development due to constitutive NF-κB activation (Akagi, 1999; Lucas, 2001). In particular, the BIR1 domain was expected to participate in this NF-κB activation mechanism by either supporting MALT1 oligomerization (Zhou, 2005) or by providing additional TRAF6 binding sites. Regarding the oligomeric state of recombinant API2-MALT1, size-exclusion chromatography revealed similar to recombinant MALT1 mostly monomeric or by the paracaspase domain dimerized conformations, indicating no influence of the BIR1 domain on the general oligomeric state of API2-MALT1 under these conditions. The crystal structure of API2-MALT1 in complex with Z-VRPR-FMK shows no additional electron density for the BIR1 domain, expecting this domain to be flexible. Superposition of API2-MALT1 in complex with Z-VRPR-FMK and MALT1 bound to hex-LRSR-AOMK shows only minor differences (Fig. 5-1 A). Interestingly, biochemical analysis revealed that the BIR1 domain of API2-MALT1 enhances the protease activity compared to the equivalent MALT1 construct (Fig. 5-1 B). Thus, the BIR1 domain provides either a transient oligomerization interface and mediates closer proximity of the paracaspase domains or directly stimulates the protease activity by an unknown mechanism. In context of MALT1 oligomerization, CBM-complex assembly induces close proximity of the paracaspase domains by generating filamentous structures mediated by CARMA1 nuclei formation (Qiao, 2013). This mechanism was published during this thesis and is mostly in line with the by EM observed filamentous structures for the complex of BCL-10 and MALT1.
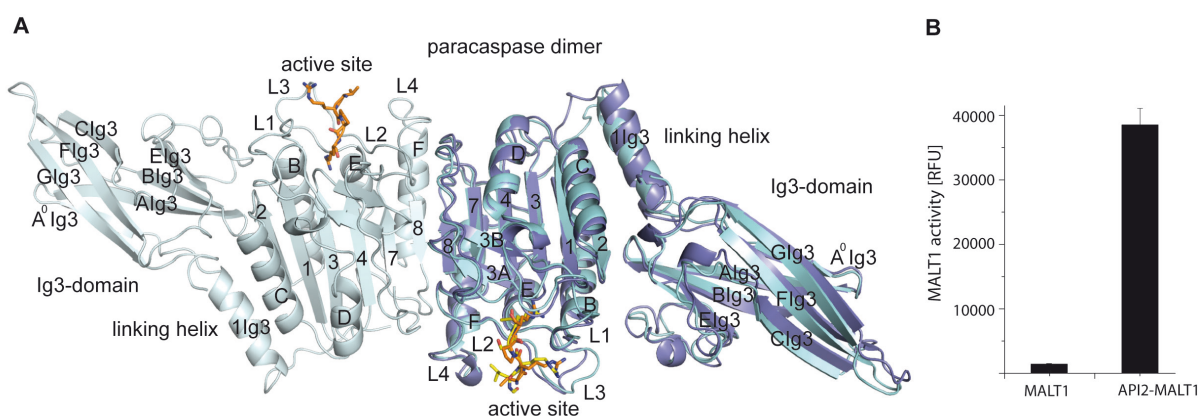
Figure: 5-1: Crystal structure and activity assay of API2-MALT1.
  A) Superposition of API2-MALT1 structure (cyan and light cyan) with Z-VRPR-FMK (orange) bound in the active site and MALT1 structure (blue) bound to hex-LRSR-AOMK (yellow).
  B) Activity assay of MALT1-6xHis and API2-MALT1-6xHis (performed by Nagel D.).

Generally, MALT1 activation is divided into two pivotal steps. Although oligomerization is needed for activity, MALT1 can adopt an auto-inhibited dimeric state where the substrate binding loops, including the active site cysteine C464 harboring L2 loop, are in an inactive conformation (Fig. 5-2 A) (Wiesmann, 2012). Hence, a second activation step needs to take place to allow the formation of an active cysteine-histidine dyad and an enzymatic functional substrate recognition groove. Substrate binding induces conformational rearrangements of the paracaspase domain into a proteolytic proficient caspase (Wiesmann, 2012).
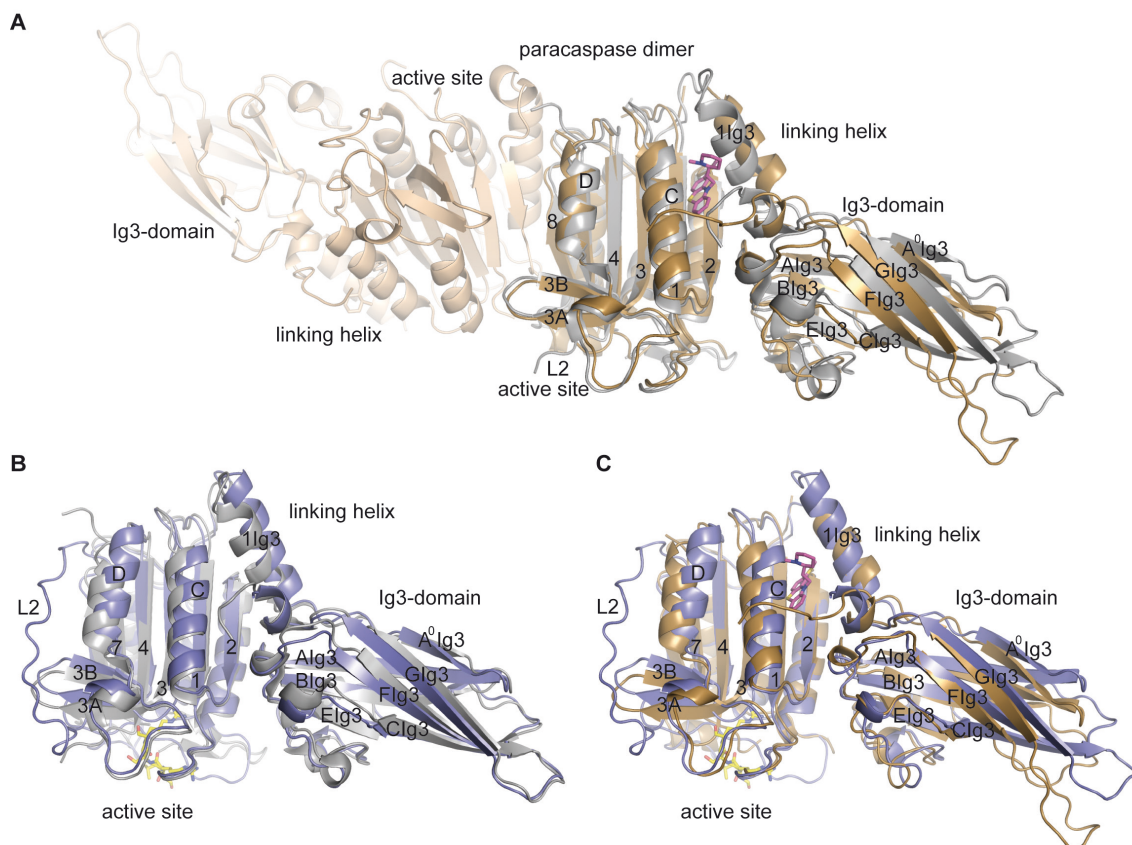
Figure: 5-2: Superposition of MALT1 crystal structures.
A) Superposition of dimeric MALT1 structure (gold) in complex with thioridazine (magenta) and ligand free MALT1 structure (grey) (Wiesmann, 2012)
B) Superposition of MALT1 structure (blue) bound to hex-LRSR-AOMK (yellow) and ligand free MALT1 structure (grey) (Wiesmann, 2012)
C) Superposition of dimeric MALT1 structure (gold) in complex with thioridazine (magenta) and MALT1 (blue) bound to hex-LRSR-AOMK (yellow)

The comparison of hex-LRSR-AOMK bound and ligand free structures illustrates the conformational changes upon substrate binding (Fig. 5-2 B). Substrate recognition mediates reorganization of the MALT1 paracaspase domain dimer interface, mainly involving β-sheet 8 and α-helix F. The active site of MALT1 is directly connected via the L4 loop to β-sheet 8. Mutation of R551 to glutamate, which is located in β-sheet 8, permits dimerization and

abolishes MALT1 protease activity (Wiesmann, 2012). In addition, K524 is located next to α-helix F and interacts with D330' and E534' of α-helix F' from the opposing monomer. Moreover, E534 is stabilized by electrostatic interactions with K557, which is located in the loop emerging from β-sheet 8 and connects the paracaspase and Ig3 domain (Fig. 5-3 A). Mutation of K524 to glutamate permits dimerization (Fig. 5-3 B) and abolishes MALT1 protease activity (Fig. 5-3 C).
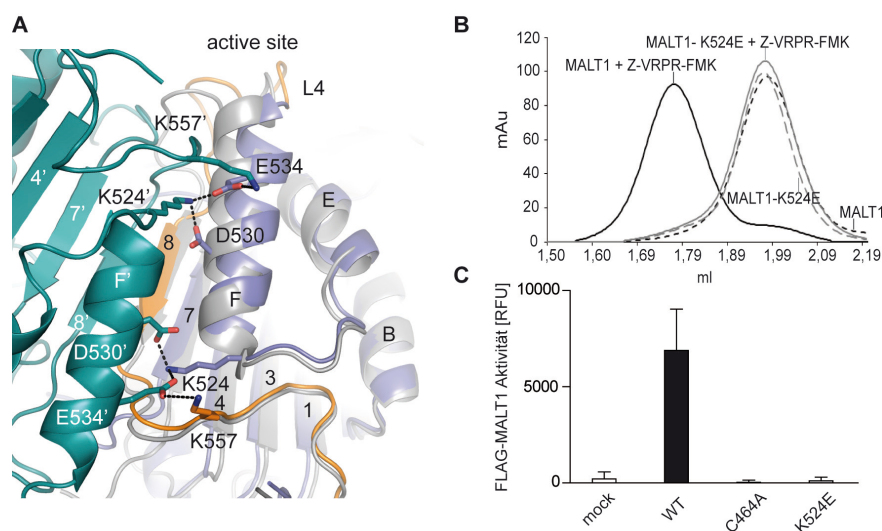

Figure: 5-3: MALT1 dimer interface presentation and analysis.

A) Close up view of MALT1 bound to hex-LRSR-AOMK dimer interface with one monomer depicted in blue and the other monomer in cyan. Structural rearrangements are shown by superposition of one monomer (blue) with ligand free dimeric MALT1 (grey) (Wiesmann, 2012). The connection between the active site and the Ig3 domain is highlighted in orange and interacting residues are illustrated as sticks.

B) Size-exclusion chromatogram of K524E mutant MALT1 after Z-VRPR-FMK incubation verifies dimer interface disruption, represented by only monomeric MALT1.

C) The MALT1 activity assay (performed by Nagel D.) confirms dimerization to be essential for activation, since K524E mutant MALT1 shows similar to C464A mutant no protease activity.

Besides dimer interface formation, substrate binding leads to reorganization of the active site loops L1-L4 implying conformational rearrangements of the whole MALT1 paracaspase domain (Fig. 5-4 A). Superposition of the ligand free and hex-LRSR-AOMK bound structure illustrates the movement of β-sheets 3A and 3B up to 3.8 Å and subsequent shift of α-helices C and D (Fig. 5-4 B). This concerted restructuring finally leads to the generation of a proteolytic proficient caspase and is directly connected via the L4 loop over β-sheet 8 and linking helix α1Ig3 to the conformation of the C-terminal Ig3 domain (Fig. 5-4 A). In summary, changes on the boundary of the caspase domain to the Ig3 domain are connected in several ways to the active site conformation.
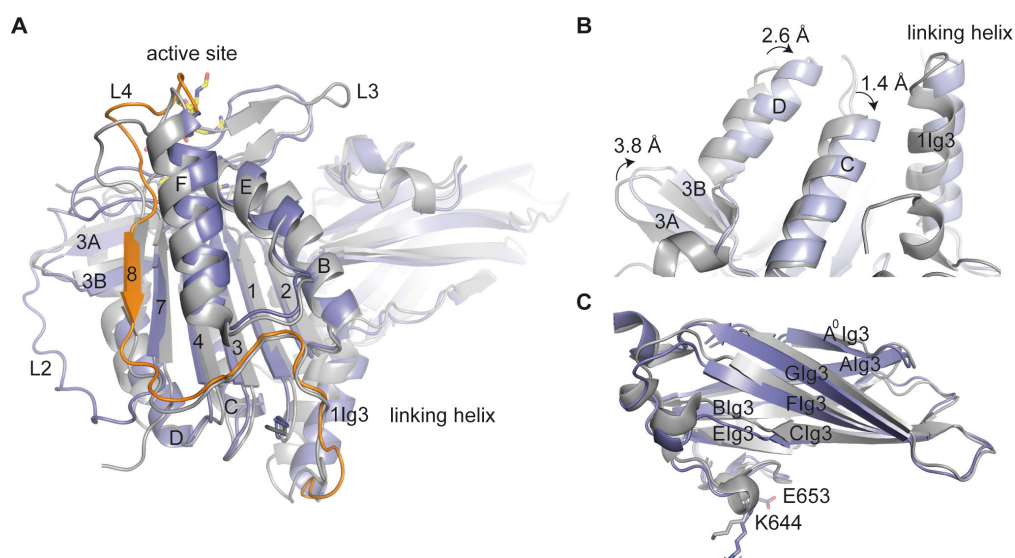
Figure: 5-4: Structural rearrangements essential for MALT1 activation.

A) Superposition of MALT1 bound to hex-LRSR-AOMK (blue) with ligand free MALT1 (grey) (Wiesmann, 2012) shows rearrangements of active site loops L2,L3 and L4. The connection between the active site and Ig3 domain connecting α-helix 1Ig3 of the hex-LRSR-AOMK bound MALT1 structure is highlighted in orange

B) Superposition of hex-LRSR-AOMK bound MALT1 (blue) and ligand free MALT1 (grey) (Wiesmann C, 2012) illustrates structural rearrangements of β-sheets 3A, 3B and α-helices C, D and 1Ig3, essential for activation.

C) Superposition of hex-LRSR-AOMK bound MALT1 (blue) and ligand free MALT1 (grey) (Wiesmann C, 2012) Ig3 domains.

Inhibition of MALT1 proteolytic activity by phenothiazines prevents RelB cleavage, IL-2 expression in activated T-cells and downregulates NF-κB gene transcription in ABC-DLBCL (Nagel, 2012). The crystal structure of MALT1 in complex with thioridazine reveals that the binding site of phenothiazine based compounds, is located on the opposite site relative to the paracaspase active site, in the interface between the paracaspase and the Ig3 domain connecting helix α1Ig3 (Fig. 5-2 A). A detailed analysis of the thioridazine binding site shows that the tricyclic ring system binds in a hydrophobic pocket composed of residues A394, F398 and L401 in α-helix C and L346, V344 and V381 in β-sheets 1 and 2, respectively. In order to determine the correct orientation of the 2-methylthiophenothiazinering, a second dataset of the same crystal was collected at a wavelength of 1.9 Å. The calculation of an anomalous difference density map allowed exact positioning of the thioridazine sulfur atoms and guaranteed correct placement of the small molecule into the refined 2Fo-Fc electron density (Fig. 5-5 A). Superposition of MALT1 bound to hex-LRSR-AOMK with the thioridazine complex structure indicates that binding of the compound in between α-helices 1Ig3 and C prevents the above described second activation step into an enzymatic proficient protease (Fig. 5-5 B). The movement of α-helices C and D is probably hampered by the sandwiched

thioridazine. Therefore, β-sheets 3A and 3B cannot perform their pivotal shift (Fig. 5-5 B) and the important L2 loop cannot be rearranged. Upon inhibitor binding, the side chain of residue W580 on α-helix 1Ig3 is flipped out of the hydrophobic groove, resulting in displacement of α-helix 1Ig3 (Fig. 5-5 A). Probably triggered by rotation of this domain connecting α-helix, the entire Ig3 domain becomes more flexible and shifts at the tip of the domain up to 9.6 Å compared to hex-LRSR-AOMK bound MALT1 (Fig. 5-5 C) or ligand free MALT1 (Fig. 5-4 C). In addition, this significant shift results in a 4 Å displacement of K644 (Fig. 5-5 C), indicating additional impact on the TRAF6 interaction and probably prevents the activation supporting mono-ubiquitination on K644 (Pelzer, 2013).
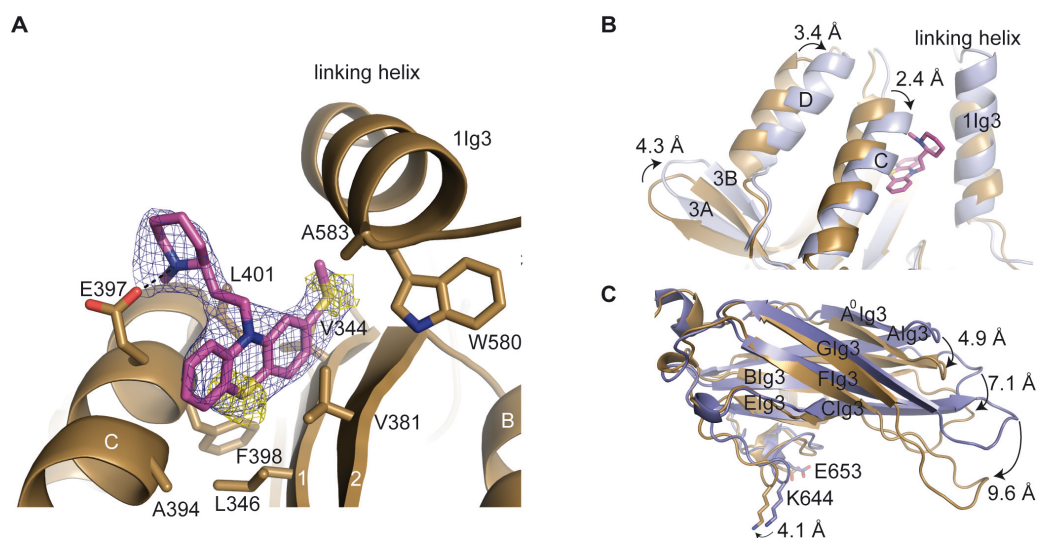
Figure: 5-5: Structural rearrangements induced by thioridazine binding.
A) Detailed view of hydrophobic pocket with interacting residues shown as sticks. The violet mesh represents the refined 2Fo-Fc electron density map (contoured at 1σ) for the ligand, shown together with the yellow highlighted anomalous difference density map (contoured at 2.2σ).
B) Superposition of hex-LRSR-AOMK bound MALT1 (blue) and thioridazine bound MALT1 (gold) illustrates structural changes essential for activation and clash of α-helix C with thioridazine.
C) Superposition of hex-LRSR-AOMK bound MALT1 (blue) and thioridazine bound MALT1 (gold) Ig3 domains represents the significant shift of the entire Ig3domain.

Biochemical and structural studies revealed that residues P2 and P3 are less selective and mainly coordinated by electrostatic interactions, while in position P4 leucine or phenylalanine are clearly preferred by the hydrophobic S4 pocket (Hachmann, 2012; Wiesmann, 2012) (Fig. 5-6 A). A detailed comparison of ligand free and hex-LRSR-AOMK bound MALT1 structures offers insights in conformational rearrangements of the active site essential for activation. The position for P1 arginine is blocked by Q494 in the ligand free structure (Wiesmann, 2012) (Fig. 5-6 B). Moreover, the L2 loop containing active site cysteine C464 is shifted in contrast to the peptide inhibitor bound structure and is stabilized in this inactive

conformation by electrostatic interaction between K466 and Y434. The charge of the active site histidine H415 is responsible for the stabilization of the negative charge of the tetrahedral intermediate and is shielded by Y434. The backbone oxygen of P357 is responsible to keep H415 in place (Fig. 5-6 B). A closer inspection of the allosteric inhibited active site reveals that Y434 interacts with R465 in contrast to K466 in the ligand free structure and stabilizes the L2 loop in the inactive conformation differently (Fig. 5-6 C).
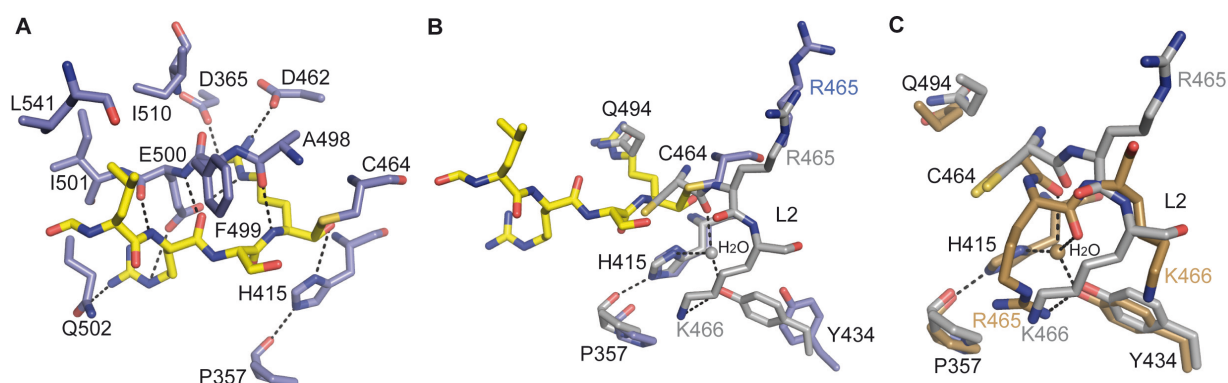
Figure: 5-6: Superposition of active site conformations.
A) Active site of hex-LRSR-AOMK (yellow) bound MALT1 (blue) with coordinating residues represented as sticks.
B) Superposition of hex-LRSR-AOMK (blue) and ligand free MALT1 (grey) (Wiesmann, 2012).
C) Superposition of thioridazine bound (gold) and ligand free MALT1 (grey) (Wiesmann, 2012).

Inhibitor binding, results in the displacement of W580 on α-helix 1Ig3 from the hydrophobic groove into a solvent exposed environment (Fig. 5-7 A). This can be measured by fluorescence quenching, since solvent exposed aromatic residues emit less fluorescence after excitation at 285 nm. The inhibitory potential of the different phenothiazines or related small molecules is represented by fluorescence quenching determined association constants (K_D). Since the association constants for monomeric and ligand free dimeric MALT1 are in a comparable range of approximately 20 μM, MALT1 is inhibited by phenothiazines or related small molecules independent of the oligomeric state (Fig. 5-7 B). Fluorescence intensity data were analyzed according to Stern-Volmer law (Eftink, 1981), pointing to a combination of dynamic and static fluorescence quenching effects (Fig. 5-7 C). In addition, the inhibitory potential of the different phenothiazines was determined by activity assay derived IC_{50}-values. MALT1 activity represents cleavage of AMC molecules from the substrate Ac-LRSR-AMC by increasing fluorescence levels, due to the generation of a conjugated electron system by the cleaved AMC molecules. To verify the allosteric binding site, the main interaction between the N-methylpiperidine group of thioridazine and E397 (Fig. 5-5 A) was disrupted by mutating glutamate to alanine (E397A).

In order to prove the proposed inhibitor-binding mechanism in cells, from DLBCL patients derived HBL-1 cells, were transduced with either wt MALT1 or E397A mutant MALT1. Expression was induced by doxycycline prior to mepazine or thioridazine treatment. Analysis of the cell viability revealed that both compounds reduced the viability of cells transduced with wt MALT1 (Fig. 5-7 D), while HBL-1 cells transduced with the E397A mutant were mostly resistant to mepazine and thioridazine treatment (Fig. 5-7 E). Thus effects of the E397A mutation verify MALT1 as target of phenothiazines *in vivo*.
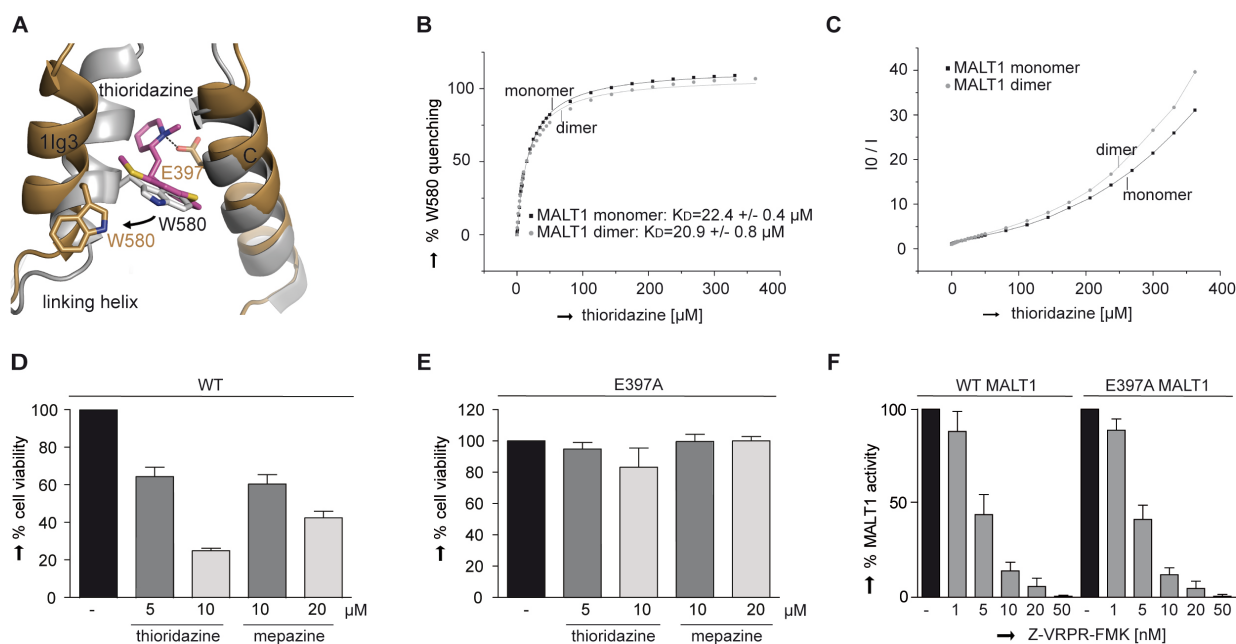
Figure: 5-7: Fluorescence quenching assay and E397A mutant analysis.
A) Close up view of W580 repositioning.
B) Fluorescence quenching assay of monomeric and dimeric MALT1-6xHis.
C) Stern-Volmer representation of fluorescence quenching assay.
D) Cell viability assay for thioridazine and mepazine using wt MALT1 (performed by Nagel D.).
E) Cell viability assay for thioridazine and mepazine with E397A MALT1 (performed by Nagel D.).
F) Activity assay of GST-MALT1 and E397A mutant GST-MALT1 (performed by Nagel D.).

Since the MALT1 cleavage assay of E397A mutant GST-MALT1 shows comparable activity to wt GST-MALT1 and increasing amounts of Z-VRPR-FMK peptide inhibitor result in an equivalent loss of activity, the E397A mutation has no influence on the general activity of MALT1 (Fig. 5-7 F). Analysis of E397A mutant MALT1 by the fluorescence quenching assay and by the MALT1 activity assay shows in comparison to wt MALT1 significant decreased inhibitory potentials, represented by 2.5 fold increased association constants and 5 fold increased IC_{50}-values for thioridazine (Fig. 5-8 A and B). In case of mepazine, 5 fold increased association constants and 60 fold increased IC_{50}-values were determined for E397A mutant MALT1 compared to wt MALT1 (Fig. 5-8 E and F). Both assays confirm the binding

mechanism and show a good correlation between association constants and IC_{50}-values. In addition, the significant increased association constants for E397A mutant MALT1 verify the fluorescence quenching assay. The crystal structure of thioridazine in complex with MALT1 indicates preferential binding of (S)-thioridazine. Both assays show only minor differences between thioridazine enantiomers, illustrated by comparable association constants of 20 μM (Fig. 5-8 C) and IC_{50}-values of 5 μM (Fig. 5-8 D). Interestingly, (S)-mepazine shows preferential binding, represented by a decreased association constant of 8.5 μM (Fig. 5-8 G) and by a 10 fold decreased IC_{50}-value of 0.36 μM (Fig. 5-8 H) compared to (R)-mepazine. Identification of stereo-selective MALT1 inhibition by (S)-mepazine is the first step towards MALT1 optimized small molecule inhibitors and might be useful for further development. Therefore, these assays provide a valuable tool to assess the impact of chemical modifications of phenothiazines on the affinity to MALT1.
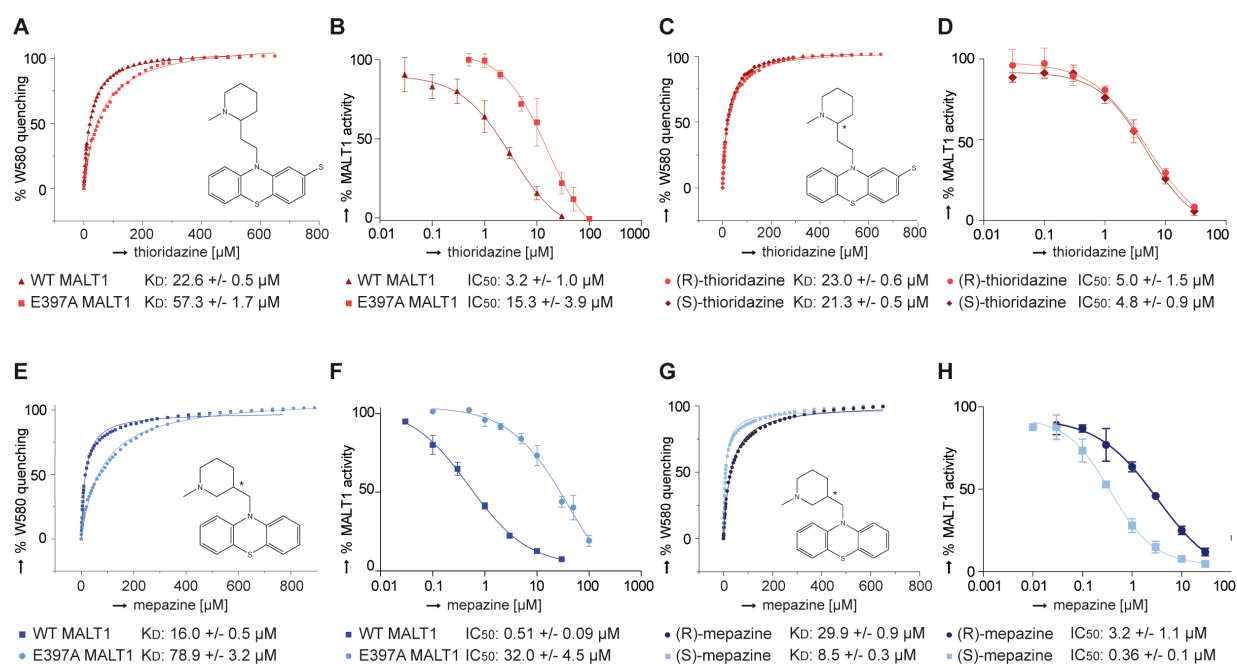
Figure: 5-8: Fluorescence quenching assay and MALT1 activity assay.
A) Fluorescence quenching assay of thioridazine with E397A mutant MALT1.
B) MALT1 activity assay of thioridazine with E397A mutant MALT1 (performed by Nagel D.).
C) Fluorescence quenching assay of thioridazine enantiomers.
D) MALT1 activity assay of thioridazine enantiomers (performed by Nagel D.).
E) Fluorescence quenching assay of mepazine with E397A mutant MALT1.
F) MALT1 activity assay of mepazine with E397A mutant MALT1 (performed by Nagel D.).
G) Fluorescence quenching assay of mepazine enantiomers.
H) MALT1 activity assay of mepazine enantiomers (performed by Nagel D.).

Furthermore, the structure of MALT1 in complex with thioridazine explains the effect of different phenothiazine modifications on their inhibitory effectiveness (Nagel, 2012). On the one hand, the phenothiazine ring system represents an optimal size to fit in the hydrophobic pocket and only minor changes that enlarge the size or enhance the solubility are tolerated, like the 2-methylthio group in thioridazine (Fig. 5-9 A). In addition, the hydrogen bond of the N-methylpiperidine nitrogen of thioridazine to E397 seems to play a major role in MALT1 recognition, as the phenothiazine backbone alone is only a very poor MALT1 inhibitor. All derivatives tested with a piperidyl ring system and nitrogen atom in a similar position to the piperidyl nitrogen atom showed an inhibitory effect in comparable range (Fig. 5-9 A and B). Modifications of the connecting alkyl chain by keto- or hydroxyl-groups (Fig. 5-9 C) result in up to 10 fold increased IC_{50}-values (Nagel, 2012). Modifications like in 3,7-dinitro-10H-phenothiazine (Fig. 5-9 D) result in a complete loss of inhibitory function (Nagel, 2012). In conclusion, both the methyl-piperidyl group and tri-cyclic ring system play equal important roles in drug recognition which is explicable with the presented complex structure.
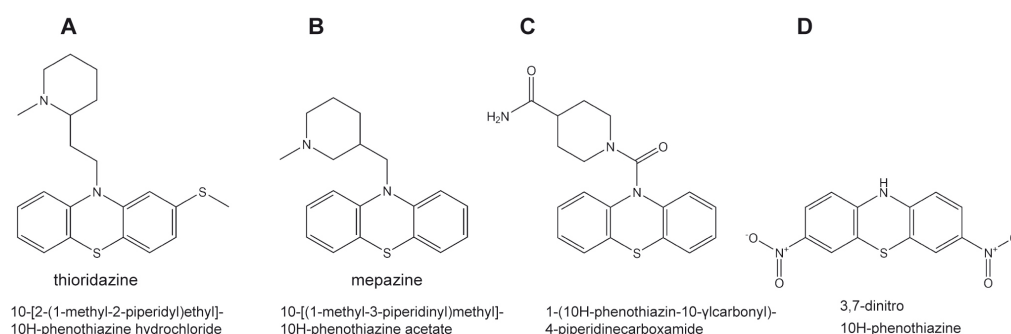
Figure: 5-9: Chemical structures of phenothiazines.
A) Thioridazine.
B) Mepazine.
C) 1-(10H-phenothiazin-10-γlcarbonyl)-4-piperidinecarboxamide.
D) 3,7-dinitro-10H-phenothiazine.

Since the catalytic center of caspases shares a similar conformation (Ivachtchenko, 2009), inhibition by peptide like inhibitors is likely to affect several caspases. In contrast, non-competitive, allosteric inhibition by small molecules is much more specific. Interestingly, thioridazine and mepazine have a clinical history as antipsychotic drugs. These molecules exert sedative effects by acting as a dopamine receptor antagonists in the brain and were used for psychiatric therapies (Seeman Lee, 1975). Recently, thioridazine attracted great attention for cancer therapy, due to a toxic effect on cancer stem cells (CSC) while having no effect on normal human pluripotent stem cells (hPSC) (Sachlos, 2012). Thioridazine affects CSC

survival by acting as dopamine receptor antagonist (Sachlos, 2012). Thus, thioridazine has the same target in psychiatric patients and CSC, leaving no option to improve effectiveness and selectivity of the anti-psychotic effect in the different diseases.

In contrast to the role in CSC, inhibition of MALT1 by thioridazine prevents RelB cleavage, IL-2 expression of activated T-cells and downregulates NF-κB gene transcription in ABC-DLBCL (Nagel, 2012). The transcription factor RelB negatively regulates NF-κB signaling by inhibiting RelA and c-Rel dependent transcription, which is usually abrogated by MALT1 processing of RelB (Hailfinger, 2011). Interestingly, MALT1 inhibition by thioridazine and mepazine reduces ABC-DLBCL growth by an MALT1 proteolytic activity depending toxic effect specific for ABC-DLBCL and does not affect GCB-DLBCL, HBL1 or TM8 cells (Nagel, 2012). Identification of the thioridazine binding pocket on the target MALT1 opens new possibilities for medicinal chemistry to develop effective MALT1 inhibitors that do not affect the dopamine receptor. Since the antipsychotic effect is proposed to origin from (R)-thioridazine (Jortani, 1993), the in this thesis identified stereo-selective mechanism of inhibition is important for the development of more specific inhibitors with less side effects.

Although, dopamine receptor antagonism might be tolerated in the treatment of high grade MALT1-dependent lymphoma, (S)-mepazine may be utilized as mild immunosuppressant that counteract overshooting immune responses in autoimmune diseases or allergic inflammation. Recently, (S)-mepazine was shown to have a significant effect on experimental autoimmune encephalomyelitis (EAE) (Mc Guire, 2014), which is the murine multiple sclerosis model and shows similar aberrant immune responses leading to tissue damage and demyelination in the CNS by auto-reactive T-cells.

In particular, Th1 and Th17 cells play a major role in EAE (Jager, 2009) involving MALT1 dependent processing of RelB. Stimulation of Th1 cells by IL-12 results in IFN-γ secretion to induce macrophages activation (Merrill, 1992) and depends on the NF-κB transcription factors c-Rel and RelB (Kontgen, 1995; Corn, 2005). Additionally, IL-23 driven GM-CSF secretion of Th17 cells is essential for EAE pathogenesis (El-Behi, 2011) and is either directly mediated by c-Rel activated transcription or indirectly by c-Rel dependent Rorγt expression (Himes, 1996; Codarri, 2011). Moreover, c-Rel is involved in T_{reg} cell differentiation by regulating FoxP3 expression (Zhang, 1999). RelA and RelB are essential for γδ-T-cell development to restrain the T_{reg} response during EAE by an IL-23 dependent mechanism (Petermann, 2010; Powolny-Budnicka, 2011).

Similar to previously described NF-κB1 (p50), c-Rel and IKKβ deficient mice (Hilliard, 1999; Hilliard, 2002; Greve, 2007), MALT1 deficient mice are resistant to EAE due to an impaired auto-reactive T-cell immune response (Mc Guire, 2013). MALT1 deficiency results in a reduced amount of Th17 cells with normal expression levels of c-Rel and Rorɣt and lead to significant high levels of RelB in the nucleus and decreased expression of the Th17 effector cytokines IL-17 and GM-CSF (Brüstle, 2012). In contrast, Th1 differentiation and their ability for IFN-ɣ and GM-CSF expression, IL-4 secretion by Th2 cells or FoxP3 expression in T_{reg} cells is not impaired in MALT1 deficient mice (Fig. 5-10) (Brüstle, 2012).

Similar to MALT1 deficient mice, MALT1-C472A knock-in mice are resistant to EAE induction, but show in contrast to MALT1 deficient mice, increased expression of IFN-ɣ by Th1 cells and IL-4 by Th2 cells, resulting in lymphocyte expansion and accumulation of activated T-cells in lymph nodes (Gewies, 2014; Jaworski, 2014). MALT1 deficient and MALT1 C472A mutant mice show increased RelB levels, proposed to be responsible for inhibition of FoxP3 dependent T_{reg} cell differentiation, since significantly reduced T_{reg} cell populations were identified in both mice (Fig. 5-10). However, no altered FoxP3 mRNA levels could be detected and impaired T_{reg} cell differentiation might depend on the MALT1 protease activity in a cell-intrinsic manner, shifting immune tolerance towards autoimmunity. MALT1 C472A mice are prone for the development of autoimmune gastritis, proposed to result from the reduced T_{reg} population (Jaworski, 2014).
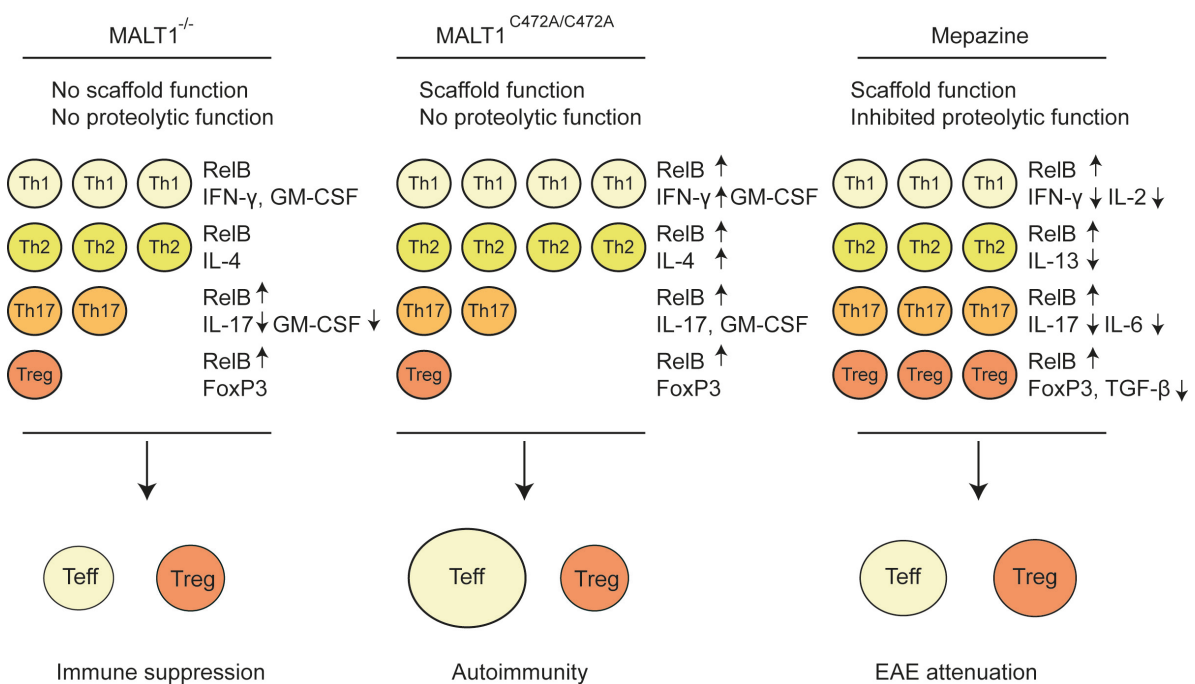
Figure: 5-10: MALT1 and T-cell immune response (adapted from Bertossi, 2014).

Since mepazine treatment in context of EAE results in decreased expression of IFN-ɣ by Th1 cells and the T_{reg} cell population is not affected (Mc Guire, 2014), effects of inhibition by phenothiazines are not comparable with MALT1 deficient or MALT1 C472A mutant mice. Moreover, the constitutive mode of inhibition by C472A mutation (Gewies, 2014) is not equivalent to the non-competitive, allosteric mode of inhibition by phenothiazines, thus therapeutic purposes are rather promising. Besides decreased expression of IFN-ɣ by Th1 cells, mepazine treatment reduces expression levels of IL-13 by Th2 cells, IL-6 and IL-17 by Th17 cells, as well as TGF-β expression by T_{reg} cells (Fig. 5-10) (Mc Guire, 2014). Thus, mepazine treatment leads to a general immune suppressive effect and rebalances immune overreaction (Bertossi, 2014), responsible for chronic inflammation and tissue damage. In particular, the combination of IL-6 with TGF-β supports the development of pathogenic Th17 cells and is reduced by mepazine treatment (Veldhoen, 2006; Bettelli, 2008; Mc Guire, 2014). Influences of MALT1 inhibition by phenothiazines on DC and NK cell activation or developmental stages of B-cells and marginal zone B-cells, observed for the C472A mutant mice (Ruefli-Brasse, 2003; Ruland, 2003; Gewies, 2014; Jaworski, 2014) are not known, but could contribute to attenuation of EAE progression. JNK signaling is not affected in MALT1 C472A mutant mice in contrast to MALT1 deficient mice, indicating that the scaffolding function of MALT1 is rather required than the proteolytic activity of MALT1 in this pathway (Ruland, 2003; Jaworski, 2014).

In conclusion, inhibition of MALT1 by (S)-mepazine is very promising for the treatment of ABC-DLBCL or MS and the identification of phenothiazines as allosteric, non-competitive MALT1 inhibitors, as well as the possibility for stereo-selective MALT1 inhibition is of great significance for further studies.

6 Abbreviations

ABC-DLBCL:	Activated B-cell like diffuse large B-cell lymphoma
ADCC:	Antibody-dependent cell-mediated cytotoxicity
AMC:	7-amido-4-methylcoumarin
Amp:	Ampicillin
APCs:	Antigen-presenting cells
API2	Inhibitor of apoptosis 2
BAFF:	B-cell activating factor
BCL-10:	B-cell lymphoma 10
BCR:	B-cell receptor
BIR:	Baculoviral IAP repeat
Btk:	Bruton's tyrosine kinase
Cam:	Chloramphenicol
CARD:	Caspase-recruitment domain
CCR7:	C-C chemokine receptor type 7
CD:	Cluster of differentiation
cDNA:	Complementary deoxyribonucleic acid
cFLIP:	Cellular FLICE-like inhibitory protein
CLPs:	Common lymphoid progenitors
CMPs:	Common myeloid progenitors
CNS:	Central nervous system
CSF:	Colony-stimulating factor
CSR:	Class-switch recombination
cTECs:	Cortical thymic epithelial cells
CYLD:	Cylindromatosis

D: Diversity

DAG: Diacylglycerol

DAP12:   DNAX-activation protein 12

DCs: Dentric cells

DD: Death domain

DLBCL: Diffuse large B-cell lymphoma

DN: Double negative

DP: Double positive

DTT: Dithiothreitol

EAE: Encephalomyelitis

EM: Electron microscopy

FDCs: Follicular dendritic cells

Fig.:   Figure

FoxP3   Forkhead-box-protein P3

GC: Germinal centres ()

GCB: Germinal center B-cell like

GM: Granulocyte macrophage

GPCR: G-protein coupled receptors

GST: Glutathione S-transferase

HC: Heavy-chain

hex-LRSR-AOMK: Hexyl-leucine-arginine-serine-arginine-acyloxymethyl ketone

HSCs: Hematopoietic stem cells

HTS: High throughput screening

IAP: Inhibitors of apoptosis

IC: Inhibitory concentration

ICOSL:	Inducible T-cell co-stimulator ligand
IFNγ:	Interferon gamma
IgLs:	Immunoglobulin light chains
IKK:	Inhibitor of NF-kB (IκB) kinase
IL:	Interleukin
ILCs:	Innate lymphoid cells
IP$_3$	Inositol triphosphate
IPTG:	Isopropyl β-D-1-thiogalactopyranoside
ITAM:	Immunoreceptor tyrosine-based activation motif
IκBα	NF-κB inhibitor α
J:	Joining
Kan:	Kanamycin
LB:	Lysogeny Broth
LPS:	Lipopolysaccharides
LTi:	Lymphoid tissue inducer cells
MAGUK:	Membrane associated guanylate kinase
MALT1	Mucosa associated lymphoid tissue lymphoma translocation protein 1
MHC:	Major histocompatibility complex
MOG:	Myelin oligodendrocyte glycoprotein
MS:	Multiple sclerosis
NaCl:	Sodium chloride
NF-κB:	Nuclear factor kappa-light-chain-enhancer of activated B-cells
NIK:	NF-κB inducing kinase
Ni-NTA:	Nickel-nitrilotriacetic acid
NK:	Natural killer

NKG2D: Natural-killer group 2, member D

NLS: Nuclear localization signal

PAMPs: Pathogen-associated molecular patterns

PCR: Polymerase chain reaction

PDK1:   Phosphoinositide-dependent kinase-1

PEG: Polyethylenglycole

pH: Pondus Hydrogenii

PI-3-K: Phosphatidyl-inositol-3-kinase

PIP2:   Phosphatidyl-inositol-2-phosphat

PIP3:   Phosphatidyl-inositol-3-phosphat

PKC: Protein kinase C

PLCγ1:   Phospholipase-C-gamma-1

PLCγ2:   Phospholipase-C-gamma-2

PRRs: Pattern-recognition receptors

PT: Pertussis toxin

PTK: Protein tyrosine kinase

RA: Rheumatoid arthritis

Ring: Really interesting new gene

SCS: Subcapsular sinus

SD: Shine-Dalgarno

SDS-PAGE: Sodium dodecyl sulfate polyacrylamide gel electrophoresis

SeMet: Seleno-methionine

SH: Src homology

SHM: Somatic hypermutation

SP: Single positive

TAK:	TGF-β activated kinase 1
T_{CM}:	Central memory T-cells
TCR:	T-cell receptor
T_{EM}:	Effector memory T-cells
T_{FH}:	Follicular helper T-cells
TGF-β:	Transforming growth factor-β
Th:	T-helper
TLRs:	Toll-like receptors
TNF:	Tumor necrosis factor
TNFR:	Tumor necrosis factor receptor
TRAF6	TNF receptor associated factor
T_{reg}:	Regulatory T-cells
TREM1:	Triggering receptor expressed on myeloid cells 1
Tris:	Tris(hydroxymethyl)-aminomethane
UBA:	Ubiquitin associated
V:	Variable
ZAP70:	Zeta-associated protein-70
Z-VRPR-FMK:	Carbobenzoxycarbonyl-val-arg-pro-arg-fluoromethylketone

7 List of figures

8 List of tables

9 References

Adams P.D., Afonine P.V., Bunkóczi G., Chen V.B., Davis I.W., Echols N., Headd J.J., Hung L.W., Kapral G.J., Grosse-Kunstleve R.W., McCoy A.J., Moriarty N.W., Oeffner R., Read R.J., Richardson D.C., Richardson J.S., Terwilliger T.C., Zwart P.H. (2010). "PHENIX: a comprehensive Python-based system for macromolecular structure solution." Acta Crystallogr D Biol Crystallogr. **66**(2): 213-221.

Agrawal A., Eastman Q.M., Schatz D.G. (1998). "Transposition mediated by RAG1 and RAG2 and its implications for the evolution of the immune system." Nature **394**(6695): 744-751.

Akagi T., Motegi M., Tamura A., Suzuki R., Hosokawa Y., Suzuki H., Ota H., Nakamura S., Morishima Y., Taniwaki M., Seto M. (1999). "A novel gene, MALT1 at 18q21, is involved in t(11;18) (q21;q21) found in low-grade B-cell lymphoma of mucosa-associated lymphoid tissue." Oncogene **18**(42): 5785-5794.

Akashi K., Traver D., Miyamoto T., Weissman I.L. (2000). "A clonogenic common myeloid progenitor that gives rise to all myeloid lineages." Nature **404**(6774): 193-197.

Alexopoulou L., Czopik Holt A., Medzhitov R., Flavell R.A. (2001). "Recognition of double-stranded RNA and activation of NF-kappaB by Toll-like receptor 3." Nature **413**(6857): 732-738.

Anderson C.L., Shen L., Eicher D.M., Wewers M.D., Gill J.K. (1990). "Phagocytosis mediated by three distinct Fc gamma receptor classes on human leukocytes." J. Exp. Med. **171**(4): 1333-1345

Arinobu Y., Iwasaki H., Gurish M.F., Mizuno S., Shigematsu H., Ozawa H., Tenen D.G., Austen K.F., Akashi K. (2005). "Developmental checkpoints of the basophil/mast cell lineages in adult murine hematopoiesis." Proc. Natl Acad. Sci. **102**(50): 18105-18110.

Badovinac V.P., Porter B.B., Harty J.T. (2002). "Programmed contraction of CD8+ T cells after infection." Nat. Immunol. **3**(7): 619-626

Bassères D.S., Baldwin A.S. (2006). "Nuclear factor-κB and inhibitor of κB kinase pathways in oncogenic initiation and progression." Oncogene **25**(51): 6817-6830.

Baxter A.G., Smyth M.J. (2002). "The Role of NK Cells in Autoimmune Disease." Autoimmunity **35**(1): 1-14.

Berridge M.J. (1993). "Inositol trisphosphate and calcium signalling. ." Nature **361**(6410): 315-325. .

Bertin J., Wang L., Guo Y., Jacobson M.D., Poyet J.L., Srinivasula S.M., Merriam S., DiStefano P.S., Alnemri E.S. (2001). "CARD11 and CARD14 are novel caspase recruitment domain (CARD)/membrane-associated guanylate kinase (MAGUK) family members that interact with BCL10 and activate NF-kappa B." The Journal of biological chemistry **276**(15): 11877-11882.

Bertossi A., Krappmann D. (2014). "MALT1 protease: equilibrating immunity versus tolerance." EMBO J. **33**(23): 2740-2742.

Bettelli E., Korn T., Oukka M., Kuchroo V.K. (2008). "Induction and effector functions of TH17 cells." Nature **453**(7198): 1051-1057.

Blink E.J., Light A., Kallies A., Nutt S.L., Hodgkin P.D., Tarlinton D.M. (2005). "Early appearance of germinal center-derived memory B cells and plasma cells in blood after primary immunization." J. Exp. Med. **201**(4): 545-554.

Blonska M., Lin X. (2011). "NF-kappaB signaling pathways regulated by CARMA family of scaffold proteins." Cell research **21**(1): 55-70.

Bonizzi G., Karin M. (2004). "The two NFkB activation pathways and their role in innate and adaptive immunity." Trends Immunol. **25**(6): 280-288.

Bricogne G., Blanc E., Brandl M., Flensburg C., Keller P., Paciorek W., Roversi P, Sharff A., Smart O.S., Vonrhein C., Womack T.O. (2011). "BUSTER." Cambridge, United Kingdom: Global Phasing Ltd.

Brown M.G., Dokun A.O., Heusel J.W., Smith H.R., Beckman D.L., Blatten-berger E.A. (2001). "Vital involvement of a natural killer cell activation receptor in resistance to viral infection." Science **292**(5518): 934-937.

Brünger A.T. (1992). "Free R value: a novel statistical quantity for assessing the accuracy of crystal structures." Nature **355**(6359): 472-475.

Brüstle A., Brenner D., Knobbe C.B., Lang P.A., Virtanen C., Hershenfield B.M., Reardon C., Lacher S.M., Ruland J., Ohashi P.S., Mak T.W. (2012). "The NF-κB regulator MALT1 determines the encephalitogenic potential of Th17 cells." J. Clin. Invest. **122**(12): 4698-4709.

Bryson K., McGuffin L.J., Marsden R.L., Ward J.J., Sodhi J.S., Jones D.T. (2005). "Protein structure prediction servers at University College London." Nucleic Acids **33**: 36-38.

Campbell I.K., Gerondakis S., O'Donnell K., Wicks I.P. (2000). "Distinct roles for the NF-κB1 (p50) and c-Rel transcription factors in inflammatory arthritis." Journal of Clinical Investigation. **105**(12): 1799-1806.

Cella M., Fuchs A., Vermi W., Facchetti F., Otero K., Lennerz J.K., Doherty J.M., Mills J.C., Colonna M. (2009). "A human natural killer cell subset provides an innate source of IL-22 for mucosal immunity." Nature **457**(7230): 722-725.

Chan P.L., Sinclair N.R. (1971). "Regulation of the immune response: An analysis of the function of the Fc portion of antibody in suppression of an immune response with respect to interaction with components of the lymphoid system." Immunology **21**(6): 967-968.

Chang D.W., Xing Z., Pan Y., Algeciras-Schimnich A., Barnhart B.C., YaishOhad S., Peter M.E., Yang X. (2002). "c-FLIP(L) is a dual function regulator for caspase-8 activation and CD95-mediated apoptosis." EMBO J. **21**(14): 3704-3714.

Che T., You Y., Wang D., Tanner M.J., Dixit V.M., Lin X. (2004). "MALT1/paracaspase is a signaling component downstream of CARMA1 and mediates T cell receptor-induced NF-kappaB activation." J Biol Chem. **279**(16): 15870-15876.

Chen W., Jin W., Hardegen N., Lei K.J., Li L., Marinos N., McGrady G., Wahl S.M. (2003). "Conversion of Peripheral CD4+CD25− Naive T Cells to CD4+CD25+ Regulatory T Cells by TGF-β Induction of Transcription Factor Foxp3." J Exp Med. **198**(12): 1875-1886.

Chen Y., Kuchroo V.K., Inobe J., Hafler D.A., Weiner H.L. (1994). "Regulatory T cell clones induced by oral tolerance: suppression of autoimmune encephalomyelitis." Science **265**(5176): 1237-1240.

Choi Y.S., Kageyama R., Eto D., Escobar T.C., Johnston R.J., Monticelli L., Lao C., Crotty S. (2011). "ICOS receptor instructs T follicular helper cell versus effector cell differentiation via induction of the transcriptional repressor Bcl6." Immunity **34**(6): 932-946.

Chung J.B., Silverman M., Monroe J.G. (2003). "Transitional B cells: step by step towards immune competence." Trends Immunol. **24**(6): 343-349.

Claudio E., Brown K., Park S., Wang H., Siebenlist U. (2002). "BAFF-induced NEMO-independent processing of NF-κB2 in maturing B cells." Nat. Immunol. **3** (10): 958-965.

Codarri L., Gyülvészi G., Tosevski V., Hesske L., Fontana A., Magnenat L., Suter T., Becher B. (2011). "RORgammat drives production of the cytokine GM-CSF in helper T cells, which is essential for the effector phase of autoimmune neuroinflammation." Nat. Immunol. **12**(6): 560-567.

Coope H.J., Atkinson P.G., Huhse B., Belich M., Janzen J., Holman M.J., Klaus G.G., Johnston L.H., Ley S.C. (2002). "CD40 regulates the processing of NF-κB2 p100 to p52." EMBO J. **21**(20): 5375-5385.

Coornaert B., Baens M., Heyninck K., Bekaert T., Haegman M., Staal J., Sun L., Chen Z.J., Marynen P., Beyaert R. (2008). "T cell antigen receptor stimulation induces MALT1 paracaspase-mediated cleavage of the NF-kappaB inhibitor A20." Nat Immunol. **9**(3): 263-271.

Corfe S.A., Paige C.J. (2012). "The many roles of IL-7 in B cell development; mediator of survival, proliferation and differentiation." Semin Immunol. **24**(3): 198-208.

Corn R.A., Hunter C., Liou H.C., Siebenlist U., Boothby M.R. (2005). "Opposing roles for RelB and Bcl-3 in regulation of T-box expressed in T cells, GATA-3, and Th effector differentiation." J. Immunol. **175**(4): 2102-2110.

Cupedo T., Crellin N.K., Papazian N., Rombouts E.J., Weijer K., Grogan J.L., Fibbe W.E., Cornelissen J.J., Spits H. (2009). "Human fetal lymphoid tissue-inducer cells are interleukin 17-producing precursors to RORC+CD127+ natural killer-like cells." Nature Immunol. **10**(1): 66-74.

Davis R.E., Ngo V.N., Lenz G., Tolar P., Young R.M., Romesser P.B., Kohlhammer H., Lamy L., Zhao H., Yang Y., Xu W., Shaffer A.L., Wright G., Xiao W., Powell J., Jiang J.K., Thomas C.J., Rosenwald A., Ott G., Muller-Hermelink H.K., Gascoyne R.D., Connors J.M., Johnson N.A., Rimsza L.M., Campo E., Jaffe E.S., Wilson W.H., Delabie J., Smeland E.B., Fisher R.I., Braziel R.M., Tubbs R.R., Cook J.R., Weisenburger D.D., Chan W.C., Pierce S.K., Staudt L.M. (2010). "Chronic active B-cell-receptor signalling in diffuse large B-cell lymphoma." Nature **463**(7277): 88-92.

Dejardin E., Droin N.M., Delhase M., Haas E., Cao Y., Makris C., Li Z.W., Karin M., Ware C.F., Green D.R. (2002). "The lymphotoxin-β receptor induces different patterns of gene expression via two NF-κB pathways." Immunity **17** (4): 525-535.

Duerr R.H., Taylor K.D., Brant S.R., Rioux J.D., Silverberg M.S., Daly M.J., Steinhart A.H., Abraham C., Regueiro M., Griffiths A., Dassopoulos T., Bitton A., Yang H., Targan S., Datta L.W., Kistner E.O., Schumm L.P., Lee A.T., Gregersen P.K., Barmada M.M., Rotter J.I., Nicolae D.L., Cho J.H. (2006). "A genome-wide association study identifies IL23R as an inflammatory bowel disease gene." Science **314**(5804): 1461-1463.

Düwel M., Welteke V., Oeckinghaus A., Baens M., Kloo B., Ferch U., Darnay B.G., Ruland J., Marynen P., Krappmann D. (2009). "A20 negatively regulates T cell receptor signaling to NF-kappaB by cleaving Malt1 ubiquitin chains." J Immunol. **182**(12): 7718-7728.

Eftink M.R., Ghiron C.A. (1981). "Fluorescence quenching studies with proteins." Anal Biochem. **114**(2): 199-227.

Eitelhuber A.C., Vosyka O., Nagel D., Bognar M., Lenze D., Lammens K., Schlauderer F., Hlahla D., Hopfner KP., Lenz G., Hummel M., Verhelst S.H., Krappmann D. (2015). "Activity-based probes for detection of active MALT1 paracaspase in immune cells and lymphomas." Chem Biol. **22**(1): 129-138.

El-Behi M., Ciric B., Dai H., Yan Y., Cullimore M., Safavi F., Zhang G.X., Dittel B.N., Rostami A. (2011). "The encephalitogenicity of T(H)17 cells is dependent on IL-1- and IL-23-induced production of the cytokine GMCSF." Nat. Immunol. **12**(6): 568-575.

Elsby L.M., Orozco G., Denton J., Worthington J., Ray D.W., Donn R.P. (2010). "Functional evaluation of TNFAIP3 (A20) in rheumatoid arthritis." Clinical and Experimental Rheumatology. **28**(5): 708-714.

Emsley P., Cowtan K. (2004). "Coot: model-building tools for molecular graphics." Acta Crystallogr D Biol Crystallogr. **60**(12): 2126-2132.

Fazilleau N., Mark L., McHeyzer-Williams L.J., McHeyzer-Williams M.G. (2009a). "Follicular helper T cells: lineage and location." Immunity 30(3): 324-335.

Fazilleau N., McHeyzer-Williams L.J., Rosen H., McHeyzer-Williams M.G. (2009b). "The function of follicular helper T cells is regulated by the strength of T cell antigen receptor binding." Nature Immunol. 10(4): 375-384.

Ferber I.A., Brocke S., Taylor-Edwards C., Ridgway W., Dinisco C., Steinman L., Dalton D., Fathman CG. (1996). "Mice with a disrupted IFN-γ gene are susceptible to the induction of experimental autoimmune encephalomyelitis (EAE)." J Immunol. 156(1): 5-7.

Ferch U., Kloo B., Gewies A., Pfänder V., Düwel M., Peschel C., Krappmann D., Ruland J. (2009). "Inhibition of MALT1 protease activity is selectively toxic for activated B cell-like diffuse large B cell lymphoma cells." J Exp Med. 206(11): 2313-2320.

Ferrao R., Wu H. (2012). "Helical assembly in the death domain (DD) superfamily." Curr. Opin. Struct. Biol. 22(2): 241-247.

Fogg D.K., Sibon C., Miled C., Jung S., Aucouturier P., Littman D.R., Cumano A., Geissmann F. (2006). "A clonogenic bone marrow progenitor specific for macrophages and dendritic cells." Science 311(5757): 83-87.

Fontan L., Yang C., Kabaleeswaran V., Volpon L., Osborne M.J., Beltran E., Garcia M., Cerchietti L., Shaknovich R., Yang S.N., Fang F., Gascoyne R.D., Martinez-Climent J.A., Glickman J.F., Borden K., Wu H., Melnick A. (2012). "MALT1 small molecule inhibitors specifically suppress ABC-DLBCL in vitro and in vivo." Cancer Cell. 22(6): 812-824.

Gaide O., Martinon F., Micheau O., Bonnet D., Thome M., Tschopp J. (2001). "Carma1, a CARD-containing binding partner of Bcl10, induces Bcl10 phosphorylation and NF-kappaB activation." FEBS Lett. 496(2-3): 121-127.

Garrison J.B., Samuel T., Reed J.C. (2009). "TRAF2-binding BIR1 domain of c-IAP2/MALT1 fusion protein is essential for activation of NF-kappaB." Oncogene 28(13): 1584-1593.

Gett A.V., Sallusto F., Lanzavecchia A., Geginat J. (2003). "T cell fitness determined by signal strength." Nat Immunol. 4(4): 355-360.

Gewies A., Gorka O., Bergmann H., Pechloff K., Petermann F., Jeltsch K.M., Rudelius M., Kriegsmann M., Weichert W., Horsch M., Beckers J., Wurst W., Heikenwalder M., Korn T., Heissmeyer V., Ruland J. (2014). "Uncoupling Malt1 threshold function from paracaspase activity results in destructive autoimmune inflammation." Cell Rep. 9(4).

Gilmore T.D. (2006). "Introduction to NFkB: players, pathways, perspectives." Oncogene 25(51): 6680-6684.

Godfrey D.I., Kennedy J., Suda T., Zlotnik A. (1993). "A developmental pathway involving four phenotypically and functionally distinct subsets of CD3−CD4−CD8− triplenegative adult mouse thymocytes defined by CD44 and CD25 expression." J. Immunol. 150(10): 4244-4252.

Greve B., Weissert R., Hamdi N., Bettelli E., Sobel R.A., Coyle A., Kuchroo V.K., Rajewsky K., Schmidt-Supprian M. (2007). "I kappa B kinase 2/beta deficiency controls expansion of autoreactive T cells and suppresses experimental autoimmune encephalomyelitis." J. Immunol. 179(1): 179-185.

Gross O., Gewies A., Finger K., Schäfer M., Sparwasser T., Peschel C., Förster I., Ruland J. (2006). "Card9 controls a non-TLR signalling pathway for innate anti-fungal immunity." Nature 442(7103): 651-656.

Gross O., Grupp C., Steinberg C., Zimmermann S., Strasser D., Hannesschläger N., Reindl W., Jonsson H., Huo H., Littman D.R., Peschel C., Yokoyama W.M., Krug A., Ruland J. (2008). "Multiple ITAM-coupled NK-cell receptors engage the Bcl10/Malt1 complex via Carma1 for NF-kappaB and MAPK activation to selectively control cytokine production." Blood **112**(6): 2421-2428.

Hachmann J., Snipas S.J., van Raam B.J., Cancino E.M., Houlihan E.J., Poreba M., Kasperkiewicz P., Drag M., Salvesen G.S. (2012). "Mechanism and specificity of the human paracaspase MALT1." The Biochemical journal **443**(1): 287-295.

Hailfinger S., Lenz G., Ngo V., Posvitz-Fejfar A., Rebeaud F., Guzzardi M., Penas E.M., Dierlamm J., Chan W.C., Staudt L.M., Thome M. (2009). "Essential role of MALT1 protease activity in activated B cell-like diffuse large B-cell lymphoma." Proc Natl Acad Sci U S A. **106**(47): 19946-19951.

Hailfinger S., Nogai H., Pelzer C., Jaworski M., Cabalzar K., Charton J.E., Guzzardi M., Decaillet C., Grau M., Dorken B., Lenz P., Lenz G., Thome M. (2011). "Malt1-dependent RelB cleavage promotes canonical NF-kappaB activation in lymphocytes and lymphoma cell lines." National Academy of Sciences of the United States of America **108**(35): 14596-14601.

Hanahan D. (1983). "Studies on transformation of Escherichia coli with plasmids. ." J Mol Biol Chem **166**(4): 557-580.

Hara H., Ishihara C., Takeuchi A., Imanishi T., Xue L., Morris S.W., Inui M., Takai T., Shibuya A., Saijo S., Iwakura Y., Ohno N., Koseki H., Yoshida H., Penninger J.M., Saito T. (2007). "The adaptor protein CARD9 is essential for the activation of myeloid cells through ITAM-associated and Toll-like receptors." Nature Immunol. **8**(6): 619-629.

Hara H., Wada T., Bakal C., Kozieradzki I., Suzuki S., Suzuki N., Nghiem M., Griffiths E.K., Krawczyk C., Bauer B., D'Acquisto F., Ghosh S., Yeh W.C., Baier G., Rottapel R., Penninger J.M. (2003). "The MAGUK family protein CARD11 is essential for lymphocyte activation." Immunity **18**(6): 763-775.

Harbertson J., Biederman E., Bennett K.E., Kondrack R.M., Bradley L.M. (2002). "Withdrawal of stimulation may initiate the transition of effector to memory CD4 cells." J. Immunol. **168**(3): 1095-1102.

Hardy R.R., Carmack C.E., Shinton S.A., Kemp J.D., Hayakawa K. (1991). "Resolution and characterization of pro-B and pre-pro-B cell stages in normal mouse bone marrow." J. Exp. Med. **173**(5): 1213-1225

Hardy R.R., Hayakawa K., Parks D.R., Herzenberg L.A. (1983). "Demonstration of B cell maturation in X-linked immunodeficient mice by simultaneous three colour immunofluorescence." Nature **306**(5940): 270-272.

Hayden M.S., Ghosh S. (2004). "Signaling to NF-kappaB." Genes Dev. **18**(18): 2195-2224.

Hilliard B., Samoilova E.B., Liu T.S., Rostami A., Chen Y. (1999). "Experimental autoimmune encephalomyelitis in NF-kappa B-deficient mice: roles of NF-kappa B in the activation and differentiation of autoreactive T cells." J. Immunol. **163**(5): 2937-2943.

Hilliard B.A., Mason N., Xu L., Sun J., Lamhamedi-Cherradi S.E., Liou H.C., Hunter C., Chen Y.H. (2002). "Critical roles of c-Rel in autoimmune inflammation and helper T cell differentiation." J. Clin. Invest. **110**(6): 843-850.

Himes S.R., Coles L.S., Reeves R., Shannon M.F. (1996). "High mobility group protein I(Y) is required for function and for c-Rel binding to CD28 response elements within the GM-CSF and IL-2 promoters." Immunity **5**(5): 479-489.

Hoffmann A., Kafatos F.C., Janeway C.A., Ezekowitz R.A. (1999). "Phylogenetic perspectives in innate immunity." Science **284**(5418): 1313-1318.

Homma Y., Emori Y., Takenawa T. (1992). "Purification of recombinant SH2/SH3 proteins of phospholipase C-gamma 1 and -gamma 2 and their inhibitory effect on PIP2-hydrolysis induced by both types of phospholipase C-gamma." Biochem Biophys Res Commun. **182**(3): 1402-1407.

Hori S., Nomura T., Sakaguchi S. (2003). "Control of regulatory T cell development by the transcription factor Foxp3." Science **299**(5609): 1057-1061.

Hozak R.R., Manji G.A., Friesen P.D. (2000). "The BIR motifs mediate dominant interference and oligomerization of inhibitor of apoptosis Op-IAP." Mol Cell Biol. **20**(5): 1877-1885.

Hsu Y.M., Zhang Y., You Y., Wang D., Li H., Duramad O., Qin X.F., Dong C., Lin X. (2007). "The adaptor protein CARD9 is required for innate immune responses to intracellular pathogens." Nat Immunol. **8**(2): 198-205.

Isaacson P.G., Du M.Q. (2004). "MALT lymphoma: from morphology to molecules." Nat Rev Cancer. **4**(8): 644-653.

Itoh M., Takahashi T., Sakaguchi N., Kuniyasu Y., Shimizu J., Otsuka F., Sakaguchi S. (1999). "Thymus and autoimmunity: production of CD25+CD4+ naturally anergic and suppressive T cells as a key function of the thymus in maintaining immunologic self-tolerance." J Immunol. **162**(9): 5317-5326.

Ivachtchenko A., Okun I., Tkachenko S., Kiselyov A., Ivanenkov Y., Balakin K., O'Brien T., Linton S. (2009). "Design of Caspase Inhibitors as Potential Clinical Agents." CRC Press.

Jacob J., Kelsoe G., Rajewsky K., Weiss U. (1991). "Intraclonal generation of antibody mutants in germinal centres." Nature **354**(6352): 389-392.

Jager A., Dardalhon V., Sobel R.A., Bettelli E., Kuchroo V.K. (2009). "Th1, Th17, and Th9 effector cells induce experimental autoimmune encephalomyelitis with different pathological phenotypes." J. Immunol. **183**(11): 7169-7177.

Jaworski M., Marsland B.J., Gehrig J., Held W., Favre S., Luther S.A., Perroud M., Golshayan D., Gaide O., Thome M. (2014). "Malt1 protease inactivation efficiently dampens immune responses but causes spontaneous autoimmunity." EMBO J. **33**(23): 2765-2781.

Jeltsch K.M., Hu D., Brenner S., Zoller J., Heinz G.A., Nagel D., Vogel K.U., Rehage N., Warth S.C., Edelmann S.L., Gloury R., Martin N., Lohs C., Lech M., Stehklein J.E., Geerlof A., Kremmer E., Weber A., Anders H.J., Schmitz I., Schmidt-Supprian M., Fu M., Holtmann H., Krappmann D., Ruland J., Kallies A., Heikenwalder M., Heissmeyer V. (2014). "Cleavage of roquin and regnase-1 by the paracaspase MALT1 releases their cooperatively repressed targets to promote T(H)17 differentiation." Nature immunology **15**(11): 1079-1089.

Jortani S.A., Poklis A. (1993). "Determination of thioridazine enantiomers in human serum by sequential achiral and chiral high-performance liquid chromatography." J Anal Toxicol. **17**(6): 374-377.

Junt T., Moseman E.A., Iannacone M., Massberg S., Lang P.A., Boes M., Fink K., Henrickson S.E., Shayakhmetov D.M., Di Paolo N.C., van Rooijen N., Mempel T.R., Whelan S.P., von Andrian U.H. (2007). "Subcapsular sinus macrophages in lymph nodes clear lymph-borne viruses and present them to antiviral B cells." Nature **450**(7166): 110-114.

Kabsch W. (2010). "XDS." Acta Crystallogr D Biol Crystallogr. **66**: 125-132.

Karlhofer F.M., Ribaudo R.K., Yokoyama W.M. (2006). "MHC class I alloanti-gen specificity of Ly-49+ IL-2 activated natural killer cells." J Immunol. **177**(9): 5761-5765.

Kawadler H., Gantz M.A., Riley J.L., Yang X. (2008). "The paracaspase MALT1 controls caspase-8 activation during lymphocyte proliferation." Mol Cell. **31**(3): 415-421.

Khader S.A., Bell G.K., Pearl J.E., Fountain J.J., Rangel-Moreno J., Cilley G.E., Shen F., Eaton S.M., Gaffen S.L., Swain S.L., Locksley R.M., Haynes L., Randall T.D., Cooper A.M. (2007). "IL-23 and IL-17 in the establishment of protective pulmonary CD4+ T cell responses after vaccination and during Mycobacterium tuberculosis challenge." Nature Immunol. **8**(4): 369-377.

Klein Wolterink R.G., Kleinjan A., van Nimwegen M., Bergen I., de Bruijn M., Levani Y., Hendriks R.W. (2012). "Pulmonary innate lymphoid cells are major producers of IL-5 and IL-13 in murine models of allergic asthma." J. Immunol. **42**(5): 1106-1116.

Kondo M., Weissman I.L., Akashi K. (1997). "Identification of clonogenic common lymphoid progenitors in mouse bone marrow." Cell **91**(5): 661-672.

Kontgen F., Grumont R.J., Strasser A., Metcalf D., Li R., Tarlinton D., Gerondakis S. (1995). "Mice lacking the c-rel proto-oncogene exhibit defects in lymphocyte proliferation, humoral immunity, and interleukin-2 expression." Genes Dev. **9**(16): 1965-1977.

Laemmli U.K. (1970). "Cleavage of structural proteins during the assembly of the head of bacteriophage T4." Nature **227**(5259): 680-685.

Landström M. (2010). "The TAK1-TRAF6 signalling pathway." Int. J. Biochem. Cell Biol. **42**(5): 585-589.

Langel F.D., Jain N.A., Rossman J.S., Kingeter L.M., Kashyap A.K., Schaefer B.C. (2008). "Multiple protein domains mediate interaction between Bcl10 and MALT1." J Biol Chem. **283**(47): 32419-32431.

Langrish C.L., Chen Y., Blumenschein W.M., Mattson J., Basham B., Sedgwick J.D., McClanahan T., Kastelein R.A., Cua D.J. (2005). "IL-23 drives a pathogenic T cell population that induces autoimmune inflammation." J. Exp. Med. **201**(2): 233-240.

Lee K.Y., D'Acquisto F., Hayden M.S., Shim J.H., Ghosh S. (2005). "PDK1 nucleates T cell receptor-induced signaling complex for NF-kappaB activation." Science **308**(5718): 114-118.

Lenz G., Davis R.E., Ngo V.N., Lam L., George T.C., Wright G.W., Dave S.S., Zhao H., Xu W., Rosenwald A., Ott G., Muller-Hermelink H.K., Gascoyne R.D., Connors J.M., Rimsza L.M., Campo E., Jaffe E.S., Delabie J., Smeland E.B., Fisher R.I., Chan W.C., Staudt L.M. (2008a). "Oncogenic CARD11 mutations in human diffuse large B cell lymphoma." Science **319**(5870): 1676-1679.

Lenz G., Wright G.W., Emre N.C.T., Kohlhammer H., Dave S.S., Davis R.E., Carty S., Lam L.T., Shaffer A.L., Xiao W., Powell J., Rosenwald A., Ott G., Muller-Hermelink H.K., Gascoyne R.D., Connors J.M., Campo E., Jaffe E.S., Delabie J., Smeland E.B., Rimsza L.M., Fisher R.I., Weisenburger D.D., Chan W.C., Staudt L.M. (2008b). "Molecular subtypes of diffuse large B-cell lymphoma arise by distinct genetic pathways." Proceedings of the National Academy of Sciences **105** (36): 13520-13525.

Linsley P.S., Brady W., Grosmaire L., Aruffo A., Damle N.K., Ledbetter J.A. (1991). "Binding of the B cell activation antigen B7 to CD28 costimulates T cell proliferation and interleukin 2 mRNA accumulation." J Exp Med. **173**(3): 721-730.

Lisurek M., Rupp B., Wichard J., Neuenschwander M., von Kries J.P., Frank R., Rademann J., Kühne R. (2010). "Design of chemical libraries with potentially bioactive molecules applying a maximum common substructure concept." Mol Divers **14**(2): 401-408.

Loder F., Mutschler B., Ray R.J., Paige C.J., Sideras P., Torres R., Lamers M.C., Carsetti R. (1999). "B cell development in the spleen takes place in discrete steps and is determined by the quality of B cell receptor-derived signals." J. Exp. Med. **190**(1): 75-89.

Lucas P.C., Kuffa P., Gu S., Kohrt D., Kim D.S., Siu K., Jin X., Swenson J., McAllister-Lucas L.M. (2007). "A dual role for the API2 moiety in API2-MALT1-dependent NF-kappaB activation: heterotypic oligomerization and TRAF2 recruitment." Oncogene **26**(38): 5643-5654.

Lucas P.C., Yonezumi M., Inohara N., McAllister-Lucas L.M., Abazeed M.E., Chen F.F., Yamaoka S., Seto M., Nunez G. (2001). "Bcl10 and MALT1, independent targets of chromosomal translocation in malt lymphoma, cooperate in a novel NF-kappa B signaling pathway." J Biol Chem. **276**(22): 19012-19019.

Mangan P.R., Harrington L.E., O'Quinn D.B., Helms W.S., Bullard D.C., Elson C.O., Hatton R.D., Wahl S.M., Schoeb T.R., Weaver CT. (2006). "Transforming growth factor-beta induces development of the T(H)17 lineage." Nature **441**(7090): 231-234.

Matechak E.O., Killeen, N., Hedrick, S. M., Fowlkes, B. (1996). " MHC class-II-specific T cells can develop in the CD8 lineage when CD4 is absent." Immunity **4**(4): 337-347.

Matsumoto R., Wang D., Blonska M., Li H., Kobayashi M., Pappu B., Chen Y., Wang D., Lin X. (2005). "Phosphorylation of CARMA1 plays a critical role in T Cell receptor-mediated NF-kappaB activation." Immunity **23**(6): 575-585.

Mauro C., Pacifico F., Lavorgna A., Mellone S., Iannetti A., Acquaviva R., Formisano S., Vito P., Leonardi A. (2006). "ABIN-1 binds to NEMO/IKKgamma and co-operates with A20 in inhibiting NF-kappaB." The Journal of biological chemistry **281**(27): 18482-18488.

Mc Guire C., Elton L., Wieghofer P., Staal J., Voet S., Demeyer A., Nagel D., Krappmann D., Prinz M., Beyaert R., van Loo G. (2014). "Pharmacological inhibition of MALT1 protease activity protects mice in a mouse model of multiple sclerosis." J Neuroinflammation **11**(124): 1742-2094.

Mc Guire C., Wieghofer P., Elton L., Muylaert D., Prinz M., Beyaert R., van Loo G. (2013). "Paracaspase MALT1 deficiency protects mice from autoimmune mediated demyelination." J Immunol **190**(6): 2896-2903.

McAllister-Lucas L.M., Inohara N., Lucas P.C., Ruland J., Benito A., Li Q., Chen S., Chen F.F., Yamaoka S., Verma I.M., Mak T.W., Núñez G. (2001). "Bimp1, a MAGUK family member linking protein kinase C activation to Bcl10-mediated NF-kappaB induction." J Biol Chem. **276**(33): 30589-30597.

McCoy A.J., Grosse-Kunstleve R.W., Adams P.D., Winn M.D., Storoni L.C., Read RJ. (2007). "Phaser crystallographic software." J Appl Crystallogr. **40**(4): 658-674.

McHeyzer-Williams L.J., Driver D.J., McHeyzer-Williams M.G. (2001). "Germinal center reaction." Curr. Opin. Hematol. **8**(1): 52-59.

Medzhitov R. (2007). "Recognition of microorganisms and activation of the immune response." Nature **449**(7164): 819-826.

Merrill J.E., Kono D.H., Clayton J., Ando D.G., Hinton D.R., Hofman F.M. (1992). "Inflammatory leukocytes and cytokines in the peptide-induced disease of experimental allergic encephalomyelitis in SJL and B10.PL mice." Proc Natl Acad Sci U S A. **89**(2): 574-578.

Micheau O., Thome M., Schneider P., Holler N., Tschopp J., Nicholson D.W., Briand C., Grutter M.G. (2002). "The long form of FLIP is an activator of caspase-8 at the Fas death-inducing signaling complex." J. Biol. Chem. **277**(47): 45162-45171.

Michie A.M., Carlyle J.R., Schmitt T.M., Ljutic B., Cho S.K., Fong Q., Zúñiga-Pflücker J.C. (2000). "Clonal characterization of a bipotent T-cell and NK-cell progenitor in the mouse fetal thymus." J. Immunol. **164**(4): 1730-1733.

Misra R.S., Russell J.Q., Koenig A., Hinshaw-Makepeace J.A., Wen R., Wang D., Huo H., Littman D.R., Ferch U., Ruland J., Thome M., Budd R.C. (2007). "Caspase-8 and c-FLIPL associate in lipid rafts with NF-kappaB adaptors during T cell activation." J Biol Chem. **282**(27): 19365-19374.

Morgan J.A., Yin Y., Borowsky A.D., Kuo F., Nourmand N., Koontz J.I., Reynolds C., Soreng L., Griffin C.A., Graeme-Cook F., Harris N.L., Weisenburger D., Pinkus G.S., Fletcher J.A., Sklar J. (1999). "Breakpoints of the t(11;18)(q21;q21) in mucosa-associated lymphoid tissue (MALT) lymphoma lie within or near the previously undescribed gene MALT1 in chromosome 18." Cancer Res. 59(24): 6205-6213.

Mosmann T.R., Cherwinski H., Bond M.W. (1986). "Two types of murine helper T cell clone. I. Definition according to profiles of lymphokine activities and secreted proteins. ." J Immunol 136(7): 2348-2357.

Motegi M., Yonezumi M., Suzuki H., Suzuki R., Hosokawa Y., Hosaka S., Kodera Y., Morishima Y., Nakamura S., Seto M. (2000). "API2-MALT1 chimeric transcripts involved in mucosa-associated lymphoid tissue type lymphoma predict heterogeneous products." Am J Pathol. 156(3): 807-812.

Murali-Krishna K., Altman J.D., Suresh M., Sourdive D.J., Zajac A.J., Miller J.D., Slansky J., Ahmed R. (1998). "Counting antigen-specific CD8 T cells: a reevaluation of bystander activation during viral infection." Immunity 8(2): 177-187.

Nagel D., Spranger S., Vincendeau M., Grau M., Raffegerst S., Kloo B., Hlahla D., Neuenschwander M., Peter von Kries J., Hadian K., Dörken B., Lenz P., Lenz G., Schendel D.J., Krappmann D. (2012). "Pharmacologic inhibition of MALT1 protease by phenothiazines as a therapeutic approach for the treatment of aggressive ABC-DLBCL." Cancer Cell. 22(6): 825-837.

Neill D.R., Wong S.H., Bellosi A., Flynn R.J., Daly M., Langford T.K., Bucks C., Kane C.M., Fallon P.G., Pannell R., Jolin H.E., McKenzie A.N. (2010). "Nuocytes represent a new innate effector leukocyte that mediates type-2 immunity." Nature 464(7293): 1367-1370.

Nemazee D., Weigert, M. (2000). "Revising B cell receptors." J. Exp. Med. 191(11): 1813-1817.

Nie Z., Du M.Q., McAllister-Lucas L.M., Lucas P.C., Bailey N.G., Hogaboam C.M., Lim M.S., Elenitoba-Johnson K.S. (2015). "Conversion of the LIMA1 tumour suppressor into an oncogenic LMO-like protein by API2-MALT1 in MALT lymphoma." Nature communications 6(5908).

Noels H., van Loo G., Hagens S., Broeckx V., Beyaert R., Marynen P., Baens M. (2007). "A Novel TRAF6 binding site in MALT1 defines distinct mechanisms of NF-kappaB activation by API2middle dotMALT1 fusions." J Biol Chem. 282(14): 10180-10189.

Ohashi P.S., DeFranco A.L. (2002). "Making and breaking tolerance." Curr. Opin. Immunol. 14(6): 744-759.

Ohoka Y., Kuwata T., Asada A., Zhao Y., Mukai M., Iwata M. (1997). "Regulation of thymocyte lineage commitment by the level of classical protein kinase C activity." J. Immunol. 158(12): 5707-5716.

Oliver A.M., Martin F., Gartland G.L., Carter R.H., Kearney J.F. (1997). "Marginal zone B cells exhibit unique activation, proliferative and immunoglobulin secretory responses." J. Immunol. 27(9): 2366-2374.

Oliver A.M., Martin F., Kearney J.F. (1999). "IgMhighCD21high lymphocytes enriched in the splenic marginal zone generate effector cells more rapidly than the bulk of follicular B cells." J. Immunol. 162(12): 7198-7207.

Pahl H.L. (1999). "Activators and target genes of Rel/NF-kappaB transcription factors." Oncogene 18(49): 6853-6866.

Pape K.A., Catron D.M., Itano A.A., Jenkins M.K. (2007). "The humoral immune response is initiated in lymph nodes by B cells that acquire soluble antigen directly in the follicles." Immunity 26(4): 491-502.

Park H., Li Z., Yang X.O., Chang S.H., Nurieva R., Wang Y.H., Wang Y., Hood L., Zhu Z., Tian Q., Dong C. (2005). "A distinct lineage of CD4 T cells regulates tissue inflammation by producing interleukin 17." Nat Immunol. **6**(11): 1133-1141.

Park S.G., Schulze-Luehrman J., Hayden M.S., Hashimoto N., Ogawa W., Kasuga M., Ghosh S. (2009). "The kinase PDK1 integrates T cell antigen receptor and CD28 coreceptor signaling to induce NF-kappaB and activate T cells." Nat. Immunol. **10**(2): 158-166.

Pelzer C., Cabalzar K., Wolf A., Gonzalez M., Lenz G., Thome M. (2013). "The protease activity of the paracaspase MALT1 is controlled by monoubiquitination." Nature immunology **14**(4): 337-345.

Pentcheva-Hoang T., Egen J.G., Wojnoonski K., Allison J.P. (2004). "B7-1 and B7-2 selectively recruit CTLA-4 and CD28 to the immunological synapse." Immunity **21**(3): 401-413.

Perkins N.D. (2006). "Post-translational modifications regulating the activity and function of the nuclear factor kappaB pathway." Oncogene **25**(51): 6717-6730.

Petermann F., Rothhammer V., Claussen M.C., Haas J.D., Blanco L.R., Heink S., Prinz I., Hemmer B., Kuchroo V.K., Oukka M., Korn T. (2010). "γδ T cells enhance autoimmunity by restraining regulatory T cell responses via an interleukin-23-dependent mechanism." Immunity **33**(3): 351-363.

Phan T.G., Paus D., Chan T.D., Turner M.L., Nutt S.L., Basten A., Brink R. (2006). "High affinity germinal center B cells are actively selected into the plasma cell compartment." J. Exp. Med. **203**(11): 2419-2424.

Pleiman C.M., Abrams C., Gauen L.T., Bedzyk W., Jongstra J., Shaw A.S., Cambier J.C. (1994). "Distinct p53/56lyn and p59fyn domains associate with nonphosphorylated and phosphorylated Ig-α." Proc Natl Acad Sci U S A. **91**(10): 4268-4272.

Powolny-Budnicka I., Riemann M., Tänzer S., Schmid R.M., Hehlgans T., Weih F. (2011). "RelA and RelB transcription factors in distinct thymocyte populations control lymphotoxin-dependent interleukin-17 production in gammadelta T cells." Immunity **34**(3): 364-374.

Pui J.C., Allman D., Xu L., DeRocco S., Karnell F.G., Bakkour S., Lee J.Y., Kadesch T., Hardy R.R., Aster J.C., Pear W.S. (1999). "Notch1 expression in early lymphopoiesis influences B- versus T-lineage determination." Immunity **11**(3): 299-308.

Qiao Q., Yang C., Zheng C., Fontán L., David L., Yu X., Bracken C., Rosen M., Melnick A., Egelman E.H., Wu H. (2013). "Structural architecture of the CARMA1/Bcl10/MALT1 signalosome: nucleation-induced filamentous assembly." Mol Cell. **51**(6): 766-779.

Raab M., Cai Y.C., Bunnell S.C., Heyeck S.D., Berg L.J., Rudd C.E. (1995). "p56Lck and p59Fyn regulate CD28 binding to phosphatidylinositol 3-kinase, growth factor receptor-bound protein GRB-2, and T cell-specific protein-tyrosine kinase ITK: implications for T-cell costimulation." Proc Natl Acad Sci U S A. **92**(19): 8891-8895.

Radtke F., Wilson A., Stark G., Bauer M., van Meerwijk J., MacDonald H.R., Aguet M. (1999). "Deficient T cell fate specification in mice with an induced inactivation of Notch1." Immunity **10**(5): 547-558.

Rebeaud F., Hailfinger S., Posevitz-Fejfar A., Tapernoux M., Moser R., Rueda D., Gaide O., Guzzardi M., Iancu E.M., Rufer N., Fasel N., Thome M. (2008). "The proteolytic activity of the paracaspase MALT1 is key in T cell activation." Nat Immunol. **9**(3): 272-281.

Robey E., Fowlkes B.J. (1994). "Selective events in T-cell development." Annu. Rev. Immunol. **12**: 675-705.

Rosebeck S., Madden L., Jin X., Gu S., Apel I.J., Appert A., Hamoudi R.A., Noels H., Sagaert X., Van Loo P., Baens M., Du M.Q., Lucas P.C., McAllister-Lucas L.M. (2011). "Cleavage of NIK by the API2-MALT1 fusion oncoprotein leads to noncanonical NF-kappaB activation." Science **331**(6016): 468-472.

Rossman J.S., Stoicheva N.G., Langel F.D., Patterson G.H., Lippincott-Schwartz J., Schaefer BC. (2006). "POLKADOTS are foci of functional interactions in T-Cell receptor-mediated signaling to NF-kappaB." Mol Biol Cell. **17**(5): 2166-2176.

Roy N., Deveraux QL, Takahashi R, Salvesen GS, Reed JC. (1997). "The c-IAP-1 and c-IAP-2 proteins are direct inhibitors of specific caspases." EMBO J. **16**(23): 6914-6925.

Ruben S.M., Klement J.F., Coleman T.A., Maher M., Chen C.H., Rosen C.A. (1992). "I-Rel: a novel rel-related protein that inhibits NF-κB transcriptional activity." Genes Dev. **6**(5): 745-760.

Rueda D., Gaide O., Ho L., Lewkowicz E., Niedergang F., Hailfinger S., Rebeaud F., Guzzardi M., Conne B., Thelen M., Delon J., Ferch U., Mak T.W., Ruland J., Schwaller J., Thome M. (2007). "Bcl10 controls TCR- and FcgammaR-induced actin polymerization." J Immunol. **178**(7): 4373-4384.

Ruefli-Brasse A.A., French D.M., Dixit V. M. (2003). "Regulation of NF-kappaB-dependent lymphocyte activation and development by paracaspase." Science **302**(5650): 1581-1584.

Ruland J., Duncan G.S., Wakeham A., Mak T.W. (2003). "Differential requirement for Malt1 in T and B cell antigen receptor signaling." Immunity. **19**(5): 749-758.

Ryseck R.P., Bull P., Takamiya M., Bours V., Siebenlist U., Dobrzanski P., Bravo R. (1992). "RelB, a new Rel family transcription activator that can interact with p50-NF-κB." Mol. Cell. Biol. **12**(2): 674-684.

Sachlos E., Risueño R.M., Laronde S., Shapovalova Z., Lee J.H., Russell J., Malig M., McNicol J.D., Fiebig-Comyn A., Graham M., Levadoux-Martin M., Lee J.B., Giacomelli A.O., Hassell J.A., Fischer-Russell D., Trus M.R., Foley R., Leber B., Xenocostas A., Brown E.D., Collins T.J., Bhatia M. (2012). "Identification of drugs including a dopamine receptor antagonist that selectively target cancer stem cells." Cell **149**(6): 1284-1297.

Saito M., Gao J., Basso K., Kitagawa Y., Smith P.M., Bhagat G., Pernis A., Pasqualucci L., Dalla-Favera R. (2007). "A signaling pathway mediating down-regulation of BCL6 in germinal center B-cells is blocked by BCL6 gene alterations in B-cell lymphoma." Cancer Cell **12**(3): 280-292.

Sakaguchi S. (2000). "Regulatory T cells: key controllers of immunologic self-tolerance." Cell **101**(5): 455-458.

Sakaguchi S., Fukuma K., Kuribayashi K., Masuda T. (1985). "Organ-specific autoimmune diseases induced in mice by elimination of T-cell subset. I. Evidence for the active participation of T cells in natural self-tolerance: deficit of a T-cell subset as a possible cause of autoimmune disease." J. Exp. Med. **161**(1): 72-87.

Salim K., Bottomley M.J., Querfurth E., Zvelebil M.J., Gout I., Scaife R., Margolis R.L., Gigg R., Smith C.I., Driscoll P.C., Waterfield M.D., Panayotou G. (1996). "Distinct specificity in the recognition of phosphoinositides by the pleckstrin homology domains of dynamin and Bruton's tyrosine kinase." EMBO J. **15**(22): 6241-6250.

Sallusto F., Lenig D., Forster R., Lipp M., Lanzavecchia A. (1999). "Two subsets of memory T lymphocytes with distinct homing potentials and effector functions." Nature **401**(6754): 708-712.

Salmena L., Lemmers B., Hakem A., Matysiak-Zablocki E., Murakami K., Au P.Y., Berry D.M., Tamblyn L., Shehabeldin A., Migon E., Wakeham A., Bouchard D., Yeh W.C., McGlade J.C., Ohashi P.S., Hakem R. (2003). "Essential role for caspase 8 in T-cell homeostasis and T-cell-mediated immunity." Genes & development **17**(7): 883-895.

Sambrook J., Russell D.W. (2001). "Molecular Cloning: A Laboratory Manual, 3rd edition." New York, Cold Spring Harbor Laboratory Press.

Saouaf S.J., Mahajan S., Rowley R.B., Kut S.A., Fargnoli J., Burkhardt A.L., Tsukada S., Witte O.N., Bolen J.B. (1994). "Temporal differences in the activation of three classes of non-transmembrane protein tyrosine kinases following B-cell antigen receptor surface engagement." Proc Natl Acad Sci USA **91**(20): 9524-9528.

Saridakis E., Chayen N.E. (2000). "Improving protein crystal quality by decoupling nucleation and growth in vapor diffusion." Protein Sci. **9**(4): 755-757.

Satoh-Takayama N., Vosshenrich C.A., Lesjean-Pottier S., Sawa S., Lochner M., Rattis F., Mention J.J., Thiam K., Cerf-Bensussan N., Mandelboim O., Eberl G., Di Santo J.P. (2008). "Microbial flora drives interleukin 22 production in intestinal NKp46+ cells that provide innate mucosal immune defense." Immunity **29**(6): 958-970.

Schrödinger LLC. (2015). "The PyMOL Molecular Graphics System, Version 1.7.4."

Seeman P. Lee T. (1975). "Antipsychotic drugs: direct correlation between clinical potency and presynaptic action on dopamine neurons." Science **188**(4194): 1217-1219.

Seeman P., Lee T., Chau-Wong M., Wong K. (1976). "Antipsychotic drug doses and neuroleptic/dopamine receptors." Nature **261**(5562): 717-719.

Sen R., Baltimore D. (1986). "Inducibility of κ immunoglobulin enhancer-binding protein NF-κB by a posttranslational mechanism." Cell **47**(6): 921-928.

Senftleben U., Cao Y., Xiao G., Greten F.R., Krähn G., Bonizzi G., Chen Y., Hu Y., Fong A., Sun S.C., Karin M. (2001). "Activation by IKKalpha of a second, evolutionary conserved, NF-kappa B signaling pathway." Science **293**(5534): 1495-1499.

Shan H., Shlomchik M., Weigert M. (1990). "Heavy-chain class switch does not terminate somatic mutation." J. Exp. Med. **172**(2): 531-536.

Shi X., Bi Y., Yang W., Guo X., Jiang Y., Wan C., Li L., Bai Y., Guo J., Wang Y., Chen X., Wu B., Sun H., Liu W., Wang J., Xu C. (2012). "Ca2+ regulates T-cell receptor activation by modulating the charge property of lipids." Nature **493**(7430): 111-115.

Shinkai Y., Koyasu S., Nakayama K., Murphy K.M., Loh D.Y., Reinherz E.L., Alt F.W. (1993). "Restoration of T-cell development in RAG-2-deficient mice by functional TCR transgenes." Science **259**(5096): 822-825.

Shinohara H., Maeda S., Watarai H., Kurosaki T. (2007). "IkappaB kinase beta-induced phosphorylation of CARMA1 contributes to CARMA1 Bcl10 MALT1 complex formation in B cells." J Exp Med. **204**(13): 3285-3293.

Shu H.B., Takeuchi M., Goeddel D.V. (1996). "The tumor necrosis factor receptor 2 signal transducers TRAF2 and c-IAP1 are components of the tumor necrosis factor receptor 1 signaling complex." Proc Natl Acad Sci U S A. **93**(24): 13973-13978.

Smith K.G., Hewitson T.D., Nossal G.J., Tarlinton D.M. (1996). "The phenotype and fate of the antibody-forming cells of the splenic foci." Eur. J. Immunol. **26**(2): 444-448.

Sommer K., Guo B., Pomerantz J.L., Bandaranayake A.D., Moreno-Garcia M.E., Ovechkina Y.L., Rawlings D.J. (2005). "Phosphorylation of the CARMA1 linker controls NF-kappaB activation." Immunity **23**(6): 561-574.

Sonnenberg G.F., Monticelli L.A., Elloso M.M., Fouser L.A., Artis D. (2011). "CD4+ lymphoid tissue-inducer cells promote innate immunity in the gut." Immunity **34**(1): 122-134.

Spits H., Di Santo J. P. (2011). "The expanding family of innate lymphoid cells: regulators and effectors of immunity and tissue remodeling." Nature Immunol. **12**(1): 21-27.

Staal J., Driege Y., Bekaert T., Demeyer A., Muyllaert D., Van Damme P., Gevaert K., Beyaert R. (2011). "T-cell receptor-induced JNK activation requires proteolytic inactivation of CYLD by MALT1." The EMBO journal **30**(9): 1742-1752.

Stahl E.A., Raychaudhuri S., Remmers E.F., Xie G., Eyre S., Thomson B.P., Li Y., Kurreeman F.A., Zhernakova A., Hinks A., Guiducci C., Chen R., Alfredsson L., Amos C.I., Ardlie K.G. (2010). "Genome-wide association study meta-analysis identifies seven new rheumatoid arthritis risk loci." Nature Genet **42**(6): 508-514.

Streb H., Irvine R.F., Berridge M.J., Schulz I. (1983). "Release of Ca2+ from a nonmitochondrial intracellular store in pancreatic acinar cells by inositol-1,4,5-trisphosphate." Nature **306**(5938): 67-69.

Streubel B., Huber D., Wöhrer S., Chott A., Raderer M. (2004). "Frequency of chromosomal aberrations involving MALT1 in mucosa-associated lymphoid tissue lymphoma in patients with Sjögren's syndrome." Clin Cancer Res. **10**(2): 476-480.

Streubel B., Lamprecht A., Dierlamm J., Cerroni L., Stolte M., Ott G., Raderer M., Chott A. (2003). "T(14;18)(q32;q21) involving IGH and MALT1 is a frequent chromosomal aberration in MALT lymphoma." Blood **101**(6): 2335-2339.

Stritesky G.L., Yeh N., Kaplan M.H. (2008). "IL-23 promotes maintenance but not commitment to the Th17 lineage." J Immunol **181**(9): 5948–5955.

Su H., Bidère N., Zheng L., Cubre A., Sakai K., Dale J., Salmena L., Hakem R., Straus S., Lenardo M. (2005). "Requirement for caspase-8 in NF-kappaB activation by antigen receptor." Science **307**(5714): 1465-1468.

Sun L., Deng L., Ea C.K., Xia Z.P., Chen Z.J. (2004). "The TRAF6 ubiquitin ligase and TAK1 kinase mediate IKK activation by BCL10 and MALT1 in T lymphocytes." Mol Cell. **14**(3): 289-301.

Suzuki H., Matsuda S., Terauchi Y., Fujiwara M., Ohteki T., Asano T., Behrens T.W., Kouro T., Takatsu K., Kadowaki T., Koyasu S. (2003). "PI3K and Btk differentially regulate B cell antigen receptor-mediated signal transduction." Nat Immunol **4**(3): 280-286.

Swain S.L., Weinberg, A.D., English M. (1990). "CD4+ T cell subsets. Lymphokine secretion of memory cells and of effector cells that develop from precursors in vitro." J. Immunol. **144**(5): 1788-1799.

Takahashi R., Deveraux Q., Tamm I., Welsh K., Assa-Munt N., Salvesen G.S., Reed J.C. (1998). "A single BIR domain of XIAP sufficient for inhibiting caspases." J Biol Chem. **273**(14): 7787-7790.

Taylor P.R., Brown G.D., Reid D.M., Willment J.A., Martinez-Pomares L., Gordon S. (2002). "The beta-glucan receptor, dectin-1, is predominantly expressed on the surface of cells of the monocyte/macrophage and neutrophil lineages." J Immunol **169**(7): 3876-3882.

Thome M. (2004). "CARMA1, BCL-10 and MALT1 in lymphocyte development and activation." Nat Rev Immunol. **4**(5): 348-359.

Titus J.A., Perez P., Kaubisch A., Garrido M.A., Segal D.M. (1987). "Human K/natural killer cells targeted with hetero-cross-linked antibodies specifically lyse tumor cells in vitro and prevent tumor growth in vivo." J. Immunol. **139**(9): 3153-3158.

Toubi E., Shoenfeld Y. (2004). "Toll-like receptors and their role in the development of autoimmune diseases." Autoimmunity **37**(3): 183-188.

Uehata T., Iwasaki H., Vandenbon A., Matsushita K., Hernandez-Cuellar E., Kuniyoshi K., Satoh T., Mino T., Suzuki Y., Standley D.M., Tsujimura T., Rakugi H., Isaka Y., Takeuchi O., Akira S., (2013). "Malt1-induced cleavage of regnase-1 in CD4(+) helper T cells regulates immune activation." Cell **153**(5): 1036-1049.

Uren A.G., O'Rourke K., Aravind L.A., Pisabarro M.T., Seshagiri S., Koonin E.V., Dixit V.M. (2000). "Identification of paracaspases and metacaspases: two ancient families of caspase-like proteins, one of which plays a key role in MALT lymphoma." Mol Cell. **6**(4): 961-967.

Varfolomeev E., Blankenship J.W., Wayson S.M., Fedorova A.V., Kayagaki N., Garg P., Zobel K., Dynek J.N., Elliott L.O., Wallweber H.J., Flygare J.A., Fairbrother W.J., Deshayes K., Dixit V.M., Vucic D. (2007). "IAP antagonists induce autoubiquitination of c-IAPs, NF-kappaB activation, and TNFalpha-dependent apoptosis." Cell **131**(4): 669-681.

Veillette A., Zuniga-Pflucker J.C., Bolen J.B., Kruisbeek A.M. (1989). "Engagement of CD4 and CD8 expressed on immature thymocytes induces activation of intracellular tyrosine phosphorylation pathways." J. Exp. Med. **170**(5): 1671-1680.

Veldhoen M., Hocking R.J., Atkins C.J., Locksley R.M., Stockinger B. (2006). "TGFbeta in the context of an inflammatory cytokine milieu supports de novo differentiation of IL-17-producing T cells. ." Immunity **24**(2): 179-189.

Vercammen D., Belenghi B., van de Cotte B., Beunens T., Gavigan J.A., De Rycke R., Brackenier A., Inzé D., Harris J.L., Van Breusegem F. (2006). "Serpin1 of Arabidopsis thaliana is a suicide inhibitor for metacaspase 9." J Mol Biol. **364**(4): 625-636.

Vercammen D., Declercq W., Vandenabeele P., Van Breusegem F. (2007). "Are metacaspases caspases?" J Cell Biol. **179**(3): 375-380.

Vivier E., Raulet D.H., Moretta A., Caligiuri M.A., Zitvogel L., Lanier L.L., Yokoyama W.M., Ugolini S. (2011). "Innate or adaptive immunity? The example of natural killer cells." Science **331**(6013): 44-49.

Wagner S., Carpentier I., Rogov V., Kreike M., Ikeda F., Löhr F., Wu C.J., Ashwell J.D., Dötsch V., Dikic I., Beyaert R. (2008). "Ubiquitin binding mediates the NF-kappaB inhibitory potential of ABIN proteins." Oncogene **27**(26): 3739-3745.

Wang D., You Y., Lin P.C., Xue L., Morris S.W., Zeng H., Wen R., Lin X. (2007). "Bcl10 plays a critical role in NF-kappaB activation induced by G protein-coupled receptors. ." Proc Natl Acad Sci USA. **104**(1): 145-150.

Wang X., Zhu L., Liao Z., Zhang F., Xu L., Xu Y., Chen S., Yang L., Zhou Y., Li Y. (2014). "Alternative expression pattern of MALT1-A20-NF-κB in patients with rheumatoid arthritis." J Immunol Res. **492872**.

Weiss A., Littman D.R. (1994). "Signal transduction by lymphocyte antigen receptors." Cell **76**(2): 263-274.

Wherry E.J., Teichgräber V., Becker T.C., Masopust D., Kaech S.M., Antia R., von Andrian U.H., Ahmed R. (2003). "Lineage relationship and protective immunity of memory CD8 T cell subsets." Nat. Immunol. **4**(3): 225-234

Wiesmann C., Leder L., Blank J., Bernardi A., Melkko S., Decock A., D'Arcy A., Villard F., Erbel P., Hughes N., Freuler F., Nikolay R., Alves J., Bornancin F., Renatus M. (2012). "Structural determinants of MALT1 protease activity." J Mol Biol. **419**(1-2): 4-21.

Wiest D.L., Yuan L., Jefferson J., Benveniste P., Tsokos M., Klausner R.D., Glimcher L.H., Samelson L.E., Singer A. (1993). "Regulation of T-cell receptor expression in immature CD4+CD8+ thymocytes by p56lck tyrosine kinase: basis for differential signaling by CD4 and CD8 in immature thymocytes expressing both coreceptor molecules." J. Exp. Med. **178**(5): 1701-1712.

Wilhelm C., Hirota K., Stieglitz B., Van Snick J., Tolaini M., Lahl K., Sparwasser T., Helmby H., Stockinger B. (2011). "An IL-9 fate reporter demonstrates the induction of an innate IL-9 response in lung inflammation." Nat. Immunol. **12**(11): 1071-1077.

Withers D.R., Gaspal F.M., Mackley E.C., Marriott C.L, Ross E.A., Desanti G.E., Roberts N.A., White A.J., Flores-Langarica A., McConnell F.M., Anderson G. and Lane P.J.L (2012). "Lymphoid Tissue Inducer Cells Maintain Memory CD4 T Cells within Secondary Lymphoid Tissue." Journal of immunology **189**(5): 2094-2098.

Wykes M., Pombo A., Jenkins C., MacPherson G.G. (1998). "Dendritic cells interact directly with naive B lymphocytes to transfer antigen and initiate class switching in a primary T-dependent response." J. Immunol. **161**(3): 1313-1319.

Xiao G., Fong A., Sun S.C. (2004). "Induction of p100 processing by NF-kappaBinducing kinase involves docking IkappaB kinase alpha (IKKalpha) to p100 and IKKalpha-mediated phosphorylation." J Biol Chem. **279**(29): 30099-30105.

Xu Y., Harder K.W., Huntington N.D., Hibbs M.L., Tarlinton D.M. (2005). "Lyn tyrosine kinase: accentuating the positive and the negative." <u>Immunity</u> **22**(1): 9-18.

Xue L., Morris S.W., Orihuela C., Tuomanen E., Cui X., Wen R., Wang D. (2003). "Defective development and function of Bcl10-deficient follicular, marginal zone and B1 B cells." <u>Nature Immunol.</u> **4**(9): 857-865.

Yablonski D., Kuhne M.R., Kadlecek T., Weiss A. (1998). "Uncoupling of Nonreceptor Tyrosine Kinases from PLC-γ1 in an SLP-76-Deficient T Cell." <u>Science</u> **218** (5375): 413-416.

Ye H., Liu H., Attygalle A., Wotherspoon A.C., Nicholson A.G., Charlotte F., Leblond V., Speight P., Goodlad J., Lavergne-Slove A., Martin-Subero J.I., Siebert R., Dogan A., Isaacson P.G., Du M.Q. (2003). "Variable frequencies of t(11;18)(q21;q21) in MALT lymphomas of different sites: significant association with CagA strains of H pylori in gastric MALT lymphoma." <u>Blood</u> **102**(3): 1012-1018.

Yu J.W., Jeffrey P.D., Ha J.Y., Yang X., Shi Y. (2011). "Crystal structure of the mucosa-associated lymphoid tissue lymphoma translocation 1 (MALT1) paracaspase region." <u>Proc Natl Acad Sci U S A.</u> **108**(52): 21004-21009.

Zhang Q., Siebert R., Yan M., Hinzmann B., Cui X., Xue L., Rakestraw K.M., Naeve C.W., Beckmann G., Weisenburger D.D., Sanger W.G., Nowotny H., Vesely M., Callet-Bauchu E., Salles G., Dixit V.M., Rosenthal A., Schlegelberger B., Morris S.W. (1999). "Inactivating mutations and overexpression of BCL10, a caspase recruitment domain-containing gene, in MALT lymphoma with t(1;14)(p22;q32)." <u>Nat Genet.</u> **22**(1): 63-68.

Zhou H., Du M.Q., Dixit V.M. (2005). "Constitutive NF-kappaB activation by the t(11;18)(q21;q21) product in MALT lymphoma is linked to deregulated ubiquitin ligase activity." <u>Cancer Cell.</u> **7**(5): 425-431.

Zhou H., Wertz L., O'Rourke K., Ultsch M., Seshagiri S., Eby M., Xiao W., Dixit V.M. (2004). "Bcl10 activates the NF-kappaB pathway through ubiquitination of NEMO." <u>Nature</u> **427**(6970): 167-171.

10 Acknowledgements

First of all, I want to thank Prof. Dr. Karl-Peter Hopfner for the opportunity to work on this extraordinary project. You always supported me by helpful advices and expert knowledge. Especially, inspirations at the right time were of importance for me during the last four years.

I want to thank Prof. Dr. Karl-Klaus Conzelmann for being the second examiner of this thesis.

Special thanks to Dr. Katja Lammens. You always supported me in various ways and taught me everything about structural biology. Discussions with you were extremely helpful and of significant importance for me to create this work. You always inspired me to try new ideas and supported me with your expert knowledge about this project.

I want to thank Prof. Dr. Daniel Krappmann for the successful collaborations and supply of the small molecules inhibitors at the right time. This was the gleam of hope after publications of the MALT1 crystal structures. In this context, special thanks to Dr. Daniel Nagel for performing the cell viability assays and MALT1 activity assays, included in the published article and in this work. In particular, MALT1 specific discussions within this collaboration encouraged the project.

I would like to thank the whole Hopfner group for the nice working atmosphere and help with an extraordinary technical and practical experience. Especially, Dr. Gregor Witte with his expertise in biophysics and structural biology was always helpful during the last four years. Many thanks to our technical assistants, they also contributed to this work and were responsible for the nice working conditions.

I want to thank Dr. Manuela Gorgel and Dr. Katja Lammens for proofreading.

I want to thank the SFB1054 for funding and the great possibilities to study immunology.

Of particular importance was for me the support by my family and by my girlfriend Julia Birg. Their permanent trust in my capabilities made this work possible.